The Thesis Committee for Breanna Rose Peterman
Certifies that this is the approved version of the following thesis:

Influence of Ground Motion Selection on Computed Seismic Sliding Block Displacement

APPROVED BY
SUPERVISING COMMITTEE:

Supervisor: _____

Ellen M. Rathje

_____

Robert B. Gilbert

Influence of Ground Motion Selection on Computed Seismic Sliding Block Displacements

by

Breanna Rose Peterman, B.S.C.E.

Thesis

Presented to the Faculty of the Graduate School of

The University of Texas at Austin

in Partial Fulfillment

of the Requirements

for the Degree of

Master of Science in Engineering

The University of Texas at Austin

May 2014

Dedication

For My Mom and Dad

Acknowledgements

I would like to thank my advisor, Dr. Ellen Rathje, for her time, support, patience, and encouragement during these past two years. Her guidance has helped shape the student, engineer, and person I am today. It has been a privilege and a pleasure to work with and learn from Dr. Rathje. I am incredibly grateful for the experience.

I would also like to thank Dr. Gilbert for reviewing my work. I greatly appreciate Dr. Gilbert's guidance and contributions to my thesis.

Abstract

Influence of Ground Motion Selection on Computed Seismic Sliding Block Displacements

Breanna Rose Peterman, M.S.E

The University of Texas at Austin, 2014

Supervisor: Ellen M. Rathje

Seismic slope stability is often evaluated via permanent displacement analyses, which quantify the cumulative, downslope displacement of a sliding mass subjected to earthquake loading. Seismic sliding block displacements provide a useful index as to the seismic performance of a slope. Seismic sliding block displacements can be computed for a suite of acceleration-time histories selected to fit a design event.

This thesis explores the effect of ground motion selection on computed seismic sliding block displacements through two approaches. First, rigid sliding block displacements were computed for ground motion suites developed to fit uniform hazard spectra (UHS), conditional mean spectra (CMS), and conditional probability distributions for peak ground velocity (PGV) and Arias Intensity (Ia). Evaluation of the suites in terms of their PGV and Ia distributions provided useful insight into the relative displacements computed for the suites. The PGV and Ia distributions of the suite selected to fit the UHS exceed the theoretical

distributions of these ground motion parameters. In fact, the scaled Ia values of motions in the UHS suite are greater than the largest Ia values in the Next Generation Attenuation (NGA) ground motion database. As such, the displacements computed for the UHS suite exceed the displacements computed for any other suite. If only two ground motion parameters are to be considered in ground motion selection we recommend those parameters be PGA and PGV. However, it is important to consider PGA, PGV, and Ia when developing ground motion suites for permanent displacement analyses.

Next, the use of simulated ground motions for permanent displacement analyses was addressed by comparing displacements computed for simulated ground motions to displacements computed for the corresponding recorded ground motion. Simulated ground motions generated via four seismological models were considered: the deterministic Composite Source Model (CSM), the stochastic model EXSIM, the deterministic-stochastic hybrid model by Graves and Pitarka (GP), and the deterministic-stochastic hybrid model developed at San Deigo State University (SDSU). The displacements computed for the SDSU simulations were the most similar to those computed using the recorded motions, with the average displacement of the SDSU simulations exceeding that of the corresponding recorded ground motion by about 6%. Additionally, the displacements from the SDSU simulations provided the smallest variability about the displacements computed for the recorded motions.

Table of Contents

List of Tables x

List of Figures xii

Chapter 1. Introduction 1

1.1 Research Significance 1

1.2 Objectives 2

1.3 Thesis Organization 2

Chapter 2. Background 4

2.1 Introduction 4

2.2 Seismic Slope Stability 5

2.3 Ground Motion Parameters Relevant to Seismic Slope Stability 11

2.4 Ground Motion Selection 13

2.4.1 Selecting Motions to Fit a Target Spectrum 14

2.4.2 Selecting Motions Using Conditional Intensity Measures 27

2.5 Ground Motion Simulation 33

2.6 Summary 39

Chapter 3. The Effect of Ground Motion Selection on Sliding Displacement 41

3.1 Introduction 41

3.2 Site Selection 41

3.3 Development of Target Acceleration Response Spectra 44

3.4 Development of GCIM Distributions for Relevant Ground Motion Parameters 46

3.5 Selected Ground Motion Suites 50

3.5.1 Ground Motion Suites Developed by the PGMD 51

3.5.2 Ground Motion Suites Developed by SigmaSpectra 57

3.5.3 Ground Motion Suites Developed by the GCIM Selection Method....63
3.5.4 Comparison of Selected Motions....67
3.6 Computed Sliding Block Displacements....73
3.7 Summary....79
Chapter 4. Comparison of Displacements from Recordings and Simulated Ground Motions....81
4.1 Introduction....81
4.2 Record Selection....81
4.3 Comparison of Recorded and Simulated Ground Motion....86
4.3.1 Ground Motion Parameter Residuals....86
4.3.2 Displacement Residuals....96
4.4 Summary....108
Chapter 5. Conclusions....110
5.1 Summary and Conclusions....110
5.2 Recommendations for Further Research....113
Appendix A....114
References....129

List of Tables

Table 3-1 Median RMSE of ground motion suites. 69
Table 3-2 Parameters used as inputs to empirical displacement models. 77
Table 4-1 Parameters of recorded ground motions considered in this study. .86
Table 4-2 Average GMP residuals of the four simulation models.....95
Table 4-3 Mixed effects regression parameters for displacement residuals for the four simulation models.....108
Table A-1 Summary of properties of PGMD selected horizontal records for Los Angeles UHS 114
Table A-2 Summary of properties of PGMD selected horizontal records for Los Angeles CMS 115
Table A-3 Summary of properties of PGMD selected horizontal records for San Jose UHS 116
Table A-4 Summary of properties of PGMD selected horizontal records for San Jose CMS 117
Table A-5 Source and site information for the ground motions composing the SigmaSpectra library 118
Table A-6 Summary of properties of SigmaSpectra selected horizontal records for Los Angeles UHS. 119
Table A-7 Summary of properties of SigmaSpectra selected horizontal records for Los Angeles CMS. 120
Table A-8 Summary of properties of SigmaSpectra selected horizontal records for San Jose UHS. 121

Table A-9 Summary of properties of SigmaSpectra selected horizontal records for San Jose CMS. 122
Table A-10 Summary of properties of selected horizontal records for Los Angeles conditional PGV distribution....123
Table A-11 Summary of properties of selected horizontal records for Los Angeles conditional Ia distribution....124
Table A-12 Summary of properties of selected horizontal records for San Jose conditional PGV distribution. 125
Table A-13 Summary of properties of selected horizontal records for San Jose conditional Ia distribution.. 126
Table A-14 Ground motion parameters of the recorded acceleration-time histories. 127
Table A-15 Rigid sliding block displacements computed for the recorded acceleration-time histories. 128

List of Figures

Figure 2.1 Pseudo-static free body diagram of a slope.....6
Figure 2.2 Rigid sliding block analogy 8
Figure 2.3 Calculation of rigid sliding block displacement 10
Figure 2.4 Variation of standard deviation with critical acceleration, k_y, normalized by peak ground acceleration, PGA 13
Figure 2.5 Seismic Hazard Curves for Riverside, CA.....15
Figure 2.6 Uniform hazard spectrum (UHS) for Riverside, CA site.....16
Figure 2.7 PSHA deaggregation for San Jose, CA 18
Figure 2.8 UHS for Riverside, CA site with the predicted median acceleration response spectrum and the median + 2σ spectrum. 20
Figure 2.9 Variation of epsilon with spectral period for an individual response spectrum. 20
Figure 2.10 Conditional mean spectrum (CMS) for Riverside, CA. 23
Figure 2.11 SigmaSpectra selection process. 26
Figure 2.12 Conditional distribution of spectral acceleration at a period of 0.5 s, Sa(0.5). 30
Figure 2.13 Ground motion selection with the GCIM algorithm.....32
Figure 2.14 Ground motion simulation schematic.....35
Figure 2.15 The stochastic approach used to simulate acceleration-time histories in the EXSIM model.....38
Figure 3.1 PSHA deaggregation for Los Angeles, CA.....43
Figure 3.2 PSHA Deaggregation for San Jose, CA. 43

Figure 3.3 UHS, CMS, and predicted median spectra for Los Angeles and San Jose sites.....45
Figure 3.4 Cumulative intensity measure distributions for Los Angeles ...48
Figure 3.5 Cumulative intensity measure distributions for San Jose 49
Figure 3.6 Acceleration response spectra of the ground motion suites developed by the PGMD.....52
Figure 3.7 Intensity measure distributions of the suites selected by the PGMD to fit Los Angeles acceleration response spectra 55
Figure 3.8 Intensity measure distributions of the suites selected by the PGMD to fit San Jose acceleration response spectra. 56
Figure 3.9 Distribution of the SigmaSpectra ground motion catalog in terms of earthquake magnitude, M_w, and rupture distance, R_{rup}. 57
Figure 3.10 Acceleration response spectra of the ground motion suites developed using SigmaSpectra 58
Figure 3.11 Intensity measure distributions of the suites selected by SigmaSpectra to fit Los Angeles acceleration response spectra 61
Figure 3.12 Intensity measure distributions of the suites selected by SigmaSpectra to fit San Jose acceleration response spectra 62
Figure 3.13 Intensity measure distributions of the suites developed using the GCIM selection approach for Los Angeles.....64
Figure 3.14 Intensity measure distributions of the suites developed using the GCIM selection approach for San Jose.....65

Figure 3.15 Acceleration response spectra of the ground motion suites developed using the GCIM approach.....67
Figure 3.16 Comparison of the median spectra of the GCIM suites with the target UHS and CMS. 68
Figure 3.17 Median rigid sliding block displacements of the suites selected to fit UHS and CMS.....74
Figure 3.18 Median displacements of the ground motion suites and empirical displacement predictions 76
Figure 4.1 Ratio of spectral acceleration (Sa) at a given V_{S30} to Sa with V_{S30} = 863 m/s. 83
Figure 4.2 V_{S30} distribution of the strong motion stations considered in the BBP GMSV project 85
Figure 4.3 GMP residuals computed for the CSM simulation model. 89
Figure 4.4 GMP residuals computed for the EXSIM simulation model.....91
Figure 4.5 GMP residuals computed for the GP simulation model. 92
Figure 4.6 GMP residuals computed for the SDSU simulation model. 94
Figure 4.7 Percentage of simulations with zero displacement versus k_y normalized by PGA 99
Figure 4.8 Displacements and residual displacements computed for the CSM simulations. 102
Figure 4.9 Displacements and residual displacements computed for the EXSIM simulations.....104
Figure 4.10 Displacements and residual displacements computed for the GP simulations. 105

Figure 4.11 Displacements and residual displacements computed for the SDSU simulations. 107

Chapter 1. Introduction

1.1 RESEARCH SIGNIFICANCE

Landslides are a global hazard that involve mass downward movements of soil and/or rock. The consequences of landslides can be catastrophic: each year landslides cause hundreds of billions of dollars in damage and hundreds of thousands of casualties around the world (U.S. Geological Survey 2013). Thus, it is of no surprise that slope stability is a critical concern for engineering geologists and geotechnical engineers.

The stability of a slope is a multivariate problem, dependent on geological setting, hydrological conditions, topographical geometry and material properties. Whether it be a natural or constructed slope, a slope will fail if the shear stress required for equilibrium exceeds the maximum shear strength mobilized along the shearing interface. This can occur through a decrease in the shear strength of the soil or through an increase in the shear stress required for equilibrium. During earthquakes, ground shaking increases the shear stress required for equilibrium through the inertial forces imposed by the ground acceleration. Earthquake shaking can also decrease the shear strength of the soil (e.g. liquefaction).

The stability of slopes under seismic loading can be assessed through several approaches. Often, permanent displacement analyses are used to estimate the cumulative, downslope displacement of the slope induced by the inertial force generated by earthquake ground shaking. The estimated displacement provides a useful index regarding the seismic performance of the slope. Permanent displacements can be estimated using empirical prediction

models or computed for a suite of acceleration-time histories selected to represent a design event. There are different approaches to select appropriate acceleration-time histories that represent the design ground motion. Suites developed to fit different ground motion targets using different ground motion catalogs and selection algorithms will likely predict different levels of permanent slope displacement. Additionally, seismological simulations of earthquake ground shaking are gaining popularity, but they have not been evaluated in terms of their use in earthquake engineering analyses.

1.2 OBJECTIVES

The main intent of this study is to investigate the effect of ground motion selection on computed seismic sliding block displacement. The first objective of this study is to compute displacements for suites selected from previously recorded earthquake ground motions using several selection methodologies and compare these displacements in light of the suites' acceleration response spectra and PGV and Ia distributions. The second objective is to evaluate four seismological simulation models in the context of seismic slope stability by comparing displacements computed for simulated ground motions with those computed for the corresponding recorded ground motions.

1.3 THESIS ORGANIZATION

This thesis is organized into five chapters:

Chapter 1 touches upon the significance of seismic slope stability research, states the objectives of this research project, and outlines the structure of this thesis.

Chapter 2 provides the background information required to understand the analyses performed in this study. Fundamentals of seismic slope stability, ground motion selection, and ground motion simulation are presented.

Chapter 3 evaluates the ground motion suites developed for consideration in this study in terms of their acceleration response spectra and intensity measure distributions. The median displacements computed for the suites are presented and compared.

Chapter 4 evaluates four seismological simulation models in the context of seismic slope stability analyses. Simulated ground motions are compared to the corresponding recorded ground motions in terms of their ground motion parameters and rigid sliding block displacements.

Chapter 5 presents the conclusions drawn from the results of this study and recommends areas for further research.

Chapter 2. Background

2.1 INTRODUCTION

Slopes that are stable under static loading conditions may fail in response to earthquake-induced ground motion. Earthquakes can cause slope failure by decreasing the shear strength mobilized along a failure surface, and/or by increasing the shear stress acting along a failure surface due to the inertial loading from earthquake shaking (Kramer 1996). This thesis will focus on the instability due to inertial loading, in which slope failures occur during earthquake ground shaking.

Several methods for the evaluation of seismic slope stability are introduced in this chapter, with emphasis placed on permanent displacement analyses. Permanent displacement analyses predict the level of slope deformation for a given level of earthquake shaking and provide an index as to the severity of the failure consequences. For a given design event, the earthquake-induced permanent displacement of a slope may be estimated using empirical prediction equations or a suite of representative acceleration-time history records.

The selection of earthquake ground motion acceleration-time histories provides an integral link between seismic hazard analyses and numerical response analyses. Through ground motion selection, a suite of appropriate ground motions are selected that are representative of the seismic hazard at a site. The motions are judged as representative based on their fit to a target acceleration response spectrum or a specified statistical distribution. This chapter presents several approaches for ground motion selection relevant to this study:

the uniform hazard spectrum, the conditional mean spectrum, and the generalized conditional intensity measure distribution. This chapter introduces ground motion selection algorithms that are utilized in this study.

The chapter concludes with a discussion of simulated ground motion. The intricacies of ground motion simulation models are beyond the scope of this study. However, as the applicability of simulated ground motions in permanent displacement analyses will be addressed later in this study, a brief introduction is provided.

2.2 SEISMIC SLOPE STABILITY

There are three main approaches to evaluate the seismic stability of slopes: pseudo-static stability analyses, stress deformation analyses, and permanent displacement analyses. The first approach, known as pseudo-static stability analysis, is attributed to Karl Terzaghi (Terzaghi 1950). In a pseudo-static analysis, the effect of earthquake ground shaking is modeled by adding a representative inertial force to the static free body diagram of a slope, as in Figure 2.1. The horizontal inertial force is the product of the weight of the sliding mass, W, and a seismic coefficient, k. The seismic coefficient associated with a factor of safety of one is referred to as the yield coefficient, or critical acceleration, k_y. When the seismic coefficient exceeds the yield coefficient the factor of safety is less than 1.0, the strength of the soil is exceeded, and movement occurs. Often pseudo-static analyses only consider horizontal components of ground motion; vertical ground shaking tends to have a negligible effect on stability, as it affects both the driving force and resisting force similarly (Jibson 2011).

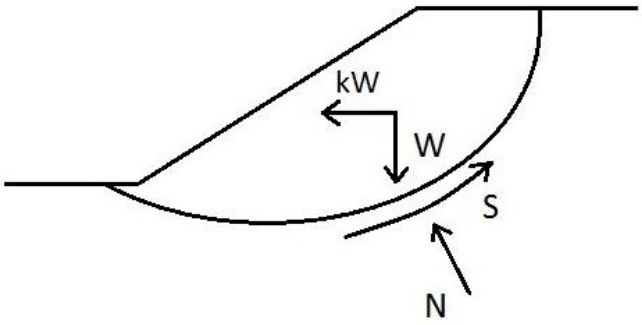

Figure 2.1 Pseudo-static free body diagram of a slope. Forces depicted include: the weight of the sliding mass, W, the normal force, N, the resisting shear force, S, and the earthquake-induced inertial force, kW.

Determination of an appropriate seismic coefficient is the most critical and difficult step in a pseudo-static analysis. In the limiting case of a perfectly rigid slope the seismic coefficient would be equal to the ground acceleration. In that case, the seismic coefficient would reach a maximum value when the peak ground acceleration occurs. A more realistic treatment of a slope, however, should account for the slope's flexibility and the transience of the peak ground acceleration. Thus, seismic coefficients used in pseudo-static stability analyses are often significantly smaller than the peak ground acceleration. Since the formulation of the pseudo-static approach in the mid-twentieth century, numerous researchers have published distinct methods for determination of a representative seismic coefficient. More recent methods, such as that of Stewart et al. (2003) and Bray and Travasarou (2009), recommend calibration of seismic coefficients based on allowable displacements.

The relatively simple pseudo-static approach is attractive to those accustomed to assessing static slope stability. However, Terzaghi (1950) recognized the theoretical limitations of the approach upon its initial formulation by stating that "the conception it conveys of earthquakes on slopes is very inaccurate" (Terzaghi 1950). In pseudo-static analyses, the dynamic and complex energy dissipated during an earthquake is represented by a constant, unidirectional pseudo-static force. Another important shortcoming of the pseudo-static approach is that, because it is a limit-equilibrium analysis, it only provides information as to whether or not failure will occur. The approach does not provide information about the consequences of the failure, which are of critical importance to engineers.

A second approach to assess the seismic stability of slopes is a stress-deformation analysis. In contrast to pseudo-static analyses, a stress-deformation analysis is a complex approach that uses dynamic finite-element modeling. The slope is modeled as a deformable system of elements that is excited by an earthquake acceleration-time history. The nonlinear stress-strain behavior of the slope materials is incorporated in the model and the permanent deformations are computed throughout the slope for the given acceleration-time history. Although theoretically robust, this method also has its drawbacks. Dynamic finite-element modeling requires a wealth of subsurface information that, unfortunately, is often hard to come by. Additionally, use of finite-element analysis and careful interpretation of the results necessitates analysis by experienced engineers.

Permanent displacement analyses are the third approach used to assess the seismic stability of slopes. Permanent displacement analyses improve upon

some of the shortcomings of the previously discussed methods. Unlike pseudo-static analyses, the deformations predicted by permanent displacement analyses represent an index of the seismic performance of the slope, rather than a mere indication of whether equilibrium is disturbed. Compared to stress deformation analyses, permanent displacement analyses require less information and are less computationally intensive.

Newmark (1965) first presented the concept of a permanent displacement analysis in his 1965 Rankine lecture. To model the seismic performance of a slope, Newmark proposed the simple analogy of a rigid block sliding along an inclined plane. A simple schematic of the analogy is presented in Figure 2.2. When applied forces are such that equilibrium cannot be maintained, the rigid block slides along the failure surface and permanent displacement occurs.

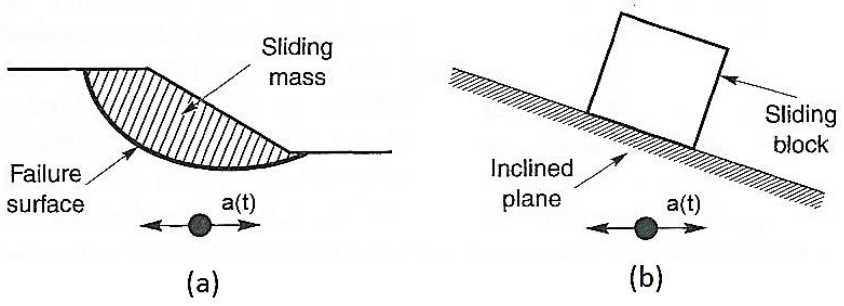

Figure 2.2 Rigid sliding block analogy: (a) slope subjected to earthquake shaking; (b) rigid sliding block analogy (Kramer 1996).

Permanent displacement is computed for a given slope, with a known failure surface and critical acceleration value, and a given acceleration-time history record. If the ground acceleration exceeds the critical acceleration, k_y, an unbalanced force disrupts equilibrium and the idealized block slides down the inclined plane. Figure 2.3 summarizes the calculation of the rigid sliding block

displacement. Movement initiates when the ground acceleration exceeds the critical acceleration of the slope. The relative velocity of the block and the inclined plane is found by numerical integration of the portion of the acceleration-time history record that exceeds the critical acceleration value. Movement continues until the relative velocity of the block and the inclined plane approaches zero. The displacement of the block is found by numerical integration of the relative velocity-time history. The cumulative, permanent displacement of the block is reached once ground shaking has ceased and the relative velocity of the block and the inclined plane has returned to zero.

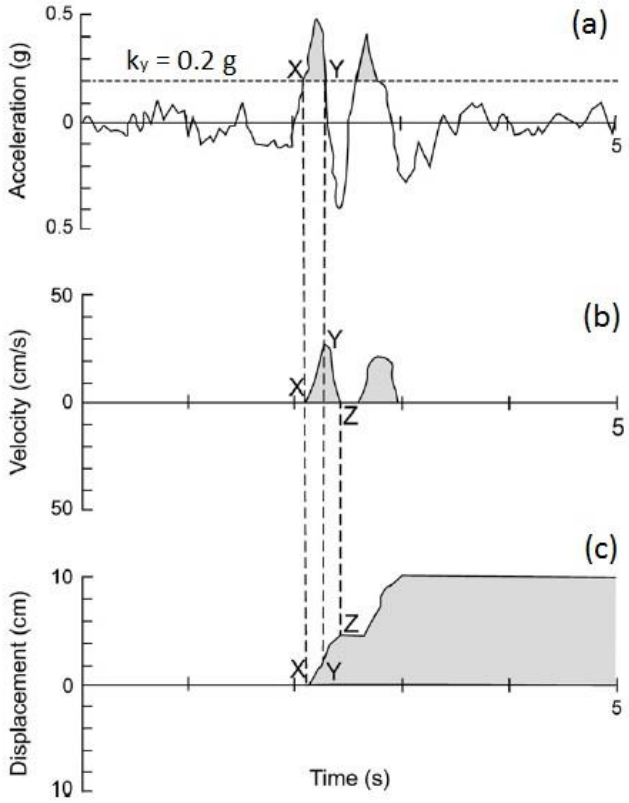

Figure 2.3 Calculation of rigid sliding block displacement: (a) acceleration-time history record with a dashed-line representing the critical acceleration value of 0.2 g; (b) relative velocity-time history; (c) permanent displacement-time history. Adapted from Jibson (2011).

While Newmark's rigid sliding block analysis is an improvement upon the simplistic pseudo-static analysis, it is not without its own shortcomings. Newmark treated the slope as a rigid block and ignored the dynamic response of the soil within the slope. Though the rigid assumption may be a rational simplification for shallow, infinite-slope type failures, the dynamic response of the soil becomes increasingly important when considering slopes with deeper shearing surfaces. Researchers have expanded the rigid sliding block approach to incorporate the dynamic response of flexible slopes with decoupled and coupled

permanent displacement analyses (e.g., Makdisi and Seed 1978, Rathje and Bray 1998, 2000, Antonakos and Rathje 2010). The details of the decoupled and coupled methods are beyond the scope of this study. The research to be presented in this thesis makes use of rigid sliding block analysis to assess the seismic stability of slopes.

2.3 GROUND MOTION PARAMETERS RELEVANT TO SEISMIC SLOPE STABILITY

The seismic design of new slopes and the assessment of the seismic performance of existing slopes often involves the computation of permanent sliding displacement. There are three main approaches to evaluate the expected permanent displacement of a slope for a given design event. The first involves selection of an appropriate suite of acceleration-time history records. The permanent displacement of the slope is calculated for each record using the k_y of the slope and the median displacement is found over all motions in the suite. The second approach uses design charts to estimate earthquake-induced sliding displacement. Design charts, such as those developed by Makdisi and Seed (1978) and Bray et al. (1998), can be used to estimate permanent displacement from various ground motion parameters and the k_y value. The third approach to evaluate the expected permanent displacement of a slope is to use empirical predictive relationships, such as those developed by Watson-Lamprey and Abrahamson (2006), Jibson (2007), Bray and Travasarou (2007), and Saygili and Rathje (2008). These empirical models essentially supersede the design charts because they more rigorously account for the effects of the characteristics of earthquake shaking. The empirical models can provide insight into the main ground motion characteristics that influence sliding displacement.

Saygili and Rathje (2008) developed several empirical models for predicting sliding displacement. These models were developed from displacements computed from a database of over 2,000 acceleration-time history records and four values of critical acceleration. A scalar model was developed, wherein sliding displacement is predicted using a single ground motion parameter, peak ground acceleration (PGA). Vector models, requiring two and three ground motion parameters to characterize the ground shaking, were developed as well. The objective of the study was to characterize the variability of the developed empirical prediction models and determine which models minimize the standard deviation of the prediction. The variation of model standard deviation with critical acceleration value normalized by peak ground acceleration (k_y/PGA) is shown for the developed models in Figure 2.4. The two parameter model that best reduces the variability in the prediction (Figure 2.4a) utilizes peak ground acceleration and peak ground velocity (PGV). It is not surprising that PGA is found to be an important ground motion parameter in assessing the seismic stability of slopes; the relative magnitude of peak ground acceleration to yield acceleration is a direct indication of whether sliding occurs at all. Both three parameter models shown in Figure 2.4b reduce the variability similarly, but Saygili and Rathje (2008) recommend the model that utilizes PGA, PGV, and Arias Intensity (Ia). The results presented in Saygili and Rathje indicate that the parameters most important in characterizing ground shaking for seismic slope stability analyses are peak ground acceleration, peak ground velocity, and Arias Intensity.

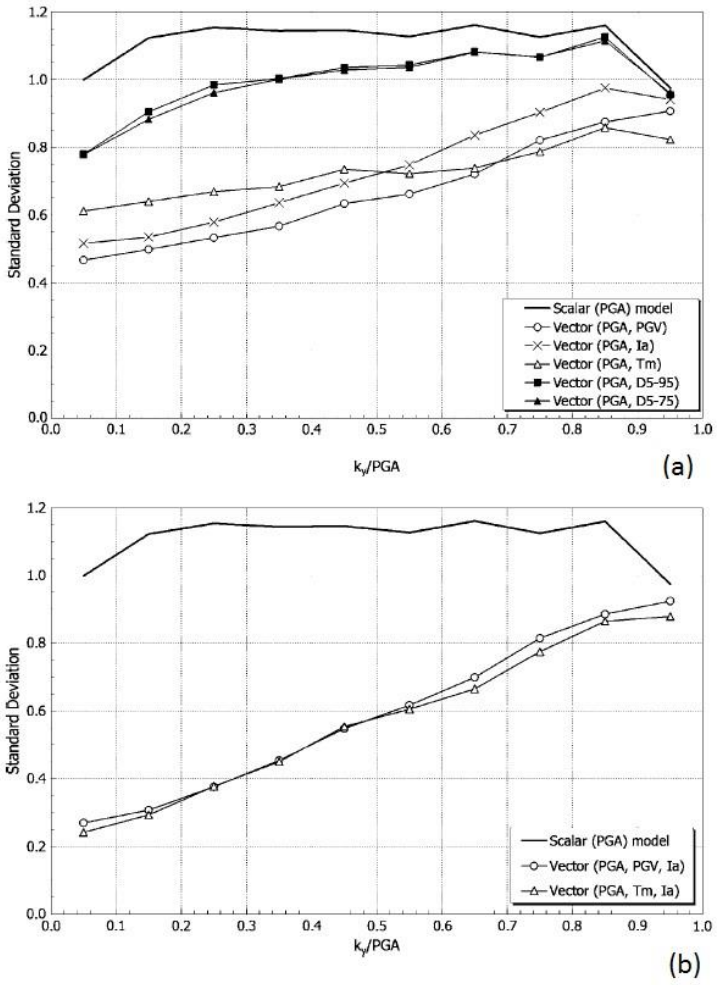

Figure 2.4 Variation of standard deviation with critical acceleration, k_y, normalized by peak ground acceleration, PGA, for (a) scalar and two-parameter models; (b) scalar and three-parameter models (Saygili and Rathje 2008).

2.4 GROUND MOTION SELECTION

As previously mentioned, one approach to estimate sliding displacement of a slope is to select a suite of representative ground motions, calculate the sliding displacement for each acceleration-time history and find the median displacement of the suite. This is just one example of an analysis in which

ground motion selection is integral to geotechnical earthquake engineering. This section will begin by introducing various approaches to specifying a target response spectrum for ground motion selection, as well as the approach to selecting motions to fit a target. Then a new approach for ground motion selection that is based on two or more ground motion parameters is described.

2.4.1 Selecting Motions to Fit a Target Spectrum

Design levels of ground shaking are estimated via probabilistic seismic hazard analysis (PSHA). There is uncertainty as to the location and size of future earthquakes, and there is significant variability in ground motions predicted for a given magnitude and distance. PSHA attempts to quantify these uncertainties and rationally combine them to predict design levels of ground shaking. PSHA yields seismic hazard curves, an example of which is shown in Figure 2.5. This curve represents the seismic hazard at a site in Riverside, CA and it was obtained from the USGS Hazard Durve Application (2008). Seismic hazard curves show the variation of the annual probability, or frequency (λ), of exceedance with ground motion intensity. Larger ground motions are associated with smaller annual frequencies of exceedance. In practice, seismic hazard curves are typically developed for spectral accelerations, as in Figure 2.5. However, seismic hazard curves can be developed for other ground motion parameters, such as peak ground velocity and Arias Intensity, as well.

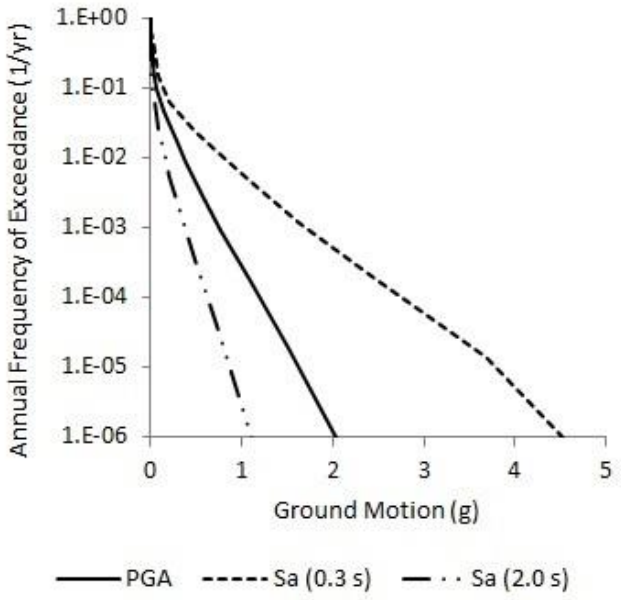

Figure 2.5 Seismic Hazard Curves for Riverside, CA (117.335°W, 33.979°N). Seismic hazard curves for PGA, spectral acceleration at a period of 0.3 s, and spectral acceleration at a period of 1 s are shown. Data from USGS Hazard Curve Application (2008).

The information provided in a seismic hazard curve can be used to define a target spectrum for ground motion selection. The uniform hazard spectrum is a commonly used target spectrum in engineering practice. The uniform hazard spectrum represents values of spectral acceleration at various periods that have the same annual frequency of exceedance. A uniform hazard spectrum can be developed for any seismic hazard level that is deemed appropriate for the system under consideration. Common design hazard levels are 10% probability of exceedance in 50 years (λ=0.0021 1/yr) and 2% probability of exceedance in 50 years (λ=0.0004 1/yr). The uniform hazard spectrum associated with a 2% probability of exceedance in 50 years for the Riverside, CA site is shown as an example in Figure 2.6.

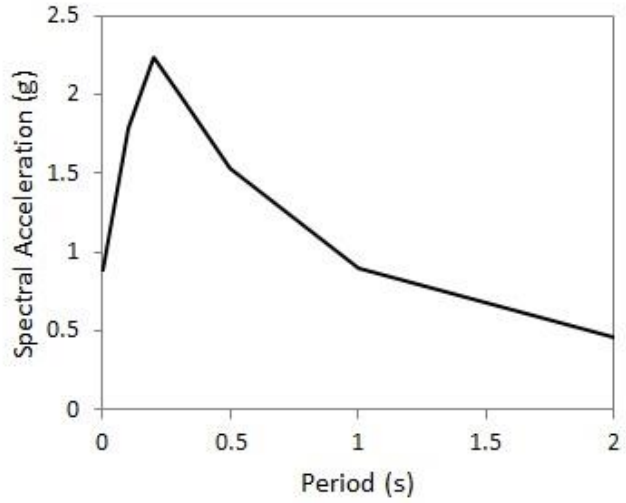

Figure 2.6 Uniform hazard spectrum for Riverside, CA site (117.335°W, 33.979°N).

The uniform hazard spectrum (UHS), as found through PSHA, is not representative of a ground motion spectrum of a single earthquake motion and is, therefore, not an ideal target for ground motion selection. There are two shortcomings of the uniform hazard spectrum. First, the seismic hazard represented in a uniform hazard spectrum is often driven by different rupture scenarios at different periods. The earthquake event (magnitude and distance) that dominates the hazard at long spectral periods is not necessarily the same event that dominates the hazard at shorter spectral periods. Deaggregation data, which breaks down the seismic hazard into contributions from different rupture scenarios (i.e., magnitude and rupture distance combinations), can be used to demonstrate this point. Example deaggregation data for San Jose, California (121.890°W, 37.340°N) is shown in Figure 2.7. Figure 2.7a shows the seismic hazard deaggregation for the PGA value that has a 2% probability of exceedance in 50 years. An earthquake with a magnitude of about 6.6 and a rupture distance

of about 12 km is seen to dominate the hazard. Figure 2.7b shows the deaggregation data for the spectral acceleration value at a period of 1.0 second that has a 2% probability of exceedance in 50 years. In this case, two earthquake scenarios contribute significantly to the seismic hazard: a magnitude of about 7.9 with a rupture distance of 20 km and a magnitude of about 6.9 at a rupture distance of about 12 km. For the same site and the same return period we see that the contributing rupture scenarios can vary with spectral period. A recorded acceleration-time history, however, is clearly the result of only one rupture scenario.

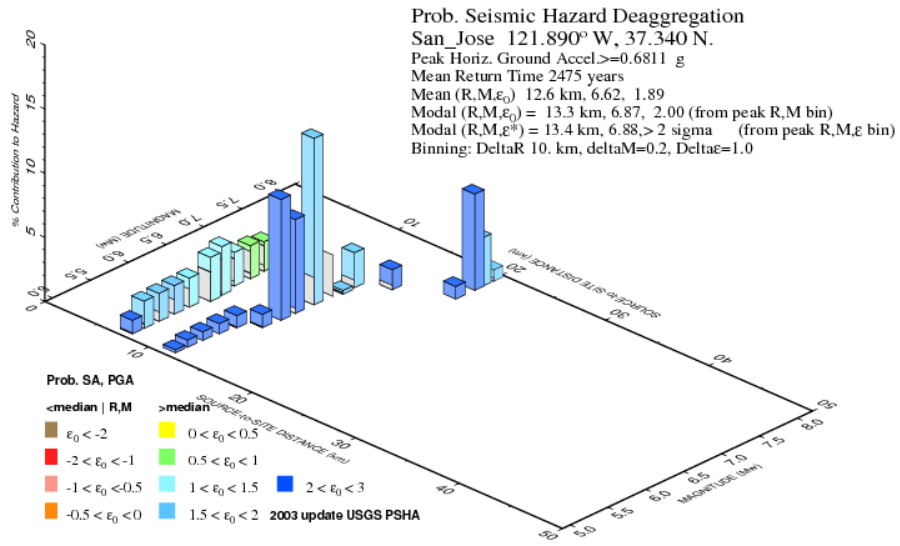

(a)

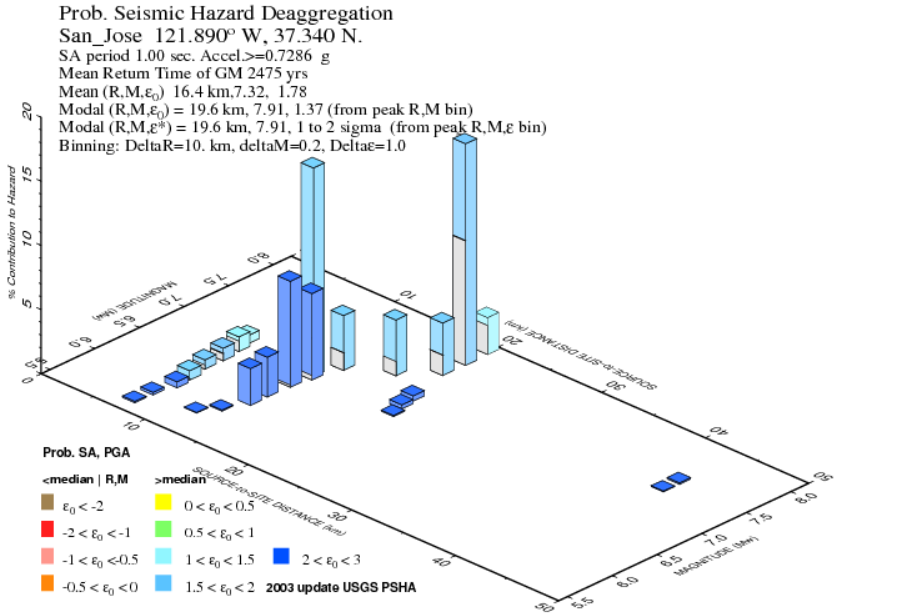

(b)

Figure 2.7 PSHA deaggregation for San Jose, CA, given exceedance of the 2% probability of exceedance in 50 years value of (a) PGA and (b) the spectral acceleration at a period of 1.0 s (USGS Custom Mapping and Analysis Tools, http://geohazards.usgs.gov/deaggint/2002/).

The second shortcoming of the uniform hazard spectrum is that it is very unlikely for an individual acceleration-time history to be equally above average across all periods (Baker 2011). Figure 2.8 shows the uniform hazard spectrum for the Riverside, CA site along with the median and median +2σ spectra for a magnitude of about 7 and distance of about 12 km, which is one of the dominant earthquake scenarios at this site. In this case, the UHS is well approximated by the predicted median +2σ spectrum. However, the acceleration response spectrum of an individual acceleration-time history varies such that the number of standard deviations by which an individual spectrum exceeds or falls short of the median changes, often significantly, with period. As an example, an individual response spectrum is shown from a recording of the 1994 Northridge earthquake (M=6.7) from the Castaic Old Ridge Route station, located 20 km from the fault rupture in Figure 2.9. The recorded ground motion exceeds the median spectrum by more than 2 standard deviations at a period of 1.0 s, but only exceeds the median spectrum by 1.2 standard deviations at a period of 0.2 s.

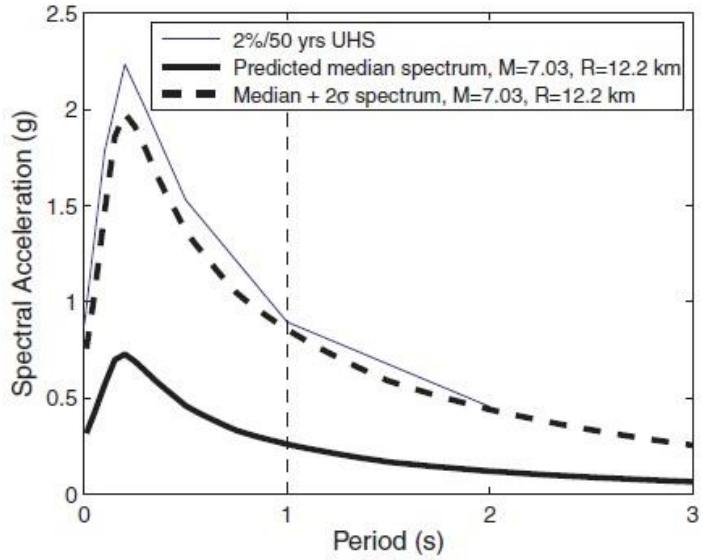

Figure 2.8 Uniform hazard spectrum for Riverside, CA site along with the predicted median acceleration response spectrum and the median + 2σ spectrum (Baker 2011).

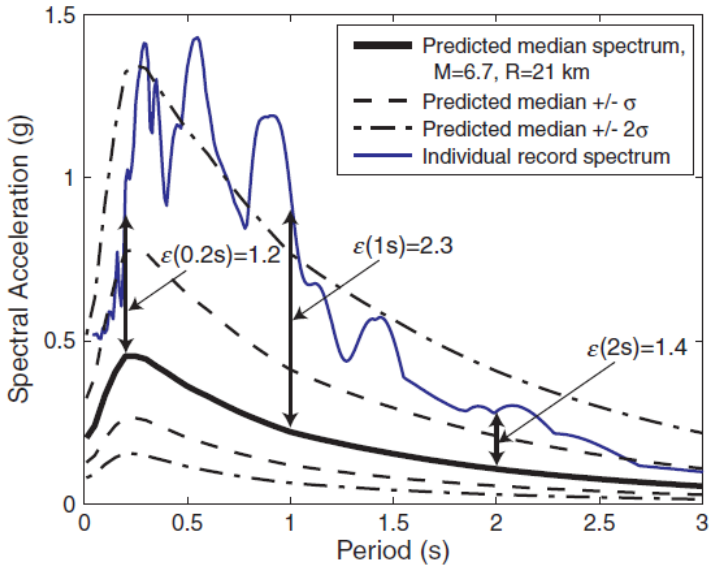

Figure 2.9 Variation of epsilon with spectral period for an individual response spectrum of the Northridge earthquake recorded at the Castaic Old Ridge Route station (Baker 2011).

The conditional mean spectrum was developed to improve upon the shortcomings of the uniform hazard spectrum. The conditional mean spectrum represents the mean values of the response spectrum, conditioned on the occurrence of a response value at a specific period of interest (Baker and Cornell 2005). The rational choice for the conditioning period is the natural period of the structure or system under consideration because a resonant condition between the earthquake ground shaking and the system's natural frequency is the worst-case scenario and will result in maximum damage to the structure. PSHA is used to define the response value at the conditioning period that is consistent with the desired seismic hazard level.

The first step in the creation of a conditional mean spectrum is the selection of the conditioning period (T*) and the response value at this period. Next, seismic deaggregation can be used to identify the mean magnitude and mean rupture distance for that ground motion level. The median acceleration response spectrum is developed for the mean magnitude and mean rupture distance using a ground motion prediction equation. Next, the number of standard deviation away from the median (i.e. epsilon) associated with the ground motion at the period of interests is computed ($\varepsilon(T*)$). Note that epsilon is computed assuming a log-normal distribution for ground motion. Epsilon is positive when a response value exceeds the median and negative when a response value falls below the median. Correlation coefficients have been developed to relate the epsilon for spectral acceleration at one period with the epsilon value for spectral acceleration at another period, $\rho_{T,T*}$ (Baker and Jayaram 2008). Generally, the correlation coefficient is close to 1.0 for periods

close to one another, and becomes less than 1.0 as periods are spaced further apart. The conditional mean spectrum is developed by updating the median response value at each period (T) by the corresponding epsilon value using

$$Sa(T) = \exp(\mu_{lnSa}(T) + \rho_{T,T*} \cdot \varepsilon(T^*) \cdot \sigma_{lnSa}(T)) \quad (2.1)$$

where $\mu_{lnSa}(T)$ and $\sigma_{lnSa}(T)$) are the predicted mean and standard deviation of ln Sa at a period of T.

An example conditional mean spectrum for the Riverside, CA site is shown in Figure 2.10. The spectrum is conditioned on the spectral acceleration at 1.0 second equal to 0.89 g, which is the motion with 2% probability of exceedance in 50 years from PSHA. The median and median + 2σ response spectrum from Figure 2.8 are replicated in Figure 2.10. Not that the CMS is equal to the +2σ spectrum at the target period of 1.0 s, but falls below the +2σ spectrum at all other periods. The smaller epsilon at the other periods is a result of the correlation coefficient between periods becoming less than 1.0 for periods further from the target period.

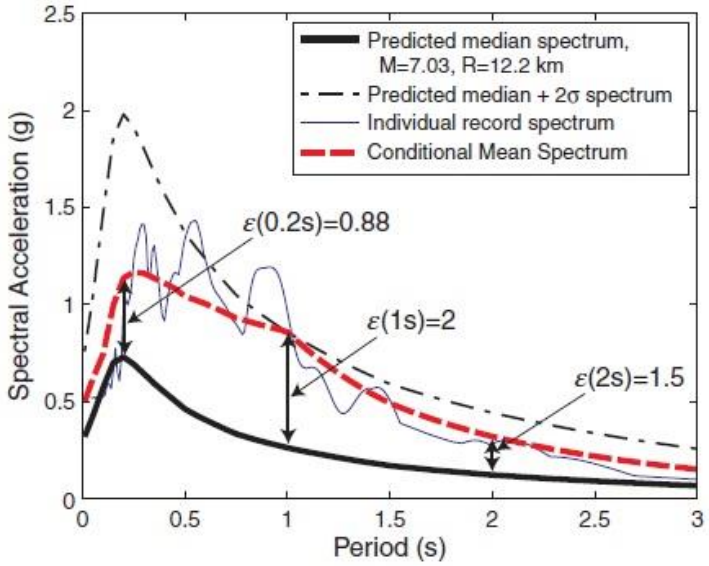

Figure 2.10 Conditional mean spectrum (CMS) for Riverside, CA conditioned on the spectral acceleration value at 1 second (Baker 2011).

After selecting a target spectrum, a suite of acceleration time histories must be selected that fit the target spectrum. This study considers two ground motion selection methods that fit a target spectrum: one that selects motions based on their individual fit to the target spectrum and one that considers how well a suite of motions work together to fit a target spectrum.

The first ground motion selection method is used by the PEER Ground Motion Database (PGMD) Web Application. A basic underlying criterion of the PGMD is that the acceleration response spectrum of a selected time history provides a "good match" to the user specified target spectrum (Pacific Earthquake Engineering Research Center 2010). After specifying the target spectrum, the user establishes the range of spectral periods over which the fit is to be evaluated and a weight function that indicates the relative importance of spectral periods within this period range. The default spectral period range is 0.1

s to 10 s and the default weight function is a uniform distribution between those values. The PGMD allows the user to place constraints on various attributes of the acceleration-time histories that are to be selected from the PEER database. For example, if the user specifies a specific fault type and/or a range of earthquake magnitudes and rupture distances then the selected time histories must meet these requirements. In the PGMD, goodness of fit is quantified with the mean square error (MSE) between the response spectrum and the target spectrum, evaluated over the spectral period range of interest defined as:

$$\mathrm{MSE} = \frac{\sum_{i} \mathrm{w}(T_i)\left\{ln\left[\mathrm{SA}^{\mathrm{target}}(T_i)\right] - ln\left[f \times \mathrm{SA}^{\mathrm{record}}(T_i)\right]\right\}^2}{\sum_{i} \mathrm{w}(T_i)} \tag{2.2}$$

where f is the scale factor applied to the response spectrum and $w(T_i)$ is the weight function defined by the user. The user has the option to select unscaled records or scaled records. Scaled records are multiplied by a factor which minimizes the MSE. After determining the MSE for each acceleration-time history that meets the user-specified criteria, the PGMD lists the records in order of increasing MSE.

The second approach for ground motion selection considered in this study is a two-step semi-automated algorithm (Kottke and Rathje 2008) available in the software program SigmaSpectra (Kottke and Rathje 2010). Required user inputs to the software include the target acceleration response spectrum and its standard deviation at each period and the range of spectral periods over which goodness of fit is to be evaluated. The user must supply the software with a library of appropriate ground motions, deemed representative of the scenario

event under consideration. Unlike in the PGMD, the user specifies the number of records desired in the ground motion suite.

The approach used in SigmaSpectra is discussed briefly here and illustrated in Figure 2.11. SigmaSpectra first identifies suites of motions from the library that, together, best match the spectral shape of the target response spectrum (Kottke and Rathje 2008). The program determines the average scale factor which, when applied to each motion, results in the best fit of the suite's median spectrum to the target spectrum (Figure 2.11a). In SigmaSpectra goodness of fit between suites is evaluated by the root mean square error (RMSE), which is defined as:

$$\mathrm{RMSE} = \sqrt{\frac{1}{n_p}\sum_{i=1}^{n_p}\left(\ln \overline{S}_a^{\mathrm{scaled}}(i) - \ln S_a^{\mathrm{target}}(i)\right)^2} \tag{2.3}$$

where n_p is the number of periods in the response spectrum, $\overline{S}_a^{scaled}(i)$ is the median spectral acceleration of the scaled suite at the i-th period, and $S_a^{target}(i)$ is the spectral acceleration of the target at the i-th period. While the average scale factor is chosen to fit the amplitude of the target spectrum, it does not control the standard deviation of the suite. Thus, the standard deviation of the suite may be quite different, probably larger, than the target spectrum (Figure 2.11b).The standard deviation of the suite can be updated to better fit the standard deviation of the target response spectrum by adjusting the scale factors of the individual ground motions in the suite (Figure 2.11c). If the individual scale factors are altered such that the average scale factor remains unchanged, the standard deviation of the suite can be controlled without affecting the median response spectrum (Figure 2.11d).

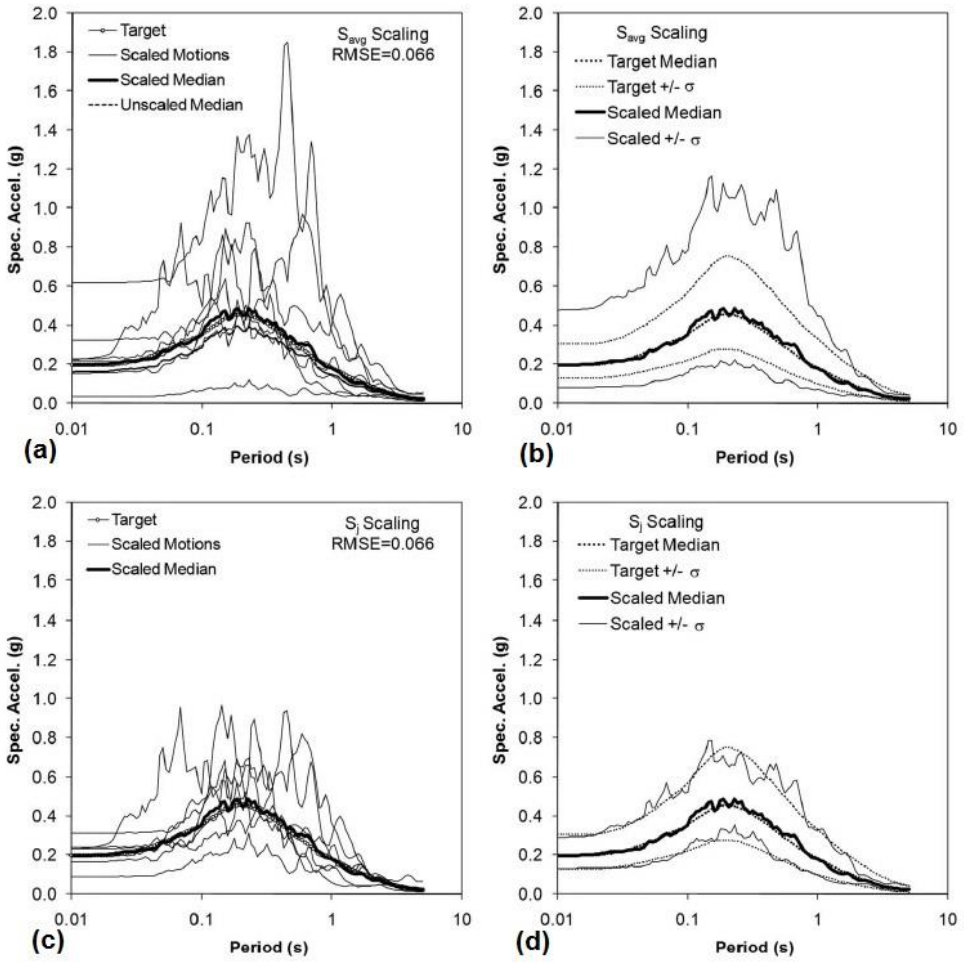

Figure 2.11 SigmaSpectra selection process: (a) ground motions scaled by average factor, s_{avg}; (b) median and median+/- σ spectrum scaled by s_{avg}; (c) ground motions scaled by individual scale factors, s_j; (d) median and median+/- σ spectrum scaled by s_j (Kottke and Rathje 2008).

There is an important difference between the ground motion selection methods used by SigmaSpectra and the PGMD. SigmaSpectra selects a suite of ground motions such that the median of the suite best fits the target spectrum. The PGMD does not develop a suite of motions, rather it lists records in order of increasing individual MSE. If a suite of N motions is desired, the first N records

on the list may be taken to compose the suite. Although the individual motions have response spectra that fit the target well, the median of the suite may not fit the target well at other periods. For example, it is possible that the suite is dominated by motions with acceleration response spectra that consistently fall above or consistently fall below the response spectrum within a specific period range.

There are important shortcomings of using a target spectrum (either a uniform hazard spectrum or a conditional mean spectrum) for ground motion selection. Acceleration response spectra only provide a partial picture of the true character of earthquake-induced ground shaking. This partial picture is a powerful tool and, for some applications, such as analysis of single-degree-of-freedom or multiple-degree-of-freedom systems, the acceleration response spectrum may be sufficient to estimate the response (Bradley 2010). However, for responses that are sensitive to other ground motion characteristics, such as duration, the response spectrum may fail to capture the characteristics of ground motion pertinent to the problem.

2.4.2 Selecting Motions Using Conditional Intensity Measures

To create a more holistic target for ground motion selection Bradley (2010) developed the generalized conditional intensity measure (GCIM) approach. The concept of the GCIM approach is similar to that used in the development of the conditional mean spectrum except that the conditional parameter can be any ground motion characteristic. In the GCIM approach conditional probability distributions are developed for relevant ground motion parameters, given the occurrence of a specific value of another ground motion parameter.

The GCIM approach has three main prerequisites. First, the value of the conditioning variable must be specified. Second, ground motion prediction equations must exist for all ground motion parameters involved. Third, the analysis requires correlation coefficients between the specified ground motion parameters. If all of the prerequisites are met the GCIM approach can be used to develop conditional distributions for ground motion parameters that are consistent with the results of PSHA.

The first step in developing a GCIM probability distribution is to specify the value of the conditioning variable. For ease of discussion, let IM_i refer to the ground motion parameter for which a conditional distribution is being developed and IM_j refer to the conditioning ground motion parameter. PSHA is used to specify the conditioning value for IM_j.

The development of a conditional distribution for a ground motion parameter can proceed in one of two ways. The first approach is similar to that used in the development of the conditional mean spectrum. Deaggregation of the seismic hazard that led to the value of the conditioning parameter, IM_j, is used to identify the mean magnitude and mean rupture distance. Next, the mean rupture scenario is used as input into the ground motion prediction equations for the two ground motion parameters to yield estimates of the median values and standard deviations of IM_i and IM_j. The epsilon value of IM_j is determined using the conditioning value, the predicted median, and the predicted standard deviation of IM_j. Next, the correlation coefficient between the two ground motion parameters is used to determine the corresponding epsilon value of IM_i. The conditional distribution of IM_i is developed by updating the first mean and

standard deviation of the unconditional distribution with the epsilon value of IM_i, using

$$\mu_{lnIM_i|Rup,IM_j}(rup_k, im_j) = \mu_{lnIM_i|Rup}(rup_k) + \sigma_{lnIM_i|Rup}(rup_k)\rho_{lnIM_i,lnIM_j}\varepsilon_{lnIM_j} \quad (2.4)$$

$$\sigma_{lnIM_i|Rup,IM_j}(rup_k, im_j) = \sigma_{lnIM_i|Rup}(rup_k)\sqrt{1 - \rho^2_{lnIM_i,lnIM_j}} \quad (2.5)$$

where $\mu_{lnIM_i|Rup,IM_j}$ and $\sigma_{lnIM_i|Rup,IM_j}$ are the conditional mean and standard deviation of $\ln IM_i$, $\mu_{lnIM_i|Rup}$ and $\sigma_{lnIM_i|Rup}$ are the unconditional mean and standard deviation of $\ln IM_i$, $\rho_{lnIM_i,lnIM_j}$ is the correlation coefficient between $\ln IM_i$ and $\ln IM_j$, and ε_{lnIM_j} is the epsilon value of $\ln IM_j$.

There is also a more rigorous approach to determine the conditional probability distribution of a ground motion parameter that considers all magnitude and rupture distance combinations that contribute to the seismic hazard. Here, a conditional distribution of IM_i is determined for each rupture scenario and each conditional distribution is weighted by its probability of occurrence, derived from the hazard deaggregation. An example conditional distribution for a site in Christchurch, NZ is shown in Figure 2.12. The GCIM distribution for spectral acceleration at 0.5 s is derived by conditioning on a spectral acceleration at 1 s, Sa (1.0), equal to 0.165 g. The value of the conditioning variable was selected from the hazard curve at 2% probability of exceedance in 50 years. The unconditional distribution for spectral acceleration at 0.5 s is shown in Figure 2.12 as well. Note that the conditional distribution results in larger values of Sa(0.5 s) than the unconditional distribution because the

conditional distribution accounts for epsilon, while the unconditional distribution assumes an epsilon of 0.0 (i.e., median ground motions).

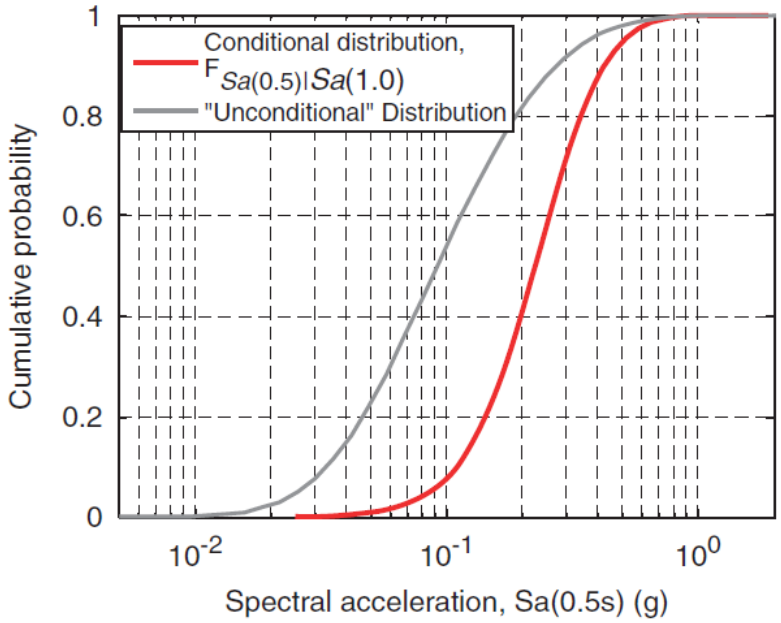

Figure 2.12 Conditional distribution of spectral acceleration at a period of 0.5 s, Sa(0.5), given that the spectral acceleration at 1.0 second, Sa(1.0), equals 0.165 g for a site in Christchurch, NZ. The unconditional distribution of Sa(0.5) is shown as well (Bradley 2010).

The GCIM selection algorithm develops a suite of ground motions that is consistent with the conditional distribution of the ground motion parameter of interest. The conditional distribution is simulated such that the continuous distribution is separated into N values of IM_i, where N is the number of motions to be selected.

Recall that the distribution for the intensity measure of interest, IM_i, is conditional on the occurrence of a specific value of another intensity measure, IM_j. An important feature of the GCIM selection algorithm is the scaling of all

records in the database to have the required value of IM_j. Thus, in the GCIM selection algorithm the scale factor for each record is known a priori (it must result in the required value of IM_j) and needs to be computed only once. For each value of IM_i in the simulated conditional distribution, a scaled motion is identified that most closely matches this value.

The empirical intensity measure distribution of a ground motion suite can be evaluated using the Kolmogorov-Smirnov (K-S) goodness-of-fit test. The K-S test statistic, D, quantifies the absolute value of the maximum difference between the continuous theoretical distribution and the empirical distribution of the suite (Ang and Tang 2007, 293-296). Once a desired confidence level, α, is chosen, a critical value of the K-S test statistic, D_α, can be defined. If the K-S test statistic is larger than the critical value then we can say that the empirical distribution is not representative of the theoretical distribution. If D_α is chosen such that the probability that D is greater than D_α is equal to α, then a band with a width equal to D_α developed around the empirical distribution will contain the theoretical distribution with probability 1-α.

The K-S test can be used for simple graphical evaluation as well. Given a particular confidence level, K-S bounds can be developed and plotted alongside the theoretical distribution. If the empirical distribution falls within the K-S bounds we can say that the empirical suite appropriately represents the theoretical distribution. However, if the empirical distribution falls outside the K-S bounds it is not representative of the theoretical distribution.

Bradley (2012) provided an example in which ground motions were selected to fit the conditional distribution for peak ground velocity (PGV). The

peak ground velocity distribution of the selected suite of motions is shown alongside the GCIM distribution for PGV in Figure 2.13. In this example, spectral acceleration at a period of 3 s, Sa(3.0), was chosen as the conditioning variable. Sa(3.0) was set equal to 0.0827 g, the value determined through PSHA to have a 10% probability of exceedance in 50 years. As the distribution of the suite falls within the Kolmogorov-Smirnov (KS) bounds, it can be said that the suite, comprised of 50 ground motions, adequately approximates the target distribution.

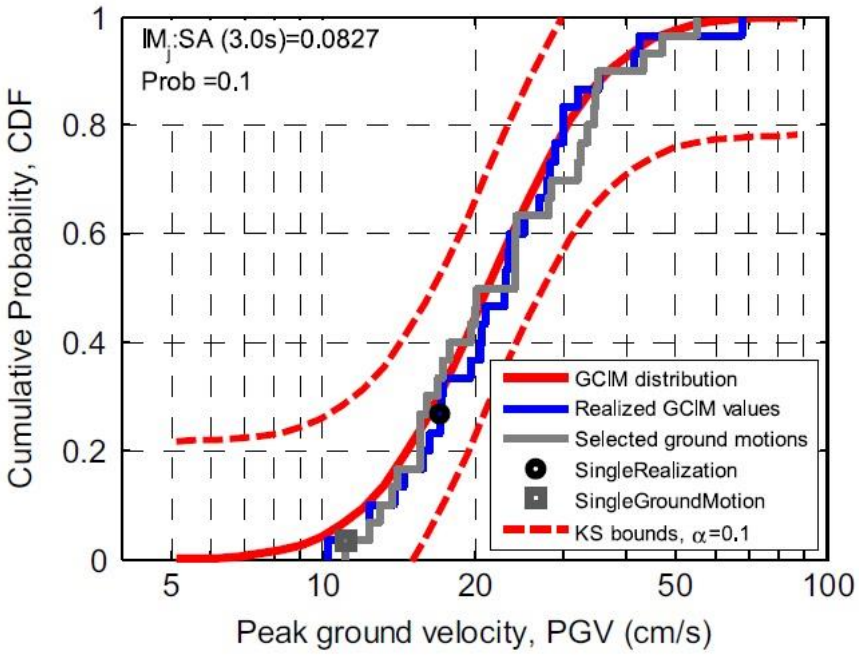

Figure 2.13 Ground motion selection with the GCIM algorithm. The peak ground velocity values for selected ground motions are shown alongside the GCIM distribution. Adapted from Bradley (2012).

In the GCIM selection approach a suite of ground motions is developed using random realizations of the conditional distribution. Therefore, if the

selection process is repeated, the random realization values, and thus the selected ground motion suite, will change. For suites comprised of a small number of ground motions, such as seven or ten, the variability between different suites may be unacceptable. To evaluate the fit of one suite compared to the fit of another, an overall residual between the target conditional distribution and the suite's distribution can be calculated. Once again, the optimal suite is the one which minimizes the residual.

2.5 GROUND MOTION SIMULATION

Recorded ground motions provide the basic underlying data in earthquake engineering and are critical to rational seismic hazard analysis and seismic design. Although the number of earthquake recordings continues to grow, there is still a limited number of records available for design level events ($M_W > 7.0$, $R < 15$ km) and these are the events of most interest for seismic design. Seismological ground motion simulations can be used to supplement recorded acceleration-time histories. This is especially useful in regions with sparse numbers of records (e.g., eastern North America).

Simulated acceleration-time histories are becoming increasingly prominent in engineering seismology. The past few decades have seen significant advancements in the ability to model earthquake ground motion. Simulated ground motions are typically generated through one of three approaches: stochastic simulation, deterministic simulation, or hybrid deterministic simulation.

The stochastic method is based upon the work presented in Hanks and McGuire (1981). In this study, seismological models of Fourier amplitude spectra

(FAS) were combined with random vibration techniques to simulate PGA and spectral accelerations. Expanding upon the work of Hanks and McGuire (1981), Boore (1983) generated acceleration-time histories using a seismological model for FAS coupled with random phase angles and a time duration enveloping function. Motions developed using this approach are commonly called stochastically simulated motions. Stochastic methods are most useful for generating ground motion at high frequencies (i.e., frequencies exceeding about 1 Hz) (Boore 2003). In stochastic methods the source can be modeled as a point or as a finite fault (Boore 1983 and Hartzell 1978). Figure 2.14a presents a schematic of the stochastic simulation method for a finite fault model. In this case FAS at a site are generated for each point on the fault plane, transformed into the time domain, and then the time series are combined based on the rupture's progression.

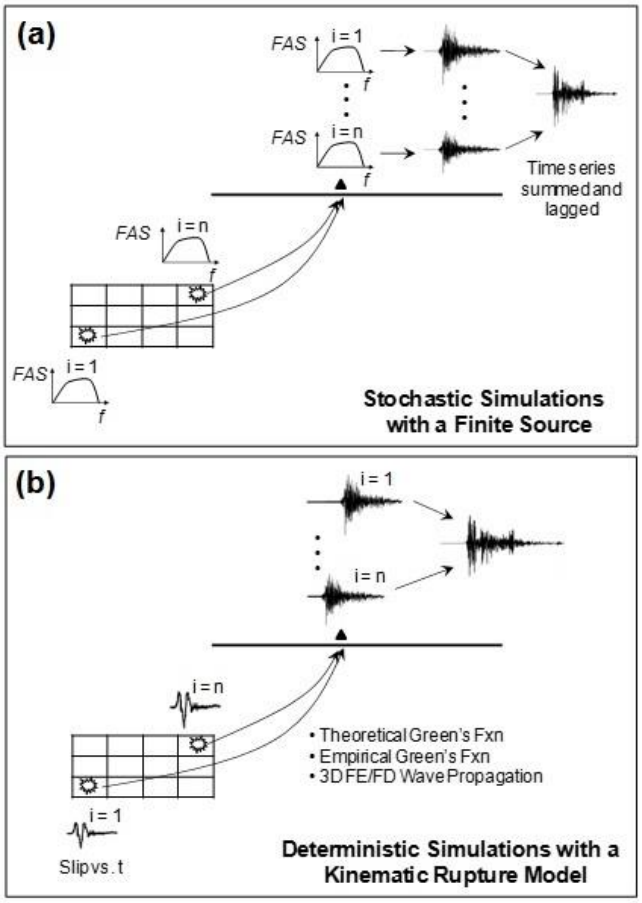

Figure 2.14 Ground motion simulation schematic for (a) stochastic simulations with a finite source, and (b) deterministic simulations with a kinematic rupture model (Rathje, personal communication).

Deterministic methods are more complex than stochastic methods and are often used to generate ground motion at lower frequencies. The schematic presented in Figure 2.14b illustrates the deterministic simulation method. A kinematic model is used to describe the fault rupture and the variation of slip in time and space. Body waves are propagated to a site using Green's functions (e.g., Hartzell and Heaton 1983) or a finite element model of the regional 3D velocity structure (e.g., Graves 1996). The deterministic methods do not

accurately model high frequencies because they cannot discretize the 3D velocity structure into small enough elements due to computational constraints. In recent years, hybrid deterministic models have been proposed to combine the strengths of the stochastic model with those of the deterministic model (Graves and Pitarka 2004). Hybrid models use time series simulated via the stochastic method at high frequencies and time series simulated via the deterministic method at low frequencies.

The intricacies of seismological models are beyond the scope of this thesis. However, as this study will evaluate four simulation models in the context of seismic slope stability the four models will be briefly presented and emphasis will be placed on the differences between the models. The four models that will be considered are CSM, EXSIM, GP, and SDSU. These models are part of the Broadband Platform (BBP) Ground Motion Simulation Verification (GMSV) project (http://collaborate.scec.org/gmsv/Main_Page).

The first model considered in this study is the Composite Source Model (CSM) that was first described by Zeng et al. (1994). The CSM is a deterministic model that generates acceleration-time histories by convolution with synthetic Green's functions. The CSM uses a kinematic rupture model and assumes that the rupture that occurs during a large earthquake can be described as the superposition of ruptures from smaller subevents. The number and size of the subevent ruptures are determined using the Guttenberg and Richter frequency-magnitude relationship and are randomly distributed across the fault plane, allowing overlap. The ground motion at a particular site is determined by

propagating the waves through a layered crustal model or through a 3D finite difference model.

EXSIM is a stochastic finite-fault simulation model developed by Motazedian and Atkinson (2005). The model is based upon the work of Boore (1983, 2003). EXSIM simulates 1D ground motion by breaking the fault plane into sub-faults. Ruptures occurring at each sub-fault are treated as point sources. The method utilized by EXSIM to simulate ground motion at a subsource is shown in Figure 2.15. First, white noise is generated (Figure 2.15a) and then windowed (Figure 2.15). The windowed time series is transformed to the frequency domain (Figure 2.15c) and then normalized to 1.0 (Figure 2.15d). Next, the model FAS is determined (Figure 2.15e) and the normalized FAS of the random time series is multiplied by the model FAS (Figure 2.15f). Finally, an inverse Fourier transform is used to develop the acceleration-time history for the subsource (Figure 2.15g). The time series of individual subsources are properly delayed and summed in the time domain to develop the final acceleration-time history.

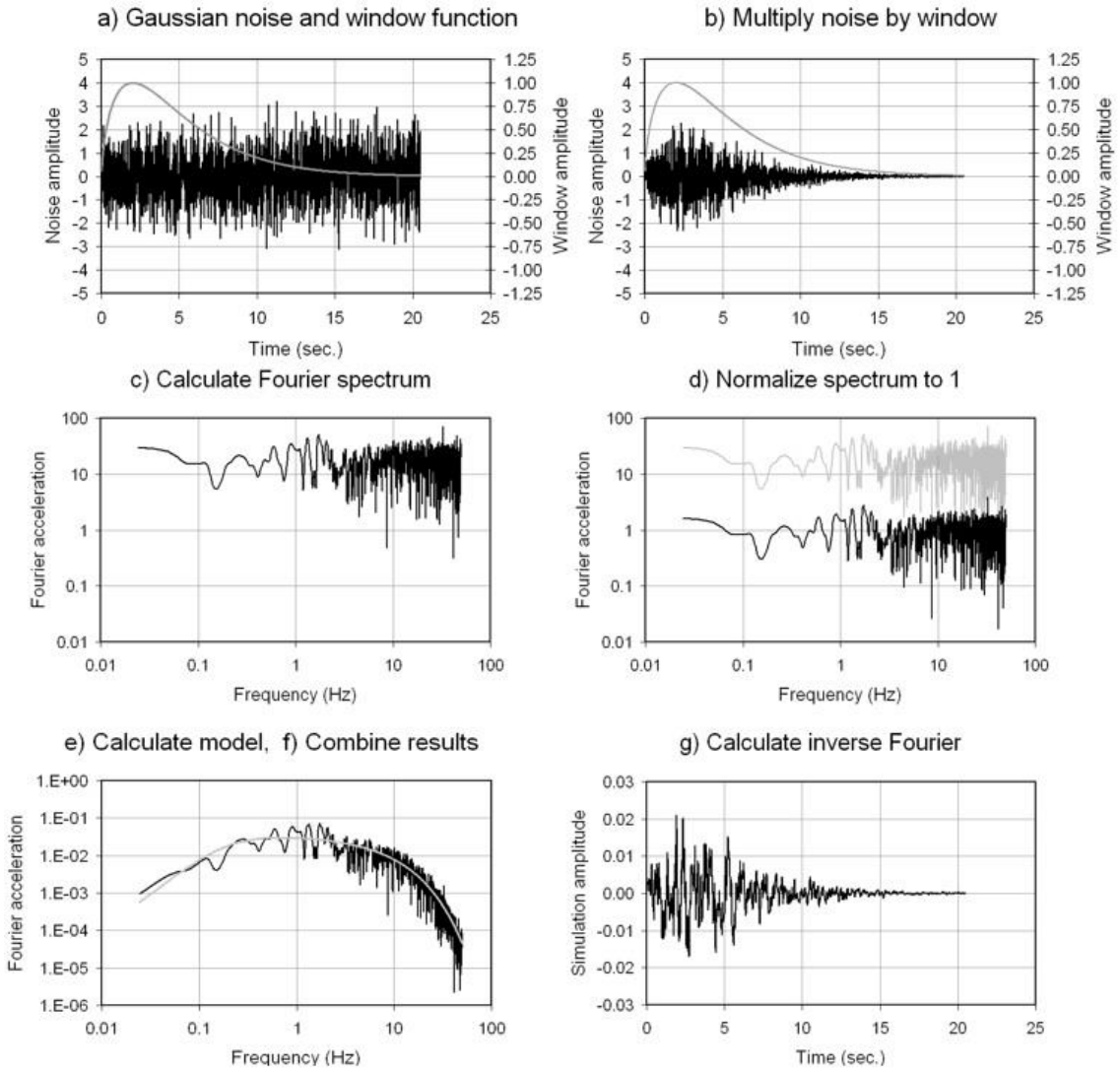

Figure 2.15 The stochastic approach used to simulate acceleration-time histories in the EXSIM model (Atkinson and Assatourians 2013).

The final two models considered, GP and SDSU, are finite-fault, hybrid deterministic models. The GP model was developed by Graves and Pitarka (2010). At low frequencies (f < 1 Hz) the GP model uses a complete kinematic representation of a heterogeneous rupture on a finite fault. Then waves are

propagated to the site using theoretical Green's functions computed for a plane-layered structure or a 3D velocity structure. At high frequencies the kinematic representation of the fault is limited and must be supplemented by stochastic methods. High frequency waves are propagated to the site with simplified 1D Green's functions.

The San Diego State University (SDSU) model was developed by Mai et al. (2010). The SDSU model assumes that the high frequency component of ground motion can be modeled as scattering from random media. Ground motion is simulated in the SDSU model through a three-stage approach. First, low frequency simulations are developed for a finite-fault rupture embedded in a 3D Earth model. Next, the high frequency scatterings are generated using path-average scattering properties and local site conditions. Site-specific Green's functions are convolved with a source-time function that describes how the rupture process varies with time. Finally, the high frequency and low frequency simulations are combined in the frequency domain.

2.6 SUMMARY

To assess the seismic stability of slopes, engineers often compute permanent displacements. Seismic sliding block displacements can be computed directly using acceleration-time history records or estimated using prediction equations requiring ground motion parameters to characterize the seismic loading. Permanent displacements provide an index as to the severity of the consequences of earthquake-induced ground shaking.

In seismically active regions, the design of new slopes and the assessment of existing slopes requires characterization of the seismic hazards. An

appropriate target acceleration response spectrum or conditional ground motion parameter distribution can be developed to represent the seismic hazard. Then, a suite of representative acceleration-time histories can be selected to fit the target via a ground motion selection algorithm. The permanent displacement associated with each record in the suite can be computed and seismic sliding block displacement may be estimated as the median of the suite.

One main objective of seismological modeling is to generate synthetic acceleration-time histories that can supplement the database of recorded ground motions. Over the years, many models of varying complexity have emerged and can be grouped into three main categories: stochastic models, deterministic models, and hybrid deterministic models. This chapter briefly introduced the four ground motion simulation models that will be considered in this study.

Chapter 3. The Effect of Ground Motion Selection on Sliding Displacement

3.1 INTRODUCTION

This chapter investigates the influence of ground motion selection on computed seismic sliding block displacements. The objective here is to gain insight into how and why ground motion suites developed through different selection methods result in different estimates of permanent displacements in slopes subjected to earthquake induced ground shaking.

First, this chapter introduces the ground motion suites developed for consideration in this study and evaluates the suites in terms of their distributions of relevant ground motion parameters. Then the rigid sliding block displacements computed for the ground motion suites are presented and compared.

3.2 SITE SELECTION

This study assesses seismic slope stability by calculating rigid sliding block displacements. The ratio of the slope's yield acceleration value to peak ground acceleration (k_y/PGA) provides a direct indication of whether failure occurs. If at some point during the earthquake loading k_y/PGA is less than 1.0, an unbalanced force disrupts equilibrium and movement occurs. Because PGA is a very important parameter in slope stability analyses, a probabilistically derived value of PGA was chosen to underlie the ground motion selection performed for this study. All of the targets and selected ground motions presented in this chapter were based on a PGA value with a 2% probability of exceedance in 50 years.

Slope stability is evaluated for two sites: one in Los Angeles, California (118.242°W, 34.052°N) and another in San Jose, California (121.890°W, 37.340°N). In Los Angeles, the PGA with a 2% PE in 50 years is 0.9n g. In San Jose the PGA with a 2% PE in 50 years is 0.7 g. These two sites were chosen because of differences in their seismic hazard deaggregation. The distribution of magnitudes and distances for PGA with a 2% probability of exceedance (PE) in 50 years is shown for Los Angeles in Figure 3.1 and San Jose in Figure 3.2. The hazard in Los Angeles is dominated by a single earthquake scenario, while the hazard in San Jose is influence by two distinct scenarios.

The modal rupture scenario for Los Angeles (Figure 3.1) is an earthquake magnitude of 6.4 and a source-to-site rupture distance of about 5 km. This scenario contributes 49.5% of the seismic hazard at the site. In fact, 91% of the hazard is contributed by earthquake events with a magnitude between 6 and 7 and a rupture distance between 4.4 and 6 km. Due to the concentration of hazard along one fault, the mean and modal rupture scenarios are quite similar. In Los Angeles the mean rupture scenario is a magnitude 6.46 event located 5.2 km from the site.

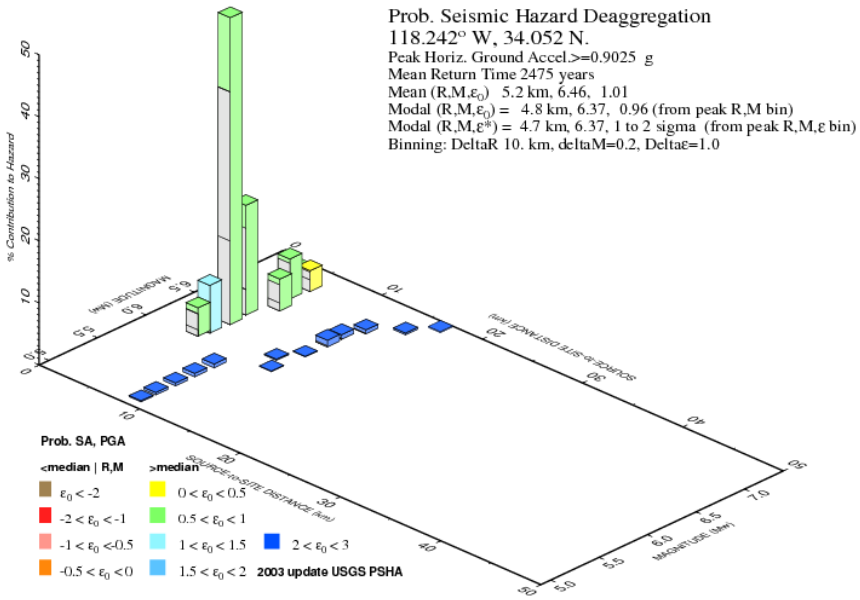

Figure 3.1 PSHA deaggregation for Los Angeles, CA, given exceedance of the PGA with a 2% PE in 50 years (USGS Custom Mapping and Analysis Tools, http://geohazards.usgs.gov/deaggint/2002/).

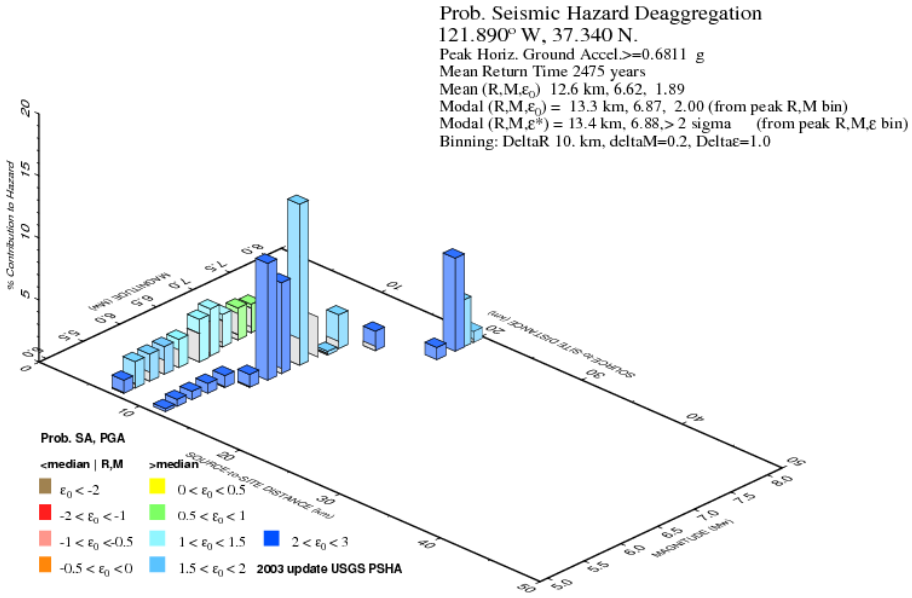

Figure 3.2 PSHA Deaggregation for San Jose, CA, given exceedance of the PGA with a 2% PE in 50 years (USGS Custom Mapping and Analysis Tools, http://geohazards.usgs.gov/deaggint/2002/).

The deaggregation for San Jose is not dominated by a single earthquake scenario (Figure 3.2), but rather by two main scenarios. The modal rupture scenario, a 6.87 magnitude earthquake located 13.3 km from the site, contributes 22.5% of the seismic hazard in San Jose and scenarios with magnitudes 6 to 7 and distances 13 to 14 km contributed 52% of the hazard. However, a meaningful contribution (13%) of the hazard comes from larger magnitudes of 7.5 to 8.0 at distances around 20 km.

Conditional probability distributions for ground motion parameters can be developed using a mean rupture scenarios, as found through seismic hazard deaggregation, or the full set of deaggregation data. The deaggregation data for Los Angeles and San Jose provide a means to evaluate the significance of the difference between the two approaches.

3.3 Development of Target Acceleration Response Spectra

Two acceleration response spectra are considered as targets for ground motion selection in this study: the uniform hazard spectrum (UHS) and the conditional mean spectrum (CMS). The UHS with a 2% probability of exceedance (PE) in 50 years is shown for Los Angeles in Figure 3.3a and for San Jose in Figure 3.3b. The UHS were derived using the U.S. Geological Survey hazard application (USGS 2008).

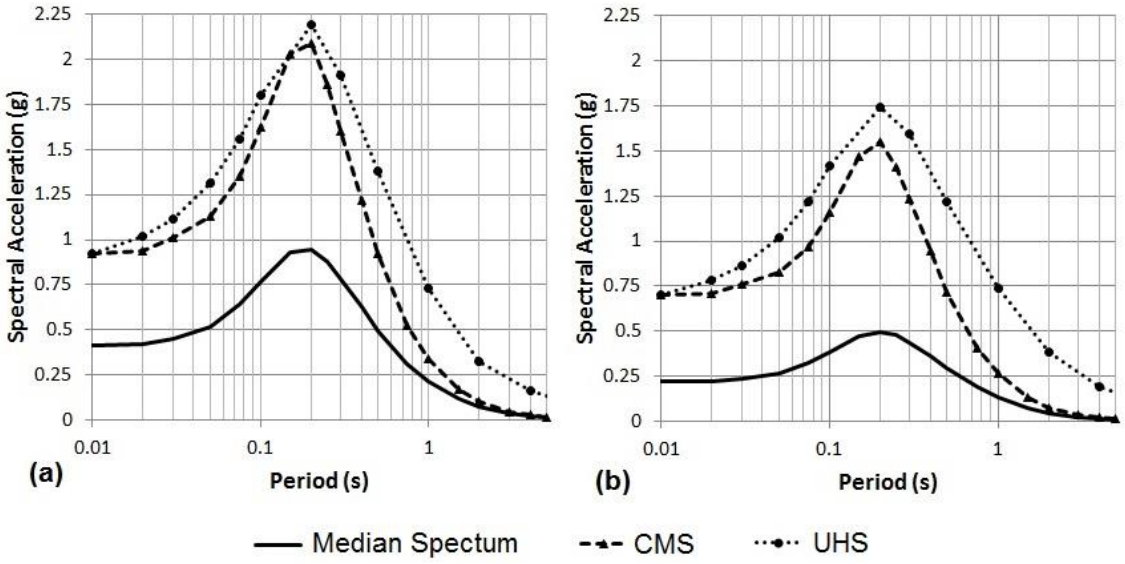

Figure 3.3 UHS with 2% PE in 50 yrs., CMS (conditional on 2% PE in 50 yrs. PGA), and predicted median spectra for (a) Los Angeles and (b) San Jose.

Figure 3.3 also shows the predicted median spectra for the two sites. The median spectra were developed using the Abrahamson and Silva (2008) Next Generation Attenuation (NGA) ground motion prediction equation (GMPE). The mean rupture scenario determined via seismic hazard deaggregation was used as input into the GMPE. For simplicity, a strike-slip fault mechanism was assumed for both sites. The shear wave velocity in the top 30 meters below the ground surface was taken as 760 m/s, such that each site could be classified as Seismic Site Class B (i.e., soft rock). Note that the UHS falls significantly above the median response spectrum for both sites.

The CMS shown in Figure 3.3 are conditioned on the PGA value with a 2% PE in 50 years. For spectral periods close to zero the UHS and CMS are similar because the CMS was conditioned on PGA from the UHS. Figure 3.3 shows that

the difference between the UHS and the CMS increases for longer periods. This is because the correlation coefficient between spectral accelerations at different periods tends to decrease as the spacing between the periods increases. As a result, at longer periods the CMS approaches the median spectrum.

3.4 Development of GCIM Distributions for Relevant Ground Motion Parameters

GCIM distributions were developed for ground motion parameters that influence sliding displacements. As noted in Chapter 2, PGA, PGV, and Arias Intensity (Ia) are important parameters that affect sliding displacement. By developing probability distributions of PGV and Ia that are conditioned on a PGA value derived from PSHA, we can establish ground motion selection targets that explicitly consider the parameters deemed relevant to seismic slope stability.

The conditioning values of PGA are the same as those discussed for the CMS. To develop the GCIM distributions for PGV and Ia, the Abrahamson and Silva (2008) GMPE was used for PGA and PGV, and the Travasarou et al. (2003) GMPE for Ia. Correlation coefficients between the ground motion parameters were taken from Rathje and Saygili (2008). The correlation coefficient between PGA and PGV is taken as 0.68 and between PGA and Ia is taken as 0.83.

The conditional intensity measure distributions for Los Angeles and San Jose are shown in Figure 3.4 and Figure 3.5, respectively. Each figure displays three functions: an unconditional distribution, a conditional distribution developed using a single magnitude and distance, and a conditional distribution developed through the more rigorous approach that considers all magnitude and distance scenarios that contribute to the seismic hazard. The unconditional

distribution ignores the correlation between intensity measures; it is developed using the unconditional mean and standard deviation.

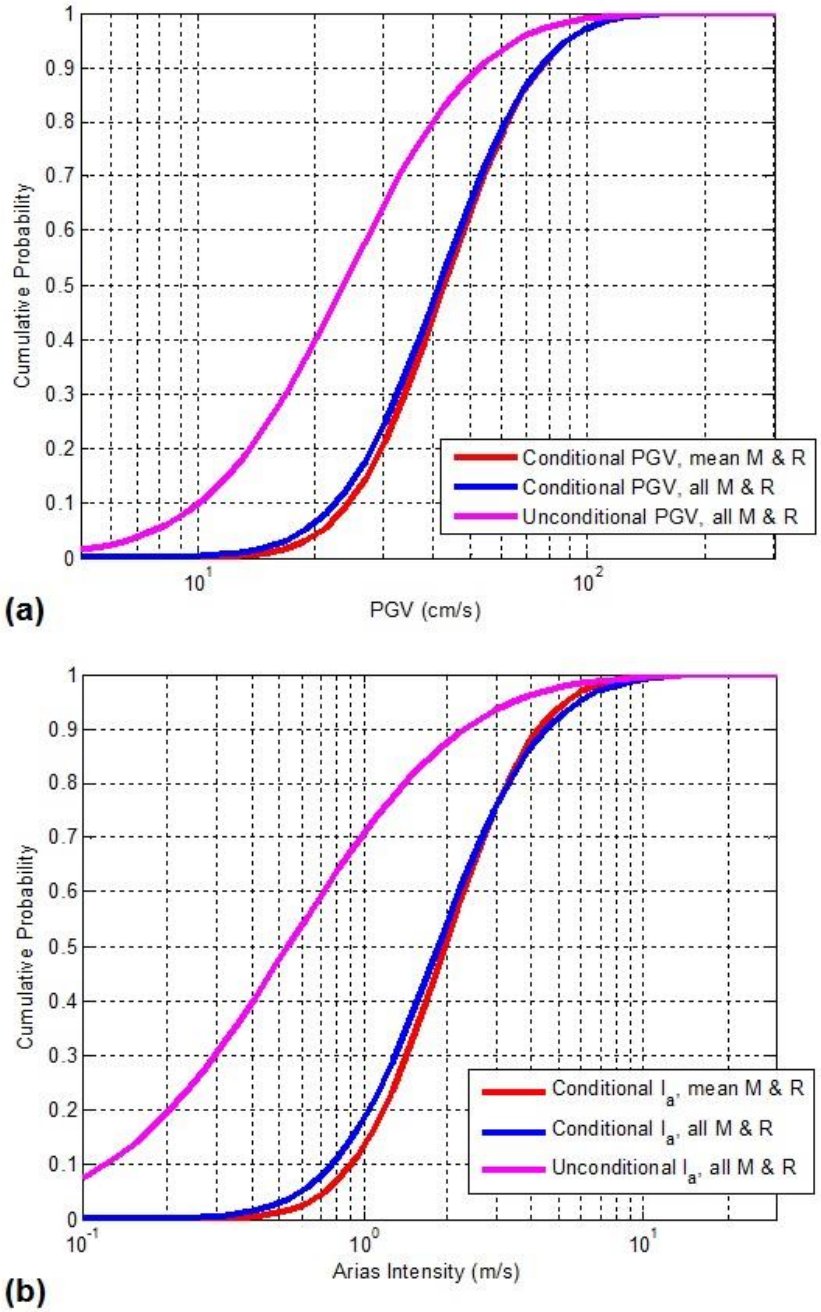

Figure 3.4 Cumulative distribution functions for (a) PGV and (b) Ia for Los Angeles, conditional on a PGA value of 0.9 g.

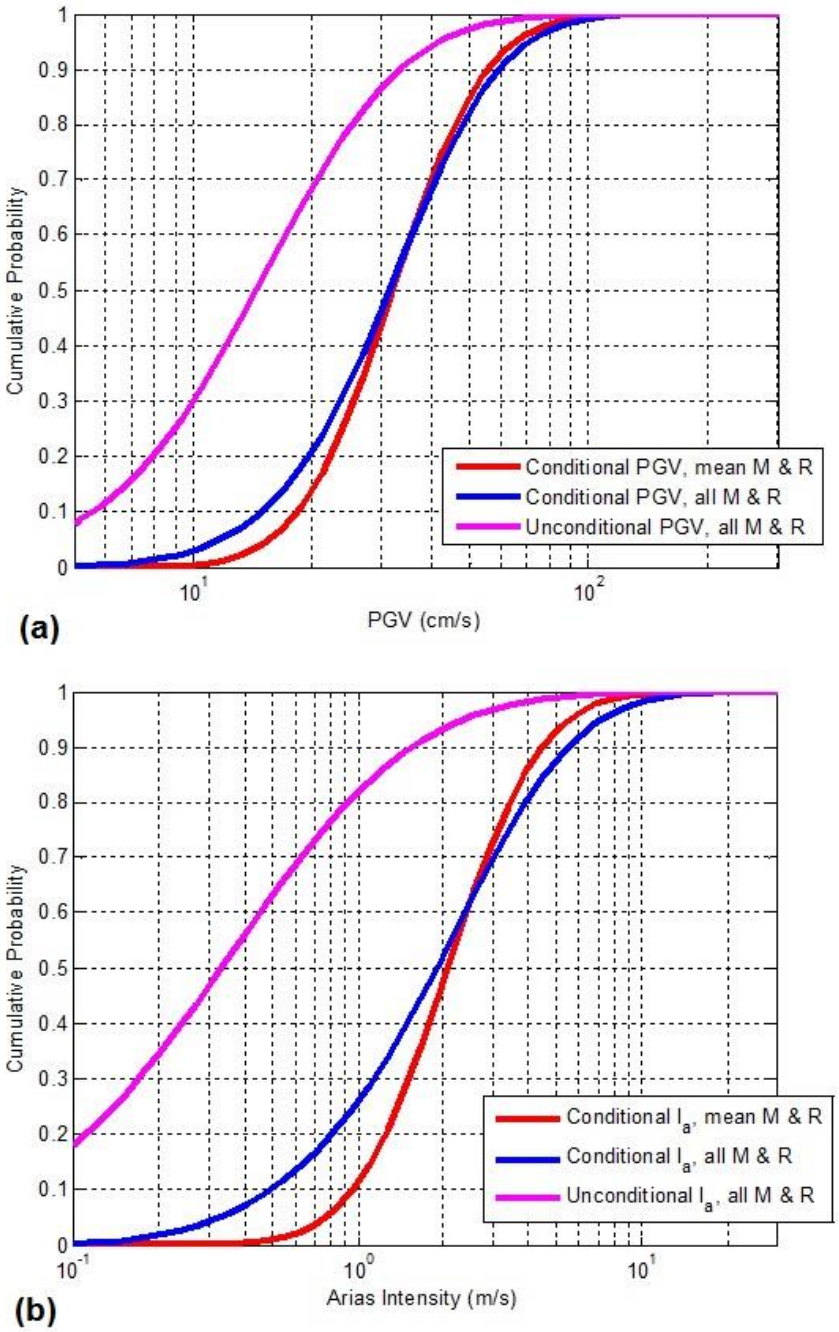

Figure 3.5 Cumulative distribution functions for (a) PGV and (b) Ia for San Jose, conditional on a PGA value of 0.7 g.

Several observations can be made through inspection of Figure 3.4 and Figure 3.5. First, the difference between the unconditional and conditional distributions is greater for Ia than PGV. This is because the standard deviation for Ia is significantly larger than for PGV (e.g. 0.60 for Ia in Los Angeles v. 0.44 for PGV in Los Angeles).

Second, the conditional distributions developed through the two approaches tend to be more similar for Los Angeles than for San Jose. This difference is most pronounced in comparing the Ia distributions for Los Angeles in Figure 3.4b with those for San Jose in Figure 3.5b. The difference can be explained considering the deaggregation plots in Figure 3.1 and Figure 3.2.

In Los Angeles the seismic hazard is dominated by one main event (magnitude ~ 6-6.5, distance ~ 5 km) and thus, the more rigorous approach for developing a conditional distribution provides little information beyond the approach that uses a single scenario. For San Jose the conditional distribution for Ia developed considering all possible rupture scenarios is broader than that of the distribution developed considering only the mean rupture scenario. This differences is a result of the seismic hazard at San Jose including non-trivial contributions from magnitudes both smaller and larger than the mean magnitude (Figure 3.2).

3.5 SELECTED GROUND MOTION SUITES

In this study, suites comprised of ten acceleration-time history records are considered. The suites selected using the various approaches are described below.

3.5.1 Ground Motion Suites Developed by the PGMD

The PGMD was used to develop suites of ground motions to fit the UHS and CMS for Los Angeles and San Jose. The search criteria used here were: earthquakes with a magnitude greater than 6.0, a source-to-site rupture distance less than 50 km, and a V_{S30} greater than 600 m/s. Spectral periods between 0.01 s and 5.0 s are considered and a uniform distribution between those bounds is used as the weighting function for spectral period.

The PGMD web application was used to select suites of ground motions to fit each of the two target acceleration response spectra at each site. The ground motions in each suite were scaled to the appropriate PGA with a 2% PE in 50 years. These PGA values are 0.9 g for ground motions selected for Los Angeles and 0.7 g for ground motions selected for San Jose. One thing to note here is that the PGMD selects ground motions using the geometric mean of the two horizontal components of ground motion recorded at a site. Thus, suites developed using the PGMD actually consist of 20 acceleration-time history records. The acceleration response spectra of the ground motion suites developed using the PGMD are shown in Figure 3.6.

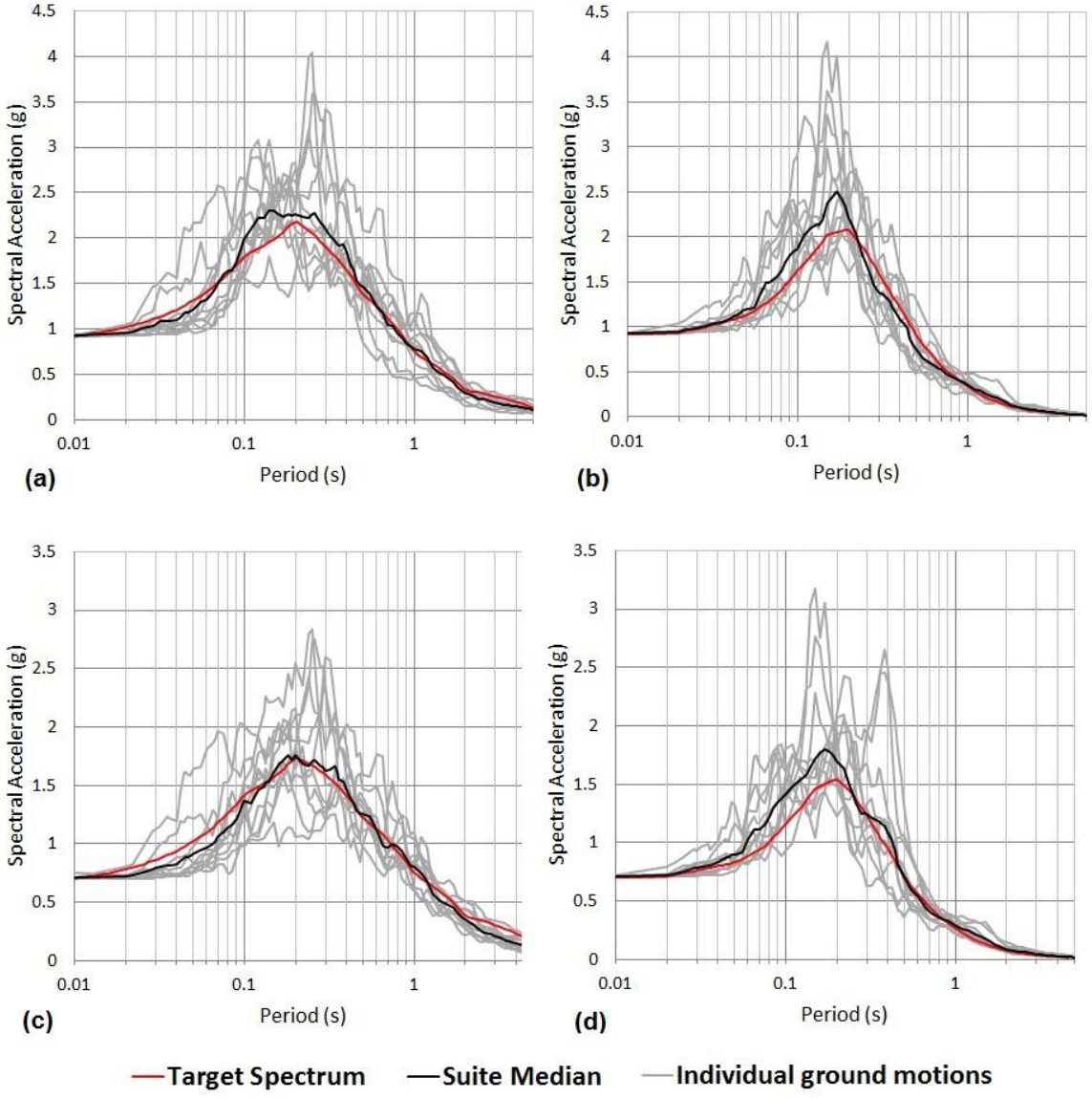

Figure 3.6 Acceleration response spectra of the ground motion suites developed by the PGMD for (a) Los Angeles UHS; (b) Los Angeles CMS; (c) San Jose UHS; (d) San Jose CMS.

Figure 3.6 shows that there are differences between the spectral shape of the median spectra and that of their respective targets. This misfit is partly due to the fact that selections were made to fit the target spectrum and then scaled to

the appropriate PGA. We see that the median spectrum of the suite shown in Figure 3.6a has a broader peak than the target Los Angeles UHS spectrum. In Figure 3.6b the peak of the median response spectrum is seen to exceed the peak of the target spectrum. Additionally, the period at which the peak spectral acceleration occurs in the median spectrum is less than that of the Los Angeles CMS. The same can be said for the ground motion suite developed to fit the San Jose CMS, shown in Figure 3.6d. At intermediate periods the median spectrum shown in Figure 3.6c approximates the San Jose UHS spectrum quite well. However, at short and long periods the median spectrum exceeds the target spectrum. For more details about the ground motion suites see Table A-1 through Table A-4 in Appendix A.

The intensity measure distributions for PGV and Ia of the suites selected to fit the Los Angeles acceleration response spectra are shown in Figure 3.7. Note that these distributions were not considered in the selection of the time histories, but it is important to consider the distribution of these ground motion parameters for the suites selected. The K-S bounds shown in Figure 3.7 were developed for α=0.05, as are the rest of the K-S bounds to be presented in this thesis. Inspection of Figure 3.7 reveals that the suite developed to fit the Los Angeles UHS has distributions for both PGV (Figure 3.7a) and Ia (Figure 3.7b) that far exceed the target conditional distributions of those parameters and fall far to the right of the upper K-S bound. The suite developed by the PGMD to fit the Los Angeles CMS, however, has PGV and Ia distributions that more closely resemble the theoretical conditional distributions. The PGV distribution of the Los Angeles CMS suite (Figure 3.7c) lies almost completely within the K-S

bounds, while the Ia distribution of the CMS suite (Figure 3.7d) improves upon that of the UHS suite, but still exceeds the upper K-S bound. The agreement between the theoretical conditional PGV distribution and the PGV distribution of the CMS suite is due to the fact that PGV is strongly related to spectral accelerations in the range of 0.5 to 1.0 s, and thus fitting an appropriate CMS results in an appropriate PGV distribution. The Ia distribution of the CMS suite does not fit the theoretical conditional distribution well because Ia is influenced by ground motion characteristics (e.g., duration) that are not captured by the response spectrum.

Similar observations can be made about Figure 3.8, which portrays the PGV and Ia distributions of the suites developed to fit the San Jose target response spectra. Once again, the distributions of the UHS suite, shown in Figure 3.8a and Figure 3.8b, fall outside the upper K-S bounds. The distributions of the CMS suite more closely fit the theoretical distributions. The PGV distribution of the San Jose CMS suite is almost completely contained within the K-S bounds. Compared to the Los Angeles CMS suite, the Ia distribution of the San Jose CMS suite is closer to the theoretical distribution.

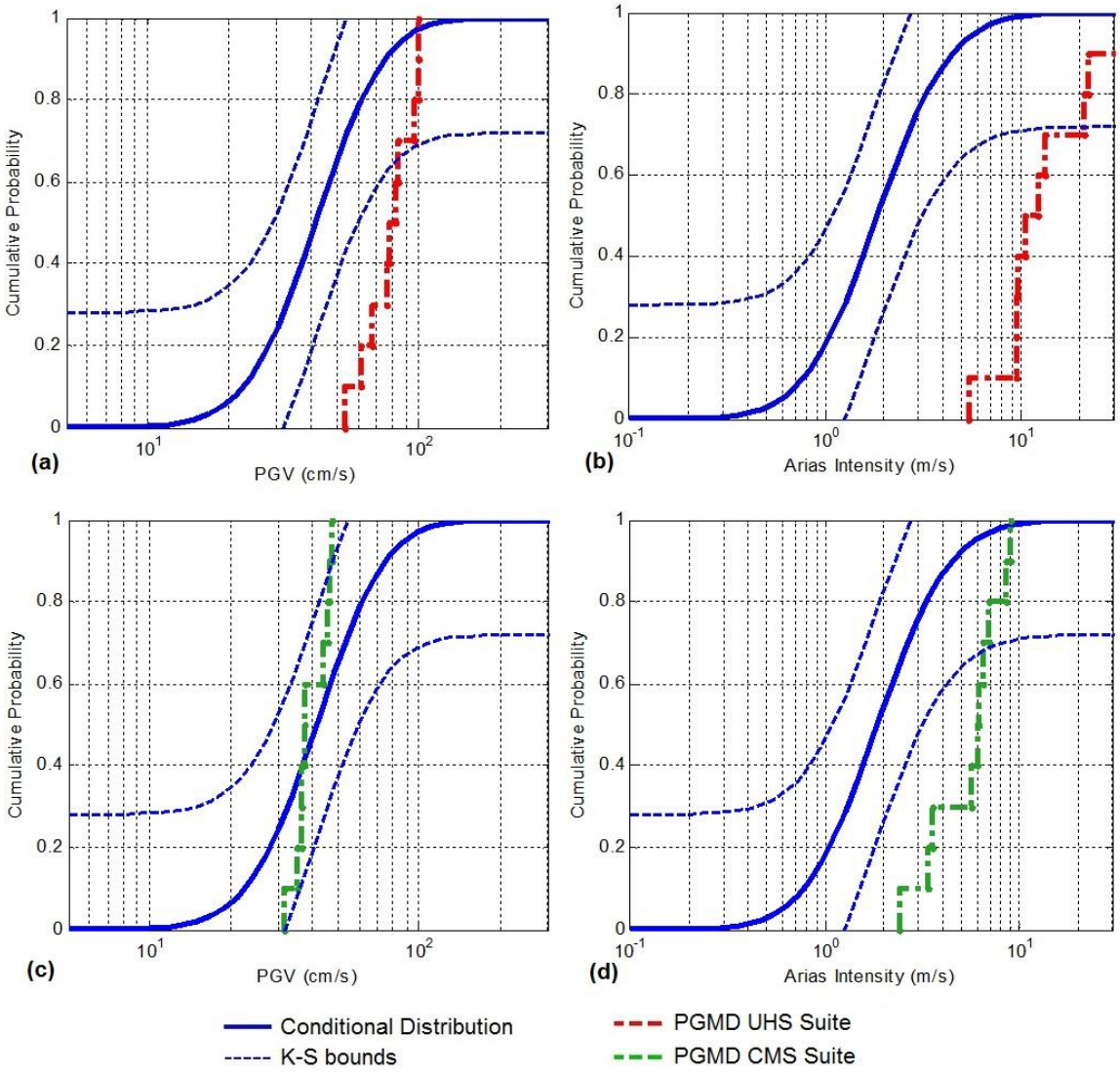

Figure 3.7 Intensity measure distributions of the suites selected by the PGMD to fit Los Angeles acceleration response spectra. K-S bounds are shown for α=0.05. Shown above are: (a) the PGV distribution of UHS suite; (b) the Ia distribution of UHS suite; (c) the PGV distribution for CMS suite; (d) the Ia distribution for CMS suite.

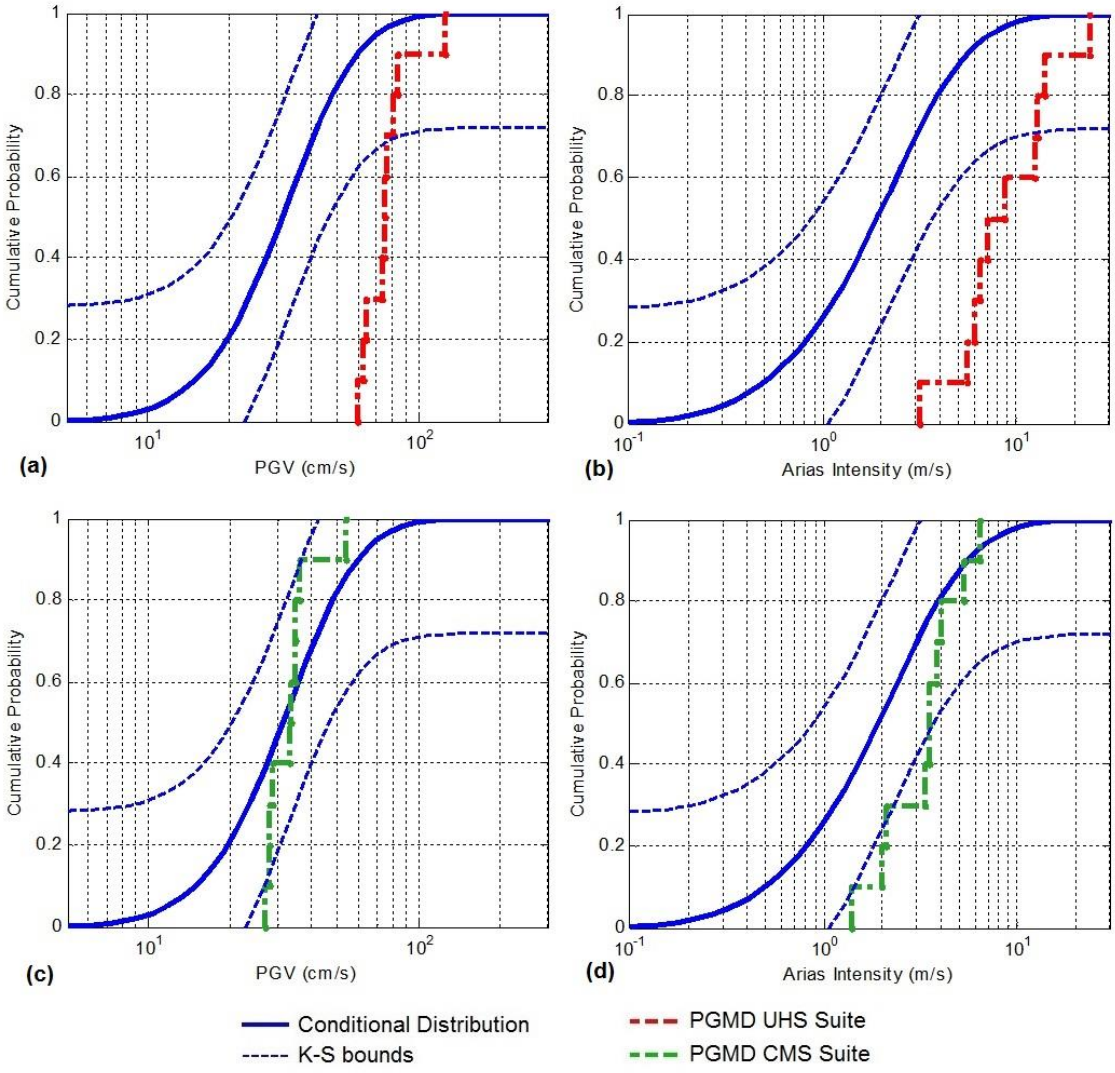

Figure 3.8 Intensity measure distributions of the suites selected by the PGMD to fit San Jose acceleration response spectra. K-S bounds are shown for α=0.05. Shown above are: (a) PGV distribution of UHS suite; (b) Ia distribution of UHS suite; (c) PGV distribution for CMS suite; (d) Ia distribution for CMS suite.

3.5.2 Ground Motion Suites Developed by SigmaSpectra

SigmaSpectra was used to develop suites of ground motions to fit the target acceleration response spectra. The search criteria used to select an appropriate catalog of motions are the same as those used in the PGMD: earthquakes with a magnitude greater than 6.0, a source-to-site rupture distance less than 50 km, and a V_{S30} greater than 600 m/s. The final catalog used for this study consists of 52 ground motions. Table A-5 in Appendix A provides more information about the individual ground motions that compose the catalog. Figure 3.9 shows the distribution of the motions in the SigmaSpectra catalog in terms of magnitude and source-to-site rupture distance.

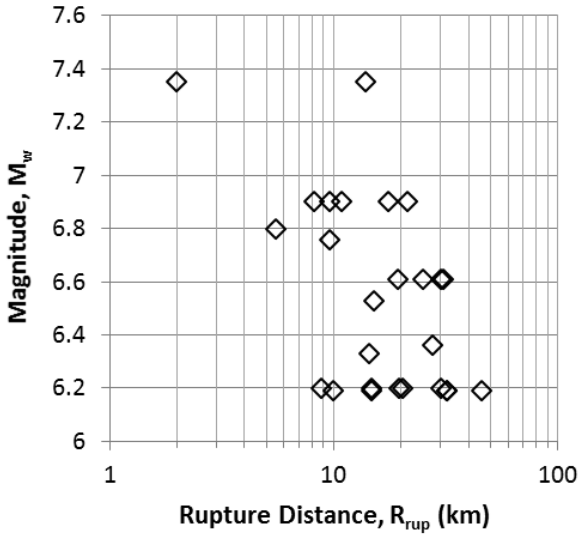

Figure 3.9 Distribution of the SigmaSpectra ground motion catalog in terms of earthquake magnitude, M_w, and rupture distance, R_{rup}.

SigmaSpectra was used to develop suites of ground motions to fit the target acceleration response spectra for Los Angeles and San Jose. Then the motions comprising each suite were scaled to the appropriate PGA value. The

acceleration response spectra of the ground motion suites developed using SigmaSpectra are shown in Figure 3.10.

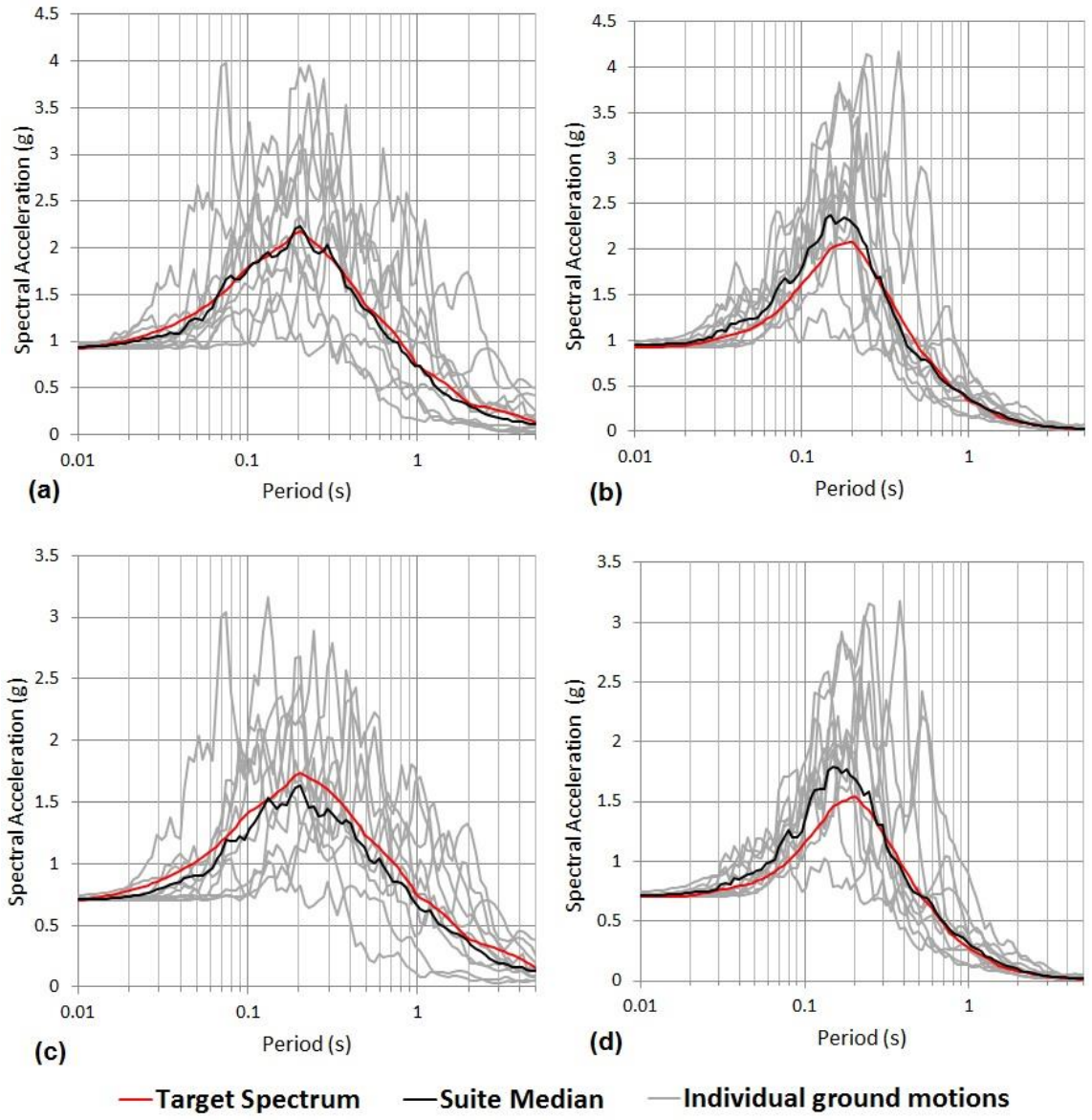

Figure 3.10 Acceleration response spectra of the ground motion suites developed using SigmaSpectra for (a) Los Angeles UHS; (b) Los Angeles CMS; (c) San Jose UHS; (d) San Jose CMS.

Once again, differences between the spectral shape of the median spectra and that of the target spectra can be seen for the suites developed by SigmaSpectra. The ground motion suite developed to fit the Los Angeles UHS, shown in Figure 3.10a, fits the target very well at periods less than 1.0 s. At periods above 1.0 s, however, the median spectrum falls slightly below the target spectrum. In Figure 3.10b the peak of the median response spectrum exceeds the peak of the target spectrum. Additionally, the period at which the peak spectral acceleration occurs in the median spectrum is less than that of the Los Angeles CMS. The same can be said for the ground motion suite developed to fit the San Jose CMS, shown in Figure 3.10d. The median spectrum of the suite developed to fit the San Jose UHS, shown in Figure 3.10c, is consistently smaller than the target spectrum. Originally, the median spectrum of the suite fit the target well. However, when all motions in the suite were scaled to have a PGA equal to 0.9 g, the suites median spectrum fell below the target spectrum. For more details about the ground motions composing the SigmaSpectra suites see Table A-6 through Table A-9 in Appendix A.

The PGV and Ia distributions of the suites selected by SigmaSpectra to fit the Los Angeles target response spectra are shown in Figure 3.11. The PGV and Ia distributions of the UHS suite exceed their respective upper K-S bounds, as shown in Figure 3.11a and Figure 3.11b. In Figure 3.11c we see that the PGV distribution of the CMS suite falls within the K-S bounds. Therefore, we can say that the PGV distribution of the CMS suite appropriately represents the target conditional distribution for Los Angeles. However, the same cannot be said for

the Ia distribution of the CMS suite, which falls above the upper K-S bound in Figure 3.11d.

The PGA and Ia distributions of the suites selected by SigmaSpectra to fit the San Jose target acceleration response spectra are shown in Figure 3.12. The same conclusions that were made for the suites developed for Los Angeles can be made for the suites developed for San Jose. In Figure 3.12a and Figure 3.12b we see that the PGV and Ia distributions of the San Jose UHS suite both exceed the upper K-S bound. In Figure 3.12c we see that the PGV distribution of the San Jose CMS suite falls within the K-S bounds. However, the Ia distribution of the San Jose CMS suite exceeds the upper K-S bound.

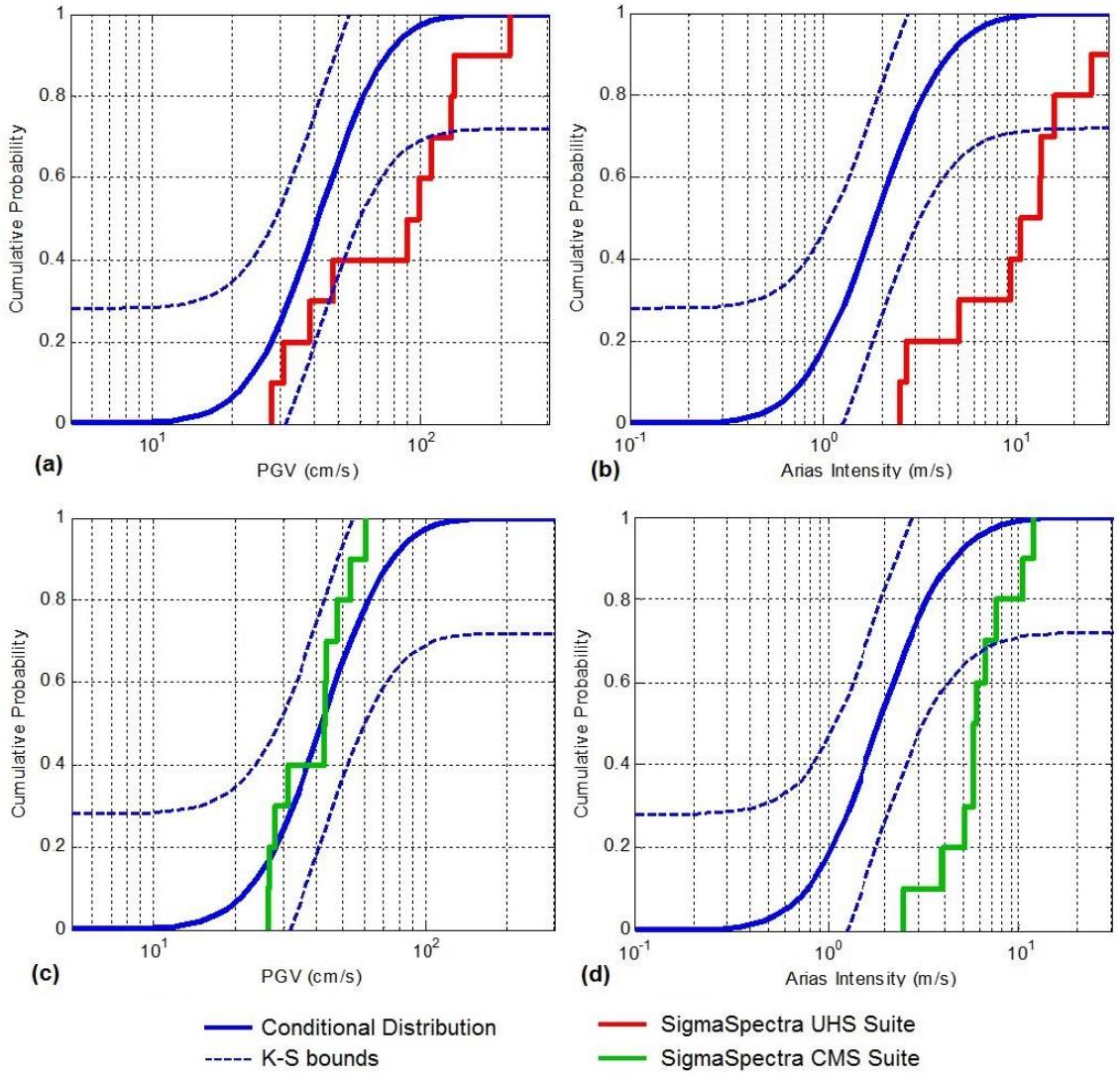

Figure 3.11 Intensity measure distributions of the suites selected by SigmaSpectra to fit Los Angeles acceleration response spectra. K-S bounds are shown for α=0.05. Shown above are: (a) PGV distribution of UHS suite; (b) Ia distribution of UHS suite; (c) PGV distribution for CMS suite; (d) Ia distribution for CMS suite.

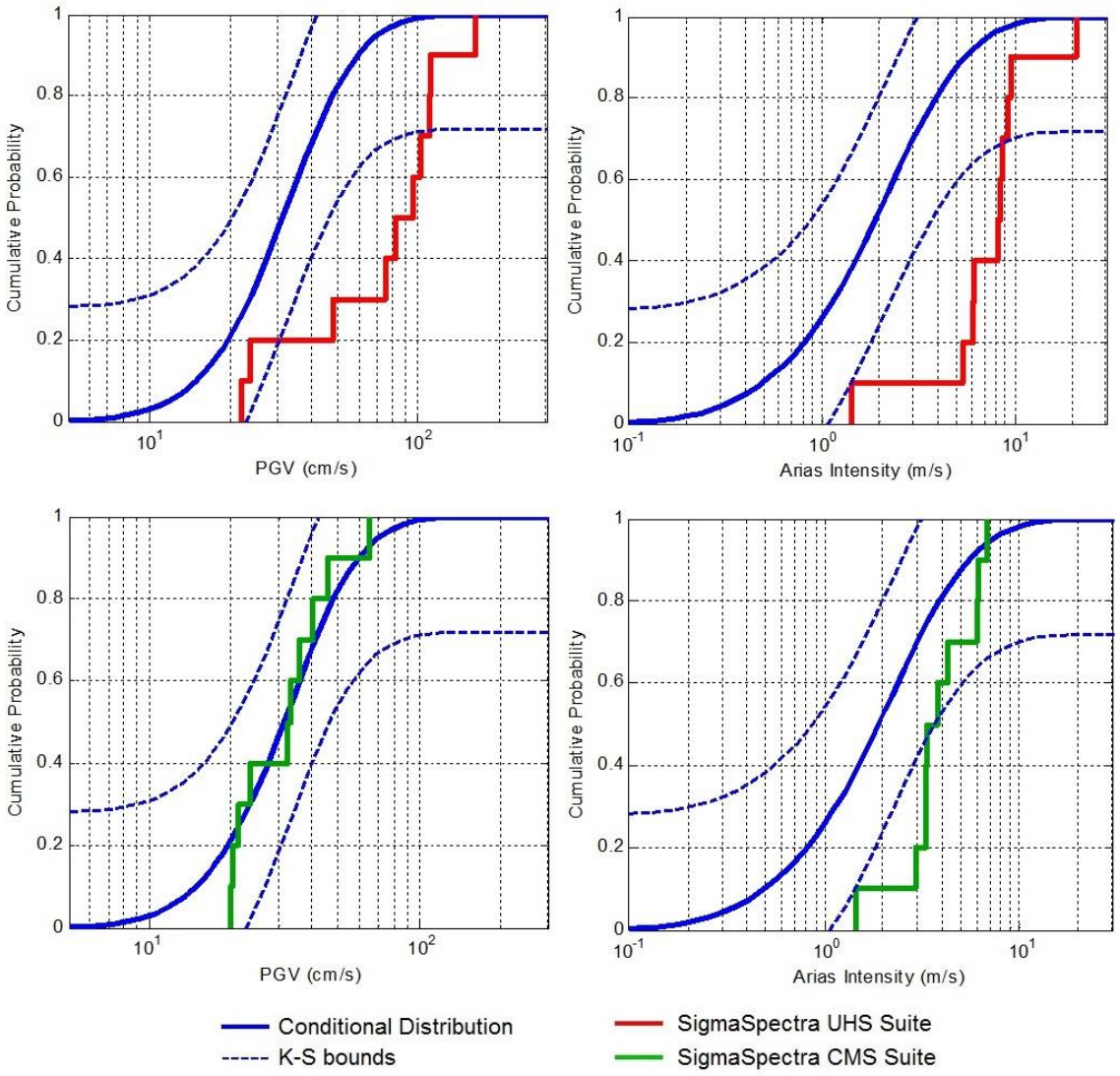

Figure 3.12 Intensity measure distributions of the suites selected by SigmaSpectra to fit San Jose acceleration response spectra. K-S bounds are shown for α=0.05. Shown above are: (a) PGV distribution of UHS suite; (b) Ia distribution of UHS suite; (c) PGV distribution for CMS suite; (d) Ia distribution for CMS suite.

3.5.3 Ground Motion Suites Developed by the GCIM Selection Method

The GCIM selection method was used to develop suites of ground motions to fit the conditional distributions of PGV and Ia. The GCIM selection method is implemented in a MATLAB code. Unlike the other two selection methods, the GCIM approach use search criteria to limit the acceleration-time histories that can be selected. Therefore, suites developed using the GCIM approach may include motions from earthquakes of any magnitude and recorded at any rupture distance. Prior to selection, the GCIM approach scaled all records in the database to the PGA value with a 2% probability of exceedance in 50 years (0.9 g for Los Angeles and 0.7 g for San Jose). These values of PGA are very large and motions recorded during very small magnitude events or very far from the fault rupture require large scale factors.

The GCIM approach selects ground motions based on the geometric mean of the ground motion parameter values of the two horizontal components. Thus, each suite developed using the GCIM selection method contains 20 ground motions. The PGV and Ia distributions of the selected ground motion suites are shown alongside the target conditional distributions for Los Angeles in Figure 3.13 and San Jose in Figure 3.14. Summaries of the properties of the selected ground motions are listed in Table A-10 through Table A-13 in Appendix A.

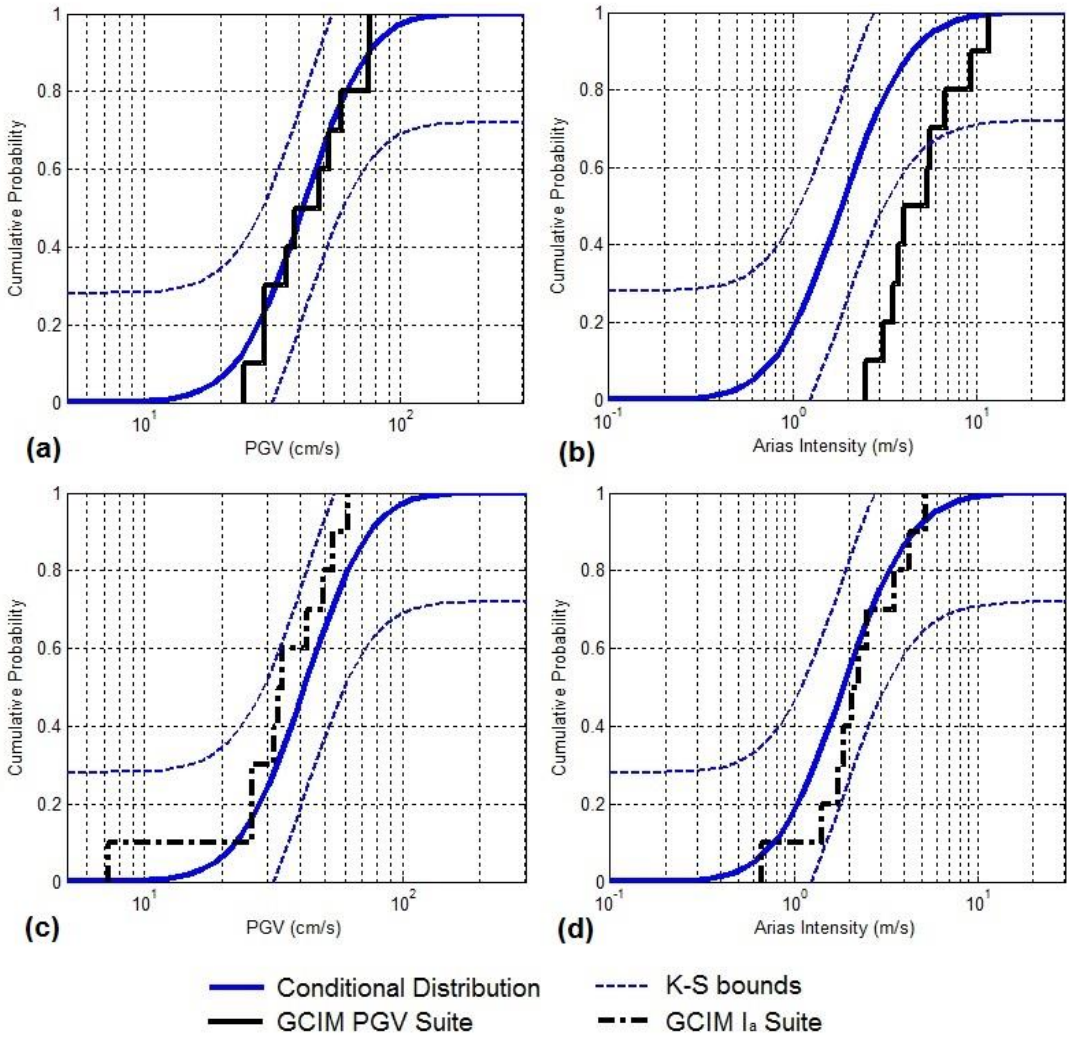

Figure 3.13 Intensity measure distributions of the suites developed using the GCIM selection approach for Los Angeles, shown alongside the target conditional distributions and K-S bounds for α=0.05. Shown above are: (a) the PGV distribution of the PGV suite; (b) the Ia distribution of the PGV suite; (c) the PGV distribution of the Ia suite; (d) the Ia distribution of the Ia suite

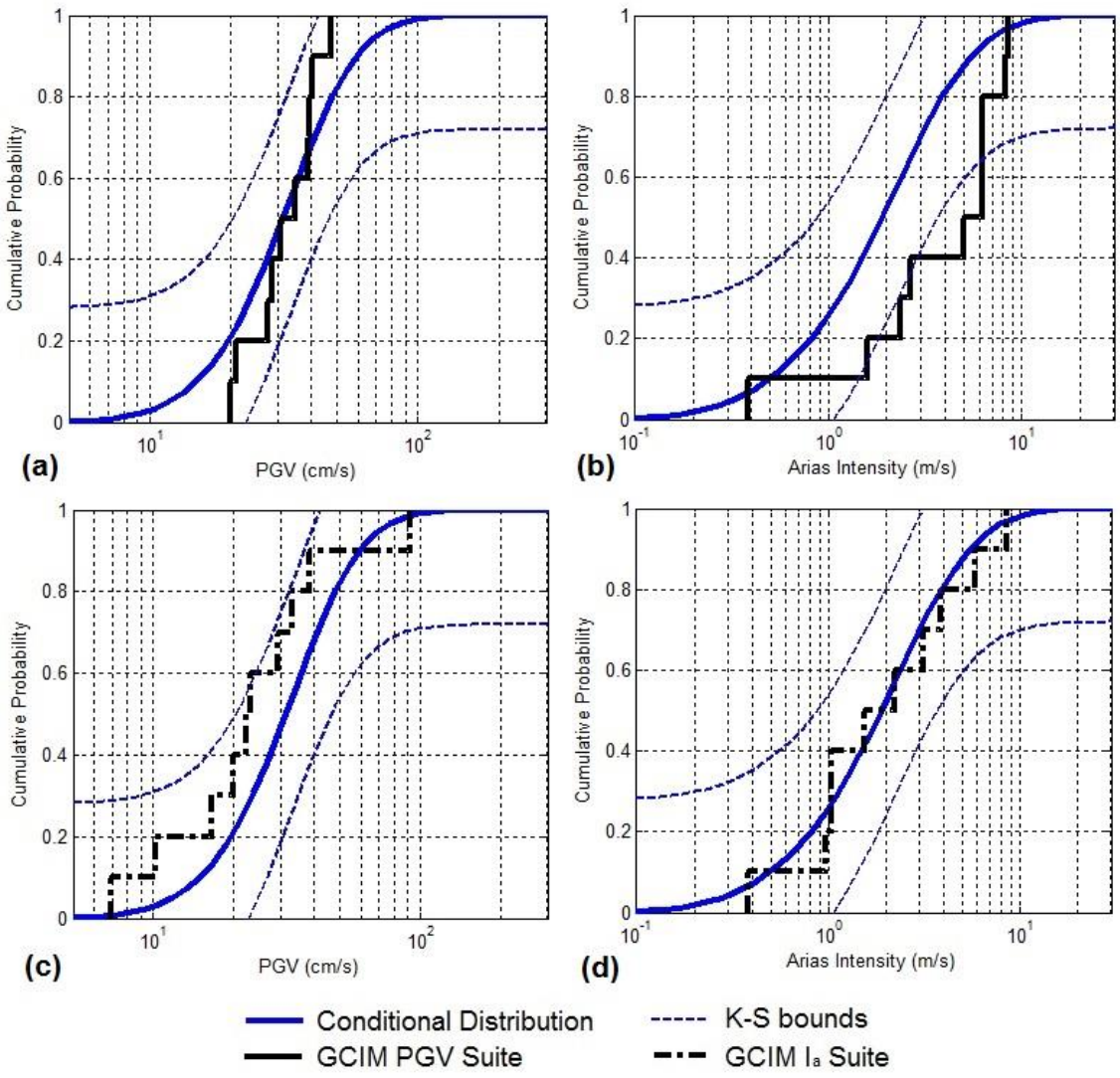

Figure 3.14 Intensity measure distributions of the suites developed using the GCIM selection approach for San Jose, shown alongside the target conditional distributions and K-S bounds for α=0.05. Shown above are: (a) the PGV distribution of the PGV suite; (b) the Ia distribution of the PGV suite; (c) the PGV distribution of the Ia suite; (d) the Ia distribution of the Ia suite.

The PGV distribution of the suite developed to fit the theoretical PGV distribution falls within the established K-S bounds (Figure 3.13a and Figure

3.14a), as expected. We also see that the Ia distribution of the suite developed to fit the theoretical Ia distribution falls within the K-S bounds (Figure 3.13d and Figure 3.14d).

It is also interesting to consider the Ia distribution of the suite developed to fit the theoretical PGV distribution. This is shown for Los Angeles in Figure 3.13b and for San Jose in Figure 3.14b. We see that the Ia distributions of the PGV suites exceed the upper K-S bounds and yield a poor fit to the theoretical Ia distributions. This is similar to the results for motions selected to fit a UHS or CMS. We can also consider the PGV distribution of the suite developed to fit the theoretical Ia distribution. This is shown for Los Angeles in Figure 3.13c and for San Jose in Figure 3.14c. Here, we see that the PGV distributions tend to fall short of the theoretical PGV distributions. In fact, in Figure 3.14c we see that the PGV distribution of the suite developed to fit the San Jose Ia distribution crosses the lower K-S bound.

The acceleration response spectra of the suites developed to fit the PGV and Ia distributions are shown in Figure 3.15. Several trends emerge through inspection of Figure 3.15. The peaks of the median spectra of the conditional PGV suites exceed the peaks of the median spectra of the conditional Ia suites. Although this is seen to occur for both sites, the difference between the maximum spectral acceleration of the median suites is more pronounced for San Jose than for Los Angeles. We also see that median spectra of the suites developed to fit the conditional Ia distributions tend to peak at lower periods than the median spectra of the PGV suites.

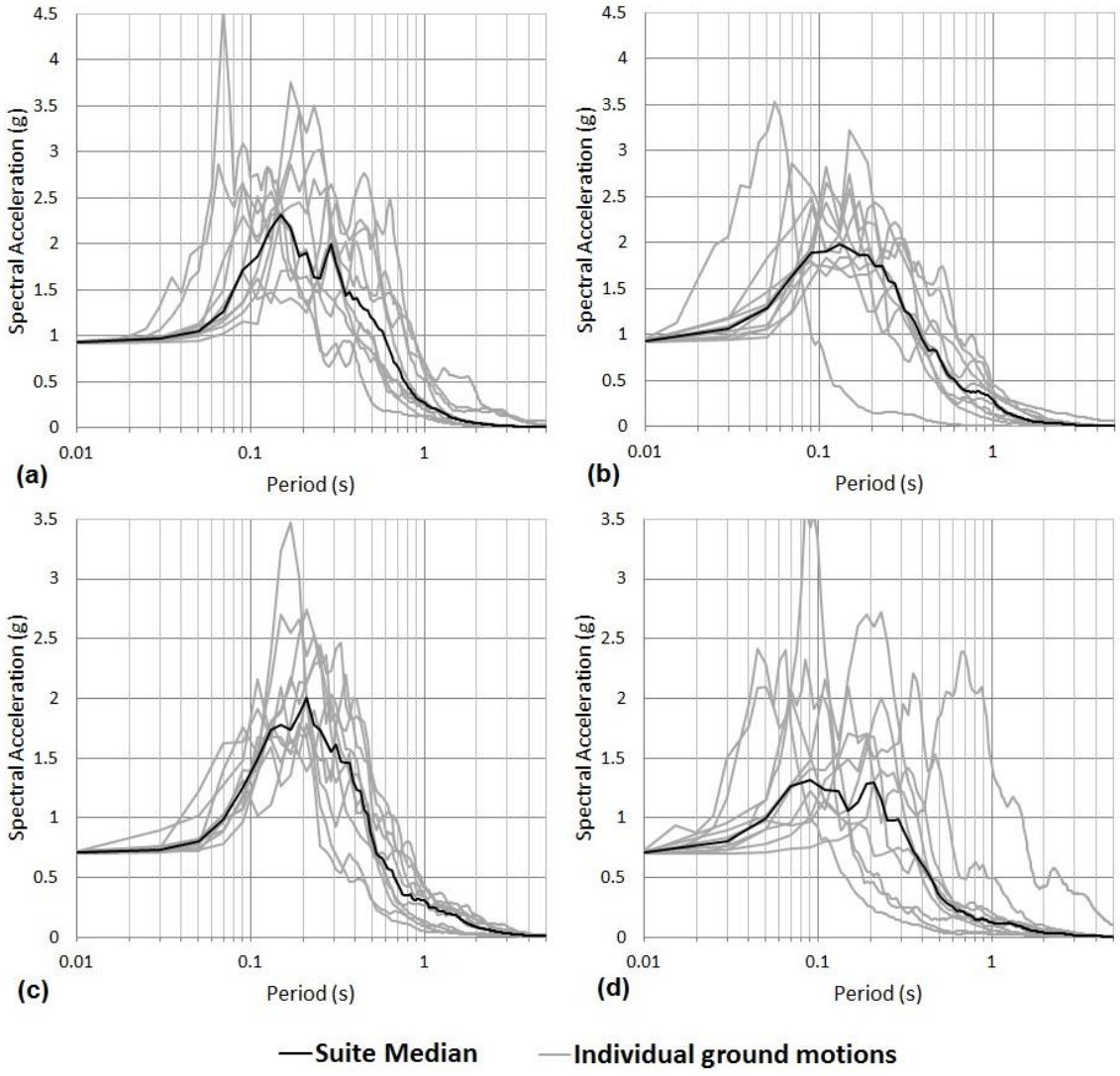

Figure 3.15 Acceleration response spectra of the ground motion suites developed using the GCIM approach for (a) Los Angeles PGV; (b) Los Angeles Ia; (c) San Jose PGV; (d) San Jose Ia.

3.5.4 Comparison of Selected Motions

The median acceleration response spectra of the suites developed using the GCIM approach are compared against the target acceleration response spectra in Figure 3.16. For Los Angeles (Figure 3.16a), the median spectrum of

the GCIM PGV suite generally matches the CMS well, while the median spectrum of the GCIM Ia suite is shifted slightly to shorter periods than the CMS. Nonetheless, the suites are generally similar and both fall significantly below the UHS at periods greater than about 0.5 s. For San Jose (Figure 3.16b), the GCIM PGV and Ia suites are more different from each other. The GCIM PGV suite peaks at periods similar to the CMS, although the maximum spectral acceleration is above the UHS. The GCIM Ia suite peaks at shorter periods and displays significantly smaller spectral accelerations in the period range of 0.1 to 2.0 s. When selecting ground motions to fit PGA and Ia alone we have seen that there is no guarantee that the spectral shape of the suite's median response spectrum will be appropriate.

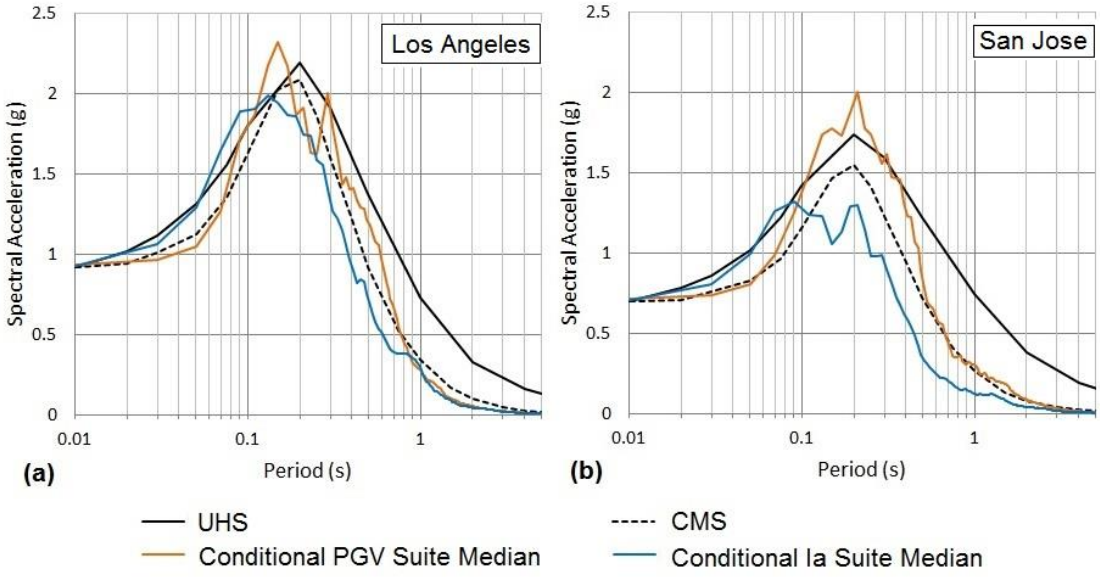

Figure 3.16 Comparison of the median spectra of the GCIM suites with the target UHS and CMS for (a) Los Angeles and (b) San Jose.

One way to compare ground motion suites is to use the root mean square error (RMSE) of the median spectrum relative to the target spectrum. The RMSE

reflects the average difference between the target spectrum and the median spectrum of the ground motion suite in terms of logarithms (Equation2.3). The RMSE of the eight suites developed to fit target acceleration response spectra are presented in Table 3-1. The smaller the RMSE, the better the fit of the selected ground motions to the target spectrum. In Table 3-1 we see that for all four target acceleration response spectra SigmaSpectra was able to develop ground motion suites with a smaller RMSE than the PGMD.

Table 3-1 Median RMSE of ground motion suites.

Selection Method	Site	Target Spectrum	Median RMSE
PGMD	Los Angeles	UHS	0.162
		CMS	0.149
	San Jose	UHS	0.120
		CMS	0.119
SigmaSpectra	Los Angeles	UHS	0.064
		CMS	0.129
	San Jose	UHS	0.107
		CMS	0.115

Several trends in the ground motion selection data have emerged through evaluation of the ground motion suites in terms of their intensity measure distributions. First, the suites selected by both the PGMD and SigmaSpectra tend to fit the theoretical PGV distribution better than the theoretical Ia distribution. Acceleration response spectra convey the intensity and frequency content of earthquake induced ground motion, but they fail to capture information about the duration of ground shaking. PGV is a measure of the intensity and frequency content of ground shaking, while Ia is the time-integral of the square of the ground acceleration and thus influenced also by the duration of ground shaking.

As a result, selecting motions to fit a response spectrum does not produce motions with appropriate values of Ia.

We also see that the suites developed to fit the CMS have intensity measure distributions that are more representative of the theoretical distributions than that of the UHS suites. This comes back to a discussion of the ways in which the CMS improves upon several shortcomings of the UHS, previously presented in Section 2.4.1. The CMS is a better target for ground motion selection because it is more representative of real ground motion spectra. The CMS in this study were developed by conditioning on the PGA with a 2% probability of exceedance in 50 years. The spectral accelerations at other periods in a CMS represent the probable values of spectral acceleration, given the occurrence of the conditioning value of PGA. Since it is very unlikely for the response spectrum for an individual acceleration-time history to be equally above average across all periods, the CMS falls below the UHS. Thus, we see that the intensity measure distributions of the UHS suites exceed that of the CMS suites and yield a poor fit to the theoretical intensity measure distributions.

We can also observe a difference in the intensity measure distributions between the suites developed using the PGMD and SigmaSpectra. The PGV and Ia distributions of the suites developed using the PGMD, shown in Figure 3.7 and Figure 3.8, tend to be steeper than the distributions of the suites developed using SigmaSpectra, shown in Figure 3.11 and Figure 3.12. This can be understood by considering the difference between the selection algorithms of the two approaches. The PGMD selects ground motions with the lowest MSE, while SigmaSpectra develops suites of ground motions to minimize the RMSE of the

suite's median response spectrum. Thus, the response spectra of the ground motions selected by the PGMD are all quite similar to the target spectrum, while the spectra of the motions selected by SigmaSpectra may vary above and below the target as long as the median spectrum of the suite remains close to the target. Because the PGMD suite is comprised of motions with very similar acceleration response spectra, the values of PGV and Ia do not tend to vary extensively across the suite. Thus, the intensity measure distributions of the SigmaSpectra suites are broader than those of the suites developed using the PGMD.

It has already been noted that all of the Ia distributions of the suites developed to fit acceleration response spectra in this study exceed the upper K-S bound of the theoretical distributions. This is especially true for the UHS suites. The Ia distribution is developed by multiplying the unscaled Ia of each record by the square of the scale factor of that particular record. Thus, if the scale factor is large (>10) then the scaled value of Ia can be more than an order of magnitude larger than the recorded Ia.

The scale factors used in the suites developed using the PGMD are all less than 10. The scale factors used in the suites developed using SigmaSpectra are all less than 16. Typically, we do not want scale factors to exceed 10 or 15 for engineering applications. Excessive scale factors may result in unrealistic acceleration-time histories and misleading results. Despite careful consideration of scale factors in the development of the ground motion suites considered in this study, the empirical values of Ia are much too large. In fact, six of the ten motions in the Los Angeles UHS suite developed by both the PGMD and SigmaSpectra

have scaled Ia values that exceed 10 m/s. The largest value of Ia in the PGMD UHS suite is 41.1 m/s and that in the SigmaSpectra UHS suite is 46.1 m/s.

Only a small handful of Ia values in excess of 10 m/s have ever been recorded, yet many of the empirical values determined for the suites in this study exceed 10 m/s. The three largest values of Ia in the NGA database are 19.5, 11.5, and 9.4 m/s. These values reflect the geometric mean of the two horizontal recordings made at each station. Therefore, it is probable that the Ia of one of the horizontal recordings exceeds the reported geometric mean. However, these values provide an indication of the upper limit we should expect for values of Ia.

Selection of ground motions to fit a UHS is one of the most common approaches used to develop input for numerical seismic response analyses in engineering practice. However, the Ia distributions of the suites selected to fit UHS in this study are inappropriately large. We have seen that the empirical distributions far exceed the theoretical Ia probability distributions. But more importantly, we have found that the scaled Ia values of motions in these suites are larger than any Ia values in the NGA database.

The information summarized in a ground motion's PGV value is also captured in the motion's acceleration response spectrum. However, as the squared time-integral of the acceleration-time history Ia characterizes information about the ground motion that is not captured in the motion's response spectrum. Thus, selection to fit an acceleration response spectrum may produce a suite with a PGV distribution that resembles the theoretical PGV distribution, but there is no guarantee that the Ia distribution of the suite will resemble the theoretical Ia distribution at the site.

If we compare the intensity measure distributions for all of the suites considered in this study we can see that the suites that best represent the theoretical distributions across multiple parameters are the suites developed to fit the theoretical Ia distributions. However, these suites are not perfect; the Ia suites tend to underestimate the theoretical PGV distributions at the two sites. Bradley (2012) developed the GCIM methodology to simultaneously consider multiple ground motion parameters in the ground motion selection process. This approach would allow both PGV and Ia to be considered when selecting motions, but this approach was not applied in this study.

3.6 COMPUTED SLIDING BLOCK DISPLACEMENTS

Rigid sliding block displacements were computed using the software program SLAMMER (Jibson et al. 2013) for each of the acceleration-time histories in each of the 12 suites. Four values of yield acceleration were considered: 0.1, 0.2, 0.3, and 0.4 g. Median displacements were determined for each suite at each of the four yield acceleration values.

The median displacements computed for the suites that were developed to fit the UHS and CMS target acceleration response spectra are plotted versus yield acceleration in Figure 3.17. Considering the two selection techniques used to fit these spectra (PGMD and SigmaSpectra), Figure 3.17 reveals that the median displacements of the suites developed by the PGMD are very similar to those computed for the suites developed by SigmaSpectra. This trend is seen for both sites. In Figure 3.17 it can be seen that there is a considerable difference between the displacements computed for the UHS suites and those computed for the CMS suites. Several ways in which the CMS improves upon the UHS as a

target for ground motion selection have already been discussed. This study has exposed another reason why the UHS is not an ideal target for ground motion selection: the intensity measure distributions of the UHS suite are inappropriately large and lead to excessively large displacements.

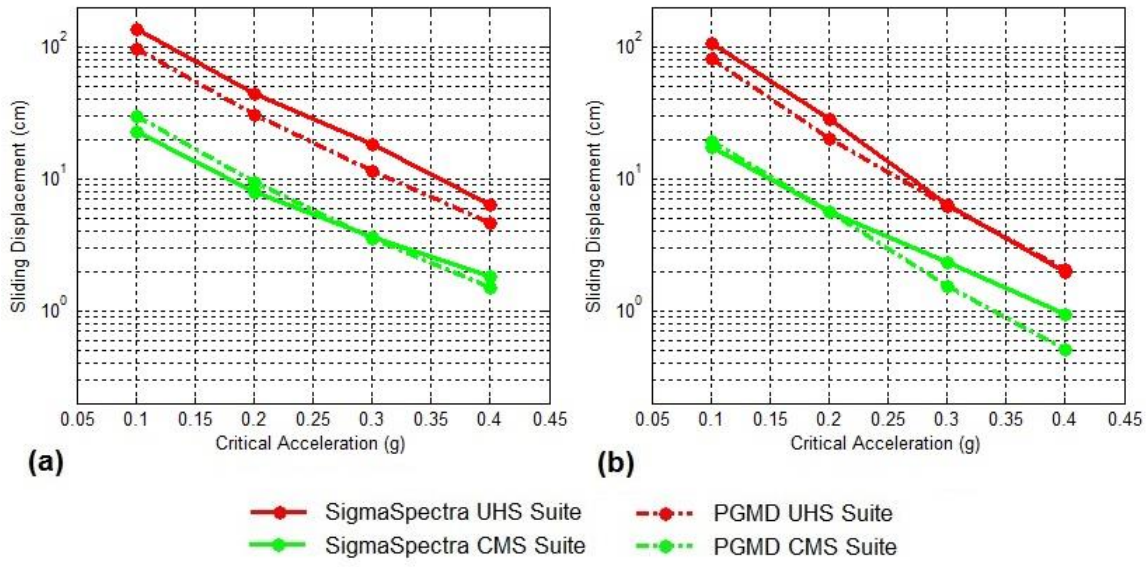

Figure 3.17 Median rigid sliding block displacements of the suites selected to fit UHS and CMS in (a) Los Angeles and (b) San Jose.

The median displacements of the UHS and CMS suites developed by SigmaSpectra are compared with the median displacements computed for the GCIM suites in Figure 3.18. The GCIM PGV suites predict displacements similar to the CMS suites for the Los Angeles and San Jose sites. This result is due to the fact that the median response spectrum of the GCIM PGV suite resembles the CMS (Figure 3.16) and the PGV distribution of the CMS suite fits the theoretical conditional PGV distribution well (Figure 3.7c and Figure 3.11c for Los Angeles and Figure 3.8c and Figure 3.12c for San Jose).

The GCIM Ia suites consistently predict displacements smaller than the GCIM PGV suites or the CMS suites. This difference is most pronounced for the San Jose site. These differences occur because the Ia values of the GCIM PGV suite and the CMS suite are much larger than those of the Ia suite (Figure 3.12d, Figure 3.14b, and Figure 3.14d). The smaller values of Ia associated with the GCIM Ia suite, as well as its smaller PGV (Figure 3.14c), lead to the smaller displacements. The difference between the displacements computed for the GCIM PGV suite and that computed for the GCIM Ia suite are more significant for San Jose (Figure 3.18b) than for Los Angeles (Figure 3.18a). First, we have seen that the Ia distributions of the GCIM PGV and GCIM Ia suites are more different for San Jose (Figure 3.14b and 3.14d) than for Los Angeles (Figure 3.13b and Figure 3.13d). We have also seen that while the median response spectrum of the GCIM Ia suite matches the CMS in Los Angeles, the median spectrum of the GCIM Ia suite falls far below the CMS in San Jose and has a different spectral shape (Figure 3.16). These results show that it is important to capture both the PGA, PGV, and Ia distribution of the design ground motion when selecting motions for sliding block displacement analyses.

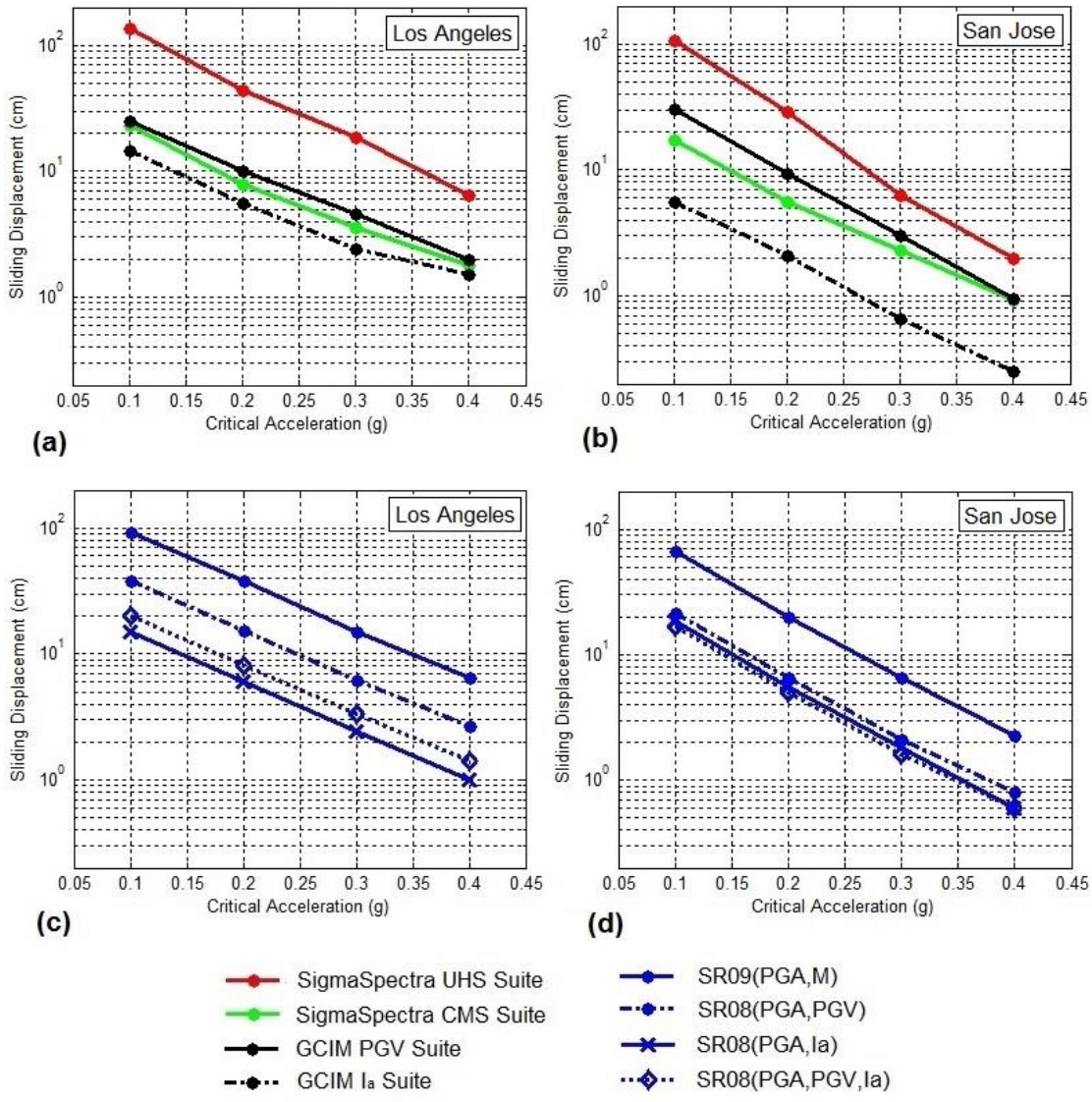

Figure 3.18 Median displacements of the ground motion suites and empirical displacement predictions: (a) Los Angeles suites; (b) empirical predictions for Los Angeles; (c) San Jose suites; (d) empirical predictions for San Jose.

Empirical predictions of rigid sliding block displacements are shown in Figure 3.18c and Figure 3.18d. Four empirical prediction equations were used to estimate the displacements featured in Figure 3.18c and Figure 3.18d: a model

published in Saygili and Rathje (2009) in which ground shaking is quantified using a combination of PGA and earthquake magnitude, M_W, and three models published in Rathje and Saygili (2008) in which ground shaking is quantified in terms of (PGA,PGV), (PGA, Ia), and (PGA, PGV, and Ia). When using these models, the PGA is taken as the 2% PE in 50 years value, M_w is taken as the mean magnitude from the deaggregation, the PGV is taken as the conditional mean PGV (i.e., mean of the GCIM PGV distribution), and the Ia is taken as the conditional mean Ia (i.e., mean of the GCIM Ia distribution). The values of the ground motion parameters used as input into the displacement prediction equations are listed in Table 3-2.

Table 3-2 Parameters used as inputs to the empirical displacement models.

Parameter	Los Angeles	San Jose
M_w	6.46	6.62
R_{rup} (km)	5.2	12.6
PGA (g)	0.92	0.7
PGV (cm/s)	42.88	31.97
Ia (m/s)	1.96	2.07

The displacements predicted by the (PGA, PGV) empirical model are consistently 30 to 50% smaller than the displacements predicted using the (PGA, M_W) model (Rathje and Saygili 2009). Seismic slope displacements are very sensitive to PGV because PGA is a measure for frequency content and the model developed in terms of PGA and M_W fails to fully capture the frequency content of the design ground motion. In Figure 3.18 we see that the displacements predicted using the (PGA, M_W) model match the median displacements computed for the UHS suites, which we've seen also fail to capture the appropriate PGV and frequency content of the design ground motion.

The median displacements of the San Jose CMS suite match the displacements predicted using the (PGA, PGV) model quite well. However, the displacements predicted by the (PGA, PGV) empirical model are larger than those computed for the Los Angeles CMS suite. We would expect the displacements computed for the CMS suite to match the displacements predicted using the (PGA, PGV) empirical model because we have seen that the PGV distribution of the CMS suite fits the theoretical PGV distribution very well. The empirical displacements predicted by the (PGA, Ia) and (PGA, PGV, Ia) models using the conditional PGV and Ia values are generally consistent with one another and with the displacements predicted by the GCIM PGV suite and the CMS suite.

It is difficult to determine which selection method yields the best estimate of rigid sliding block displacement. The GCIM PGV suites tend to have Ia larger than predicted by the theoretical Ia conditional distributions (Figure 3.13b and Figure 3.14b), while the GCIM Ia suites tend to have PGV smaller than predicted by the theoretical PGV conditional distributions (Figure 3.13c and Figure 3.14c). The CMS suites appear to have appropriate values of PGV, but the values of Ia tend to be larger than the theoretical Ia conditional distributions. Nonetheless, the GCIM PGV suites and CMS suites tend to predict displacements consistent with the empirical model that uses (PGA, PGV, and Ia) despite the fact that the Ia for these suites are larger than expected. This result may indicate that PGV is more important in predicting sliding displacement than Ia.

3.7 SUMMARY

This chapter presents and compares the displacements computed for the 12 suites of ground motions considered in this study. Evaluation of the suites in terms of their acceleration response spectra and distributions of relevant intensity measures has provided insight into the differences between the computed displacements.

Both the PGV distribution and the Ia distribution of the UHS suite exceed the theoretical distributions of these parameters, with the difference between the Ia distributions being especially pronounced. In fact, the scaled Ia values of several motions in the UHS suite exceed the largest recorded values of Ia in the NGA ground motion database. The information summarized in a ground motion's PGV value is also portrayed in the motion's response spectrum. However, the same cannot be said for Ia. Thus, selecting motion to fit an acceleration response spectrum alone can result in inappropriate distributions of Ia. As a result of the PGV and Ia values of motions in the UHS suite exceeding the expected values of these parameters, the displacements computed for the UHS suite are much larger than the displacements computed for suites developed through other selection methods.

The displacements computed for the Ia suite are smaller than the displacements computed for suites developed through other selection methods. The median acceleration response spectrum of the Ia suite lies below the median spectra of the suites developed through other selection methods. In addition, the PGV distribution of the Ia suite tends to underestimate the theoretical PGV distribution. Thus, the displacements computed for the Ia suite are likely to be unconservative estimates of permanent displacement.

Finally, the PGV distributions of the CMS suite and the PGV suite both fit the theoretical PGV distribution, while their Ia distributions exceed the theoretical Ia distribution. The median acceleration response spectra of the suites are very similar as well. Therefore, the displacements computed for the CMS suite and the PGV suite are very similar. The displacements computed for the CMS suite and the PGV suite are likely to be conservative estimates of permanent displacement.

If suites are to be developed for seismic slope stability analyses considering only two ground motion parameters, we recommend selecting motions to fit a PGV distribution that is conditional on PGA. Selecting motions to fit the CMS is also appropriate, as the PGV distribution of the CMS suite has generally been shown to fit the theoretical PGV distribution. However, for seismic slope stability analyses it is important to select motions that adequately fit the PGA, PGV, and Ia distributions expected at the site.

Chapter 4. Comparison of Displacements from Recordings and Simulated Ground Motions

4.1 Introduction

In this chapter four ground motion simulation models are evaluated within the context of rigid sliding block displacement analyses. First, the ground motion parameters of the simulations are compared to the ground motion parameters of the recorded ground motions. Then the displacements computed for the simulated ground motions are compared to the displacements computed for the recorded ground motions. A mixed effects regression is performed to quantify the bias and variability of displacements computed for each simulation model.

4.2 Record Selection

The Broadband Platform (BBP) Ground Motion Simulation Verification (GMSV) project (http://collaborate.scec.org/gmsv/Main_Page) is evaluating ground motion simulation techniques by simulating motions at strong motion stations that recorded previous earthquakes and quantitatively comparing the simulations to the actual recordings. Recordings from seven earthquakes are currently available: Loma Prieta, Northridge, Whittier Narrows, North Palm Springs, Landers, Tottori, and Niigata. For each of the seven earthquake events, ground motions were simulated for approximately 40 strong motion stations.

The ground motions considered in the Broadband Platform GMSV project were simulated for sites with a V_{S30} of 863 m/s (i.e. soft rock). However, the V_{S30} of the recording sites varies from station to station and many do not correspond with soft rock conditions. To avoid the need to model site effects in the

simulations to compare them with the recordings, only stations with V_{S30} close to the simulated value of 863 m/s are considered.

Ground motions were selected for evaluation based on the V_{S30} of the station at which they were recorded. The NGA ground motion prediction equations (GMPE) were used to estimate the effect of V_{s30} on the spectral acceleration at different periods. The predicted spectral acceleration (Sa) given a value of V_{S30} was normalized by the Sa predicted for V_{S30} = 863 m/s and plotted versus V_{S30}. The spectral acceleration at three periods was considered: PGA (0.0 s), 0.3 s, and 1.0 s. Three source-to-site rupture distances were considered as well: 100 km, 30 km, and 10 km. Equal weight was assigned to each of the four NGA GMPEs in the prediction of the Sa values. The ratios were calculated for a strike-slip fault mechanism and an earthquake magnitude (M_W) of 6.5. The results are presented in Figure 4.1.

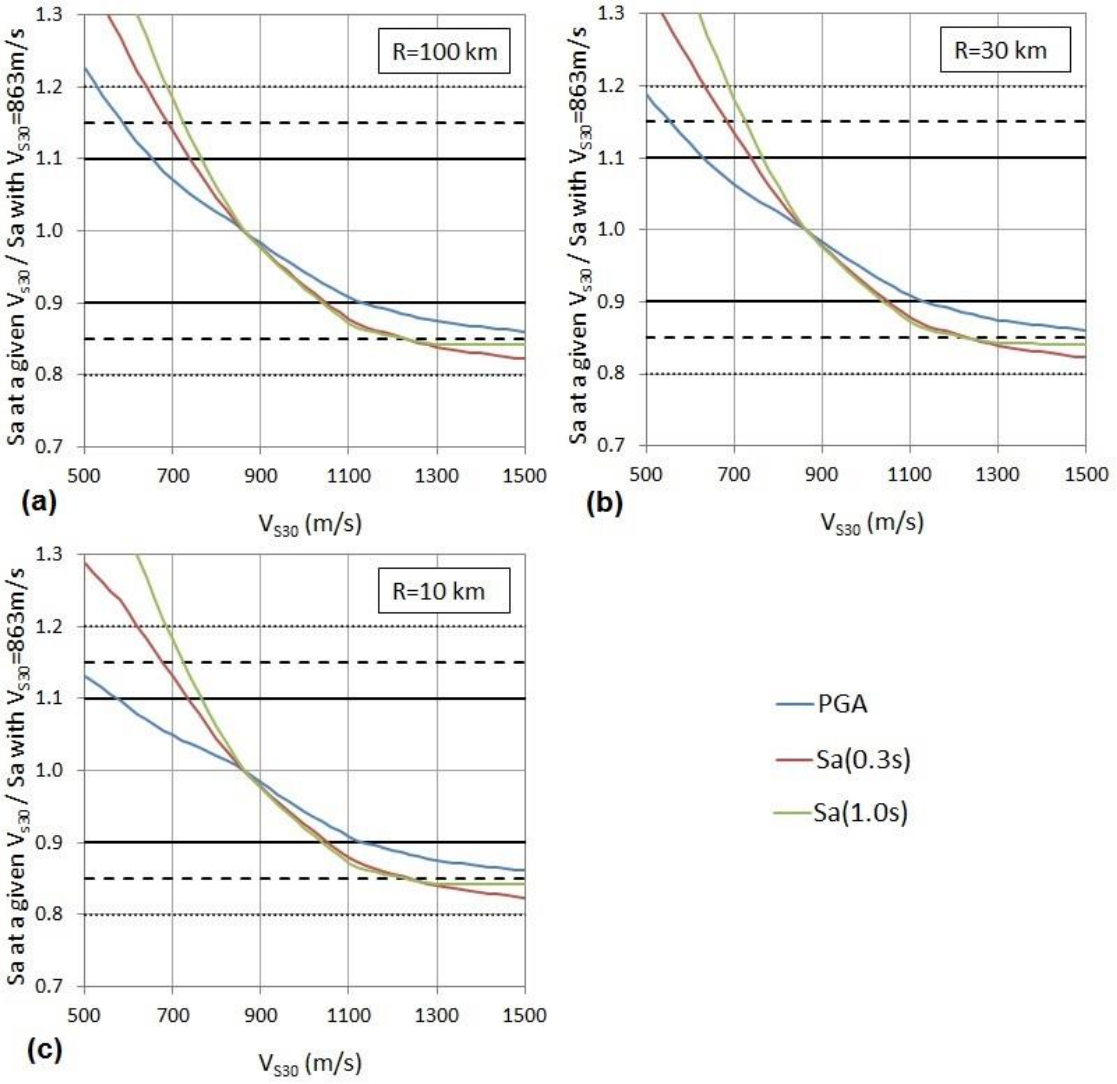

Figure 4.1 Ratio of spectral acceleration (Sa) at a given V_{S30} to Sa with V_{S30} = 863 m/s for (a) R_{rup} = 100 km; (b) R_{rup} = 30 km; and (c) R_{rup} = 10 km. 10%, 15%, and 20% error bounds are shown.

A difference in 10% relative to the Sa for V_{S30} equal to 863 m/s was deemed acceptable for this study. For the three periods and three rupture distances considered, shear wave velocities between 780 m/s and 1020 m/s yield less than a 10% difference in Sa, as shown in Figure 4.1. Of the three periods considered V_{S30}

was most restricted by the ratio of Sa at 1.0 s and least restricted by PGA. Thus the range of V_{S30} that yields less than a 10% difference in the Sa at 1.0 s was used to set the bounds on the V_{S30} of stations considered in this study. Figure 4.1 also shows that the ratio of Sa is not very sensitive to rupture distance; regardless of the rupture distance, nearly the same V_{S30} bounds were established for Sa at 1.0 s.

The V_{S30} distribution of the 270 stations considered in the BBP GMSV project is shown in Figure 4.2. Only nine stations have a V_{S30} between 780 m/s and 1020 m/s. Three acceleration-time history records are available for each station: a North-South component, an East-West component, and an Up-Down component. Since rigid sliding block displacements are computed for horizontal components of ground motion, this study compares the rigid sliding block displacements computed for 18 recordings with that of their respective simulations. Note that 50 simulations were performed for each recording. The records considered in this analysis are listed in Table 4-1.

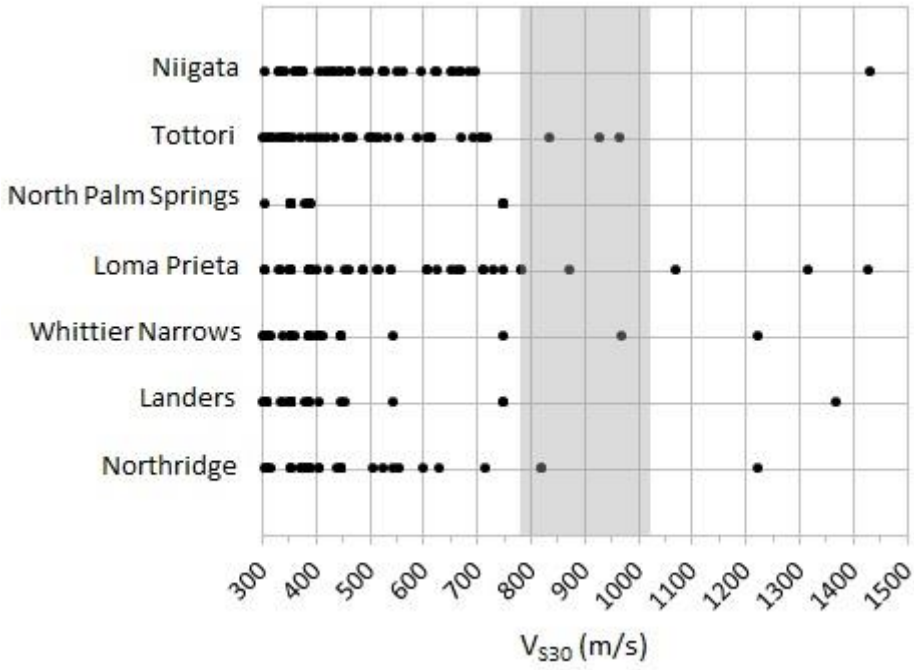

Figure 4.2 V_{S30} distribution of the strong motion stations considered in the BBP GMSV project. Shaded region indicates acceptable V_{S30} range.

Table 4-1 Parameters of the records considered for this study.

Recording Number	Event Station ID	Component	Earthquake	R_{Rup} (km)	V_{S30} (m/s)	M_W
1	15008-OKYH0	E-W	Tottori	15.23	929	6.59
2		N-S				
3	15020-SMNH1	E-W	Tottori	15.59	967	6.59
4		N-S				
5	15025-HYG00	E-W	Tottori	108.34	835	6.59
6		N-S				
7	2027-ATB	E-W	Northridge	46.91	822	6.73
8		N-S				
9	2033-ACI	E-W	Northridge	68.93	822	6.73
10		N-S				
11	5005-A-KRE	E-W	Whittier Narrows	18.12	969	5.89
12		N-S				
13	8028-XSP	E-W	Loma Prieta	48.39	782	6.94
14		N-S				
15	8029-RIN	E-W	Loma Prieta	74.14	873	6.94
16		N-S				
17	8031-CFH	E-W	Loma Prieta	78.68	782	6.94
18		N-S				

4.3 Comparison of Recorded and Simulated Ground Motion

The simulations selected for consideration in this study are first evaluated in terms of the ground motion parameters that are relevant to seismic slope stability analyses. Then, the rigid sliding block displacements computed for the simulated ground motions are compared with those computed for the corresponding acceleration-time history records.

4.3.1 Ground Motion Parameter Residuals

Three of the ground motion parameters that are important for characterizing ground motion for seismic slope stability analyses have already been discussed: PGA, PGV, and Ia. Another ground motion parameter that is

important for characterizing ground motion for seismic slope stability analyses is mean period (T_m). T_m is a parameter that describes the frequency content of a ground motion (Rathje et al. 1998, 2004). It is evaluated from the Fourier Amplitude Spectrum and is defined as:

$$T_m = \frac{\sum C_i^2 \left(\frac{1}{f_i}\right)}{\sum C_i^2} \qquad for\ 0.25 \leq f_i \leq 50\ Hz \tag{4.1}$$

where C_i are the Fourier amplitude coefficients and f_i are the Fourier amplitude frequencies.

The PGA, PGV, Ia, and T_m of the 18 acceleration-time history records considered in this study are listed in Table A-14 in Appendix A. To compare the ground motion parameters of the simulations with that of the recorded ground motions, the residual between the ground motion parameter (GMP) of the recorded ground motion and that of the simulated ground motion is computed in natural logarithmic space as:

$$GMP_{residual} = ln(GMP_{record}) - ln(GMP_{simulation}) \tag{4.2}$$

The smaller the absolute value of $GMP_{residual}$ the better the simulation approximates the recorded motion. A positive value of $GMP_{residual}$ indicates that the simulation underestimates the GMP of the record, while a negative value of $GMP_{residual}$ indicates that the simulation overestimates the GMP of the record.

Fifty ground motion simulations were generated for each acceleration-time history record. The GMP residuals computed for the four simulation models are shown versus the respective GMP of the recorded ground motion in Figure 4.3 through Figure 4.6. Each point indicates the residual of one ground motion simulation. The data presented in these figures are vertically aligned because the

GMP residuals computed for the 50 simulations are all plotted at the same position on the x-axis (i.e. the GMP of the recorded ground motion).

The GMP residuals computed for the motions simulated via the CSM model are shown in Figure 4.3. Inspection of Figure 4.3a reveals that there is a lot of variability in the PGA values of the simulated motions for each record simulated. However, the PGA residuals tend to be distributed about zero, meaning that the average PGA of the simulations is close to the PGA of the recorded ground motion. The same observation can be made for Ia in Figure 4.3c. Figure 4.3b shows that when the PGV of the recorded acceleration-time history is small (i.e. less than 5 cm/s) the PGV residuals tend to be negative. This means that the simulations tend to overestimate PGV when the recorded PGV is less than 5 cm/s. For PGV values greater than 5 cm/s the average PGV of the simulations is similar to the recorded PGV. A similar trend also exists between the T_m residuals and the T_m of the recorded ground motion (Figure 4.3d). When the T_m of the recorded ground motion is small the simulation tends to overestimate T_m. However, in this case when the T_m of the recorded ground motion is large the simulation tends to underestimate T_m.

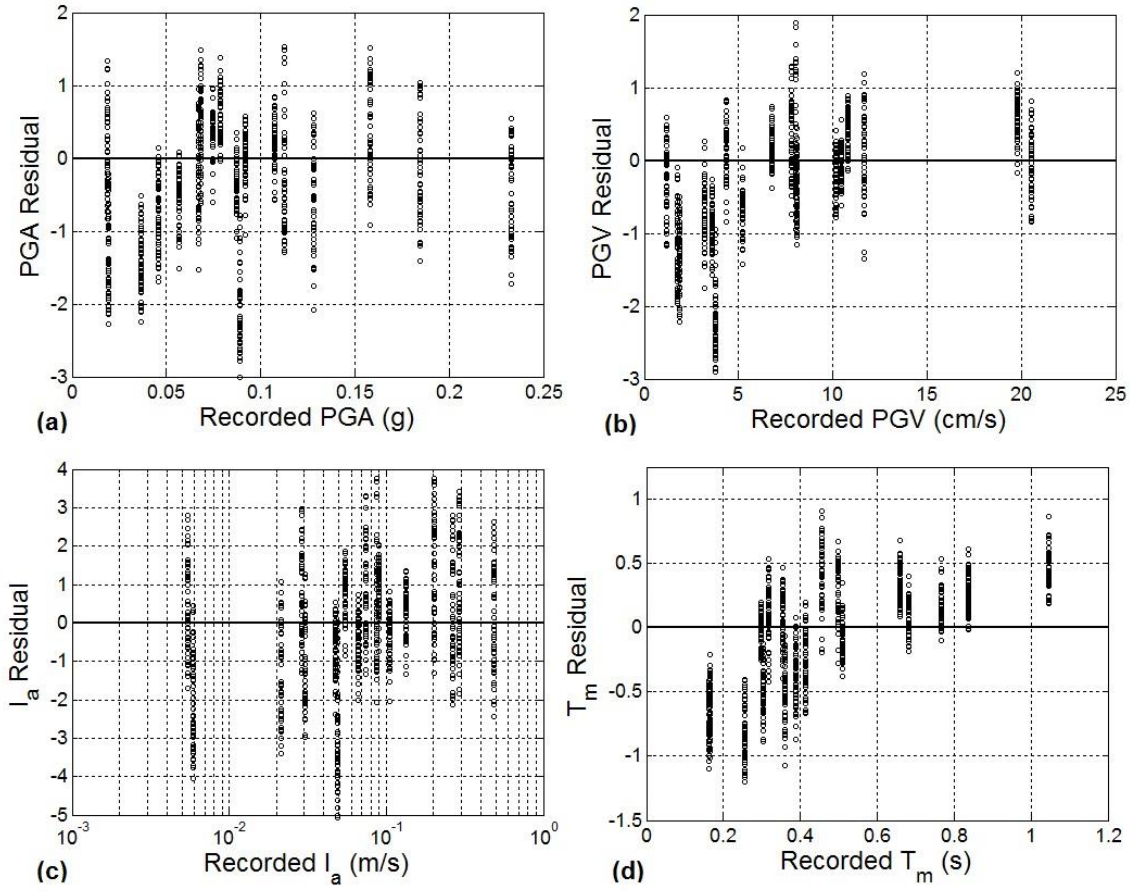

Figure 4.3 GMP residuals computed for the CSM simulation model.

The GMP residuals computed for the motions simulated via the EXSIM model are shown in Figure 4.4. One thing to note about the EXSIM model is that it only generates one horizontal ground motion. The North-South and East-West, components of ground motion are the same because the model essentially predicts the maximum component of ground motion. For the other simulation models, the North-South component of the simulated ground motion is compared to the North-South component of the recorded ground motion, and the same for the East-West component of motion. For EXSIM, we compare the

sole EXSIM ground motion to both the north-south and east-west components of the recorded ground motion.

The range of GMP residuals for a given record is seen to be considerably smaller for the EXSIM model than that observed for the CSM model. Figure 4.4a and Figure 4.4c show that the EXSIM model simulates well the PGA and Ia of the recordings. However, the same cannot be said for PGV and T_m; distinct positive trends are observed in Figure 4.4b and Figure 4.4d. When the PGV of the recorded ground motion is small the EXSIM simulations tend to overestimate PGV. When the PGV of the recorded motion is large, however, the simulations tend to underestimate PGV. The same trend is observed for T_m in Figure 4.4d.

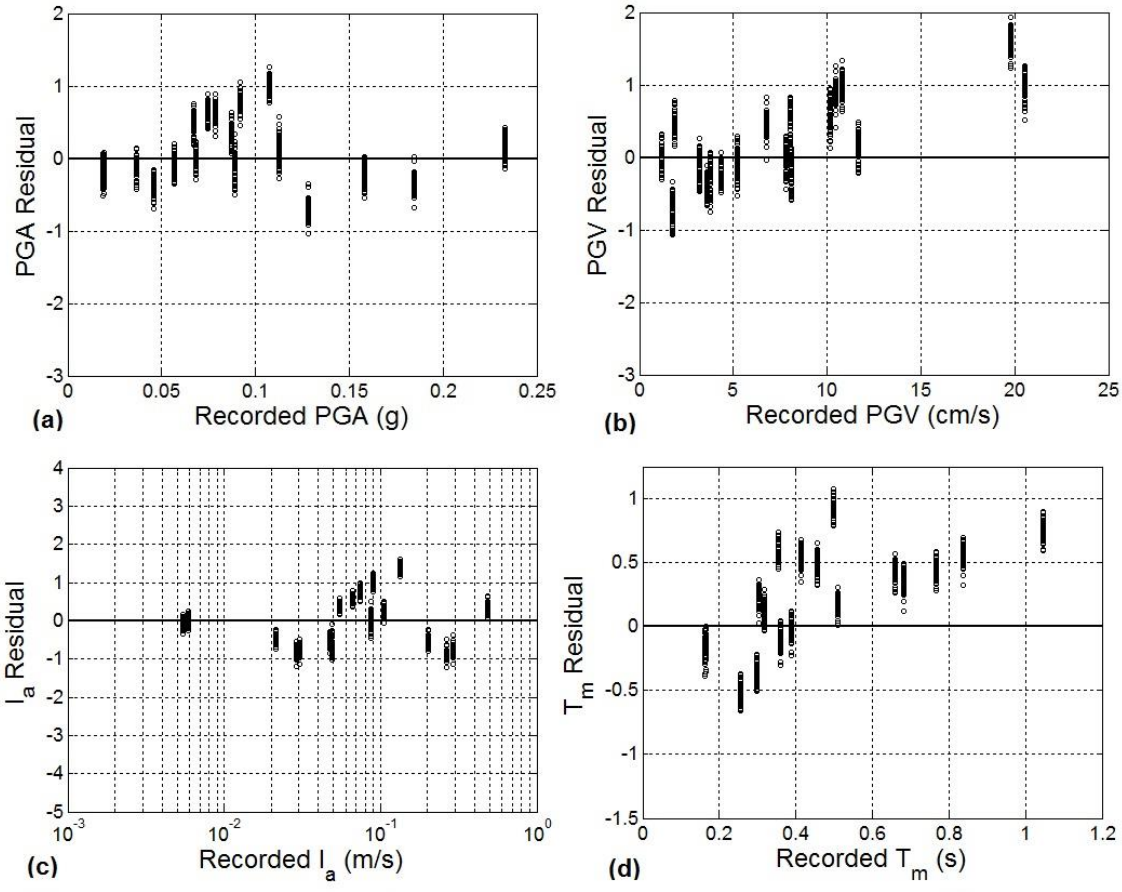

Figure 4.4 GMP residuals computed for the EXSIM simulation model.

The GMP residuals computed for the motions generated via the GP simulation model are shown in Figure 4.5. The variability of the GMP residuals of the GP simulations is smaller than that observed for the CSM simulations, but larger than observed for the EXSIM model. The GP model produces simulations with PGA and Ia that match those of the recordings quite well, as shown in Figure 4.5a and Figure 4.5c, respectively. For PGV a slight positive trend can be observed (Figure 4.5b); when the PGV of the recorded motion is small the simulation tends to overestimate PGV and when the PGV of the recorded motion

is large the simulation tends to underestimate PGV. Figure 4.5d shows that when the recorded ground motion has a small value of T_m the GP model tends to produce simulations with a T_m that is too large. The fit is better at larger values of T_m.

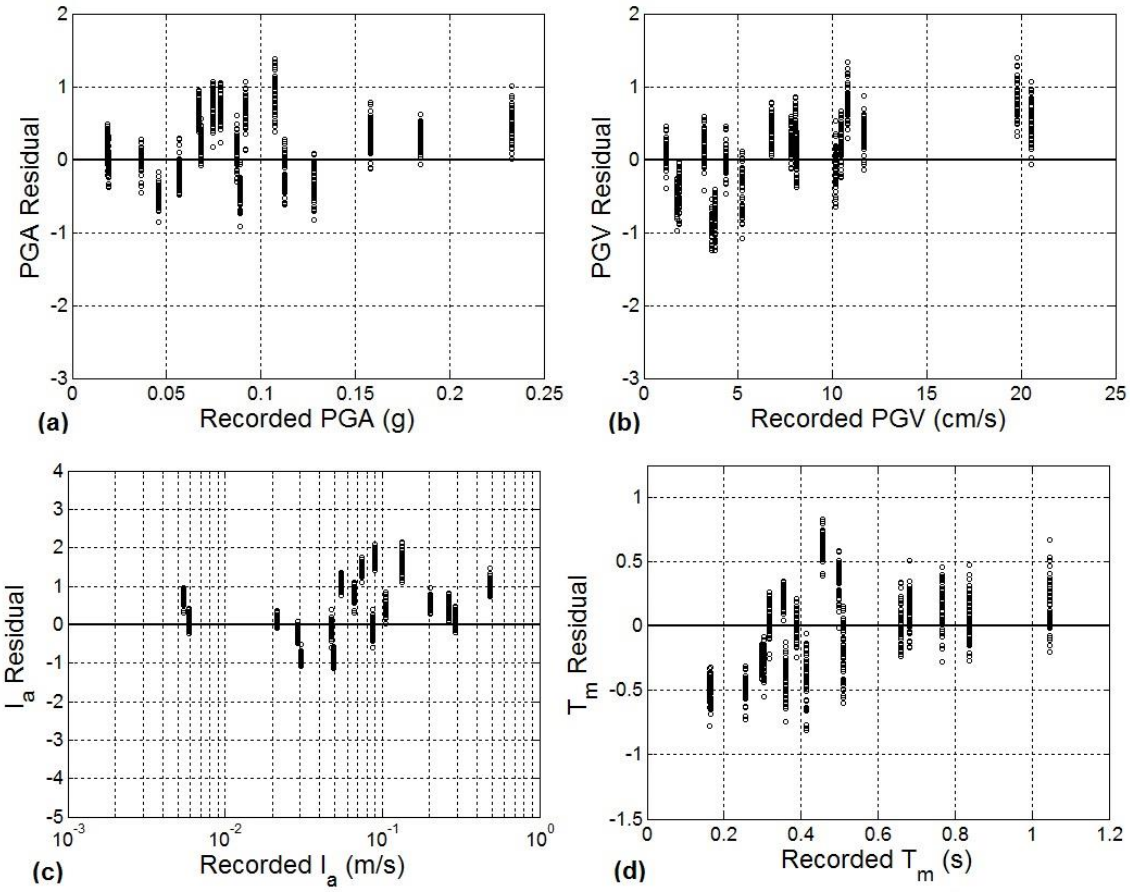

Figure 4.5 GMP residuals computed for the GP simulation model.

The GMP residuals computed for the motions simulated via the SDSU model are shown in Figure 4.6. The range of the GMP residuals computed for the SDSU appears to be less than for the CSM model, but greater than the range for the EXSIM and GP models. The GMP residuals computed for the SDSU model

differ from the residuals computed for other simulation models. For the previous three simulation models, the range of GMP residuals was relatively consistent from one recording to another. The range of GMP residuals computed for the SDSU model, however, varies considerably from one record to another. It can be seen in Figure 4.6a that the PGA residuals computed for some recordings vary over a range that is about 10 times as large as that computed for other recordings (e.g., compare the motions at recorded PGA = 0.05 g and 0.15 g). This can also be seen for Ia in Figure 4.6c. On average, the PGA and Ia of the SDSU simulations match that of the recorded ground motion. A slight positive trend is observed in Figure 4.6b; i.e., when the PGV of the recorded ground motion is small, the PGV of the simulated motion tends to be large, and when the PGV of the recorded ground motions is larger, the PGV of the simulated motion tends to be smaller. Figure 4.6d shows that the SDSU model tends to simulate motion with a T_m that is too large when the T_m of the ground motion is small. However, when the T_m of the recorded motion is larger the residuals tend to be distributed about zero.

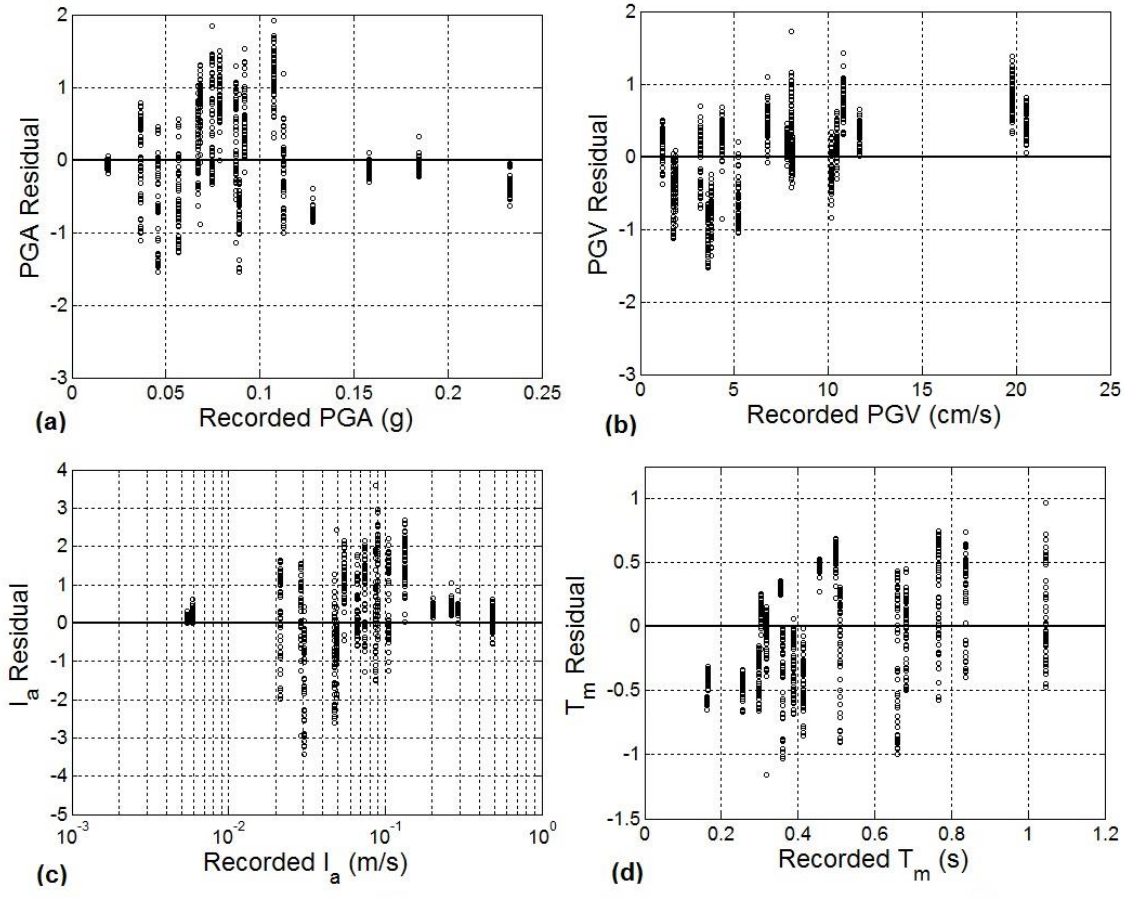

Figure 4.6 GMP residuals computed for the SDSU simulation model.

Of the four simulation models considered, the range of GMP residuals is seen to be largest for the simulations generated by the CSM model and smallest for the simulations generated by the EXSIM model. The variability of the GMP of the simulated ground motions is not our only concern; we are also interested in the average GMP residuals for each simulation model. The average GMP residuals of the four simulation models are computed across the motion-specific residuals. Only a subset of the motions are considered in computing the average GMP residuals because the smallest value of yield acceleration considered in this

study is 0.05 g. Records with a PGA less than 0.05 g will have zero displacement and therefore are not relevant for the calculation of the displacement residuals. In an attempt to ensure that the ground motion parameter residuals will be informative for interpreting the displacement results, ground motions with a PGA less than 0.05 g are ignored in the calculation of average GMP residuals. This reduces the number of acceleration-time history records to 14 and the average residuals for PGA, PGV, Ia, and T_m for these 14 motions and the 4 simulation models are listed in Table 4-2.

Table 4-2 Average GMP residuals of the four simulation models.

Simulation	PGA	PGV	I_a	T_m
CSM	-0.17	-0.16	0.18	-0.03
EXSIM	0.17	0.35	0.04	0.28
GP	0.29	0.19	0.57	0.01
SDSU	0.13	0.17	0.46	-0.02

On average, the CSM model produces simulations with PGA and PGV that exceed that of the recorded ground motion (i.e., negative residuals), while the Ia of the CSM simulations tends to underestimate the Ia of the recorded ground motions (i.e., positive residuals). The average T_m residual is close to zero. The over-prediction for PGA and PGV are about 15%-20%, while the under-prediction for Ia is about the same. On average, the EXSIM and GP models underestimate most of the GMP of the recorded ground motions. For EXSIM, the under-prediction of PGA, PGV, and T_m ranges from 15%-30%, while the average residual for Ia is close to zero. For GP, under-prediction occurs for PGA, PGV, and Ia (between 20 to 50% smaller) and the average residual for T_m is close to zero. Finally, the SDSU model tends to produce simulations with PGA, PGV, and

Ia that are smaller than the values of the recorded ground motion (15%-40% under-prediction), while the residuals are about zero for T_m. Note that these average residuals do not account for the systematic variation in residuals with GMP, as shown in Figure 4.3 through Figure 4.6.

Inspection of Figure 4.3 through Figure 4.6 reveals that the simulation model that generates ground motions with the least variability in GMP is the EXSIM model. However, the average T_m residual computed for the EXSIM model is considerably larger than the average T_m residuals computed for the other models. So while the EXSIM model may produce 50 simulations that all have a similar value of T_m, the simulations are likely to have a T_m that is considerably smaller than that of the recorded ground motion. In Table 4-2 we see that the T_m residuals computed for the CSM, GP, and SDSU models are smaller than the PGA, PGV, and Ia residuals computed for these models. This means that these three models can simulate T_m better than they can simulate PGA, PGV, and Ia.

4.3.2 Displacement Residuals

Before presentation of the displacement residuals computed for the four simulation models some details concerning the treatment of displacement data must be clarified. When the displacement computed for a simulated ground motion is zero (i.e. PGA < k_y) and the displacement computed for the recorded ground motion is nonzero the residual is equal to infinity. For this reason, displacement residuals are computed only for simulations with nonzero displacement. Nonetheless, when the PGA of the simulation is very close to k_y the computed displacement can become very small and very large residuals can occur.

Despite omission of the acceleration-time history records with a PGA less than 0.05 g, the GMP residuals presented in Section 4.3.1 are not fully informative for interpreting displacement residuals. For each simulation model, all 50 simulations developed for each of the 14 recordings with PGA greater than 0.05 g were considered in calculation of the average GMP residuals. However, simulations for which the computed displacements are zero were removed from the analysis of displacement residuals. This issue may cause the trends for the displacement residuals to be different than for the GMP residuals.

For each acceleration-time history two values of sliding block displacement can be computed. The normal displacement is found by integration of the portion of the acceleration-time history that exceeds the critical acceleration value. The inverse displacement is found by multiplying the acceleration-time history by -1 and then integrating the portion that exceeds the critical acceleration value. In this study we compared the maximum of the normal and inverse displacement computed for the recorded ground motion with the maximum of the normal and inverse displacement computed for the simulated ground motion.

A two-part approach is used to evaluate the displacements computed for simulated ground motions. First, simulated acceleration-time histories with zero displacement are considered. Next, simulated time histories with nonzero displacement are evaluated through computation of displacement residuals and a mixed effects regression analysis.

The rigid sliding block displacements computed for the 18 acceleration-time history records and three k_y values considered in this study are listed in

Table A-15 in Appendix A. To evaluate the models in terms of their ability to simulate motion with zero displacement the percentage of simulations with zero displacement are plotted versus the ratio of k_y to PGA in Figure 4.7. In computing k_y/PGA, the PGA of the recorded motion is used. Each point in Figure 4.7 represents the percentage of simulations with zero displacement for a given recorded motion and k_y value. The 54 values in each plot represent the 18 records and 3 k_y values. Ideally, 0% of the simulations should have zero displacement when k_y/PGA is less than 1.0 (i.e., the displacement of the recorded motion is nonzero) and 100% of the simulations should have zero displacement when k_y/PGA is greater than 1.0 (i.e., the displacement of the recorded motion is zero). Inspection of Figure 4.7a reveals that the CSM model performs poorly when evaluated relative to his criterion: as few as 60% of the simulations have zero displacement even when k_y/PGA of the recorded motion is greater than 5. This result agrees with the fact that the CSM model tends to over-predict the PGA of the recorded motions (Table 4-2). In Figure 4.7b and Figure 4.7c we see that for the EXSIM and GP models there is more of a rapid increase in the percentage of simulations with D = 0 at k_y/PGA equal to 1.0. Thus, the EXSIM and GP models are better able to simulate whether a motion will have zero displacement, which agrees with the PGA residuals in Table 4-2 that show that these models most accurately capture the PGA of the recordings. Finally, Figure 4.7d shows that the SDSU model has a more gradual transition between 0% and 100% at k_y/PGA equal to 1.0, which again agrees with the fact that the SDSU model has a larger PGA residual.

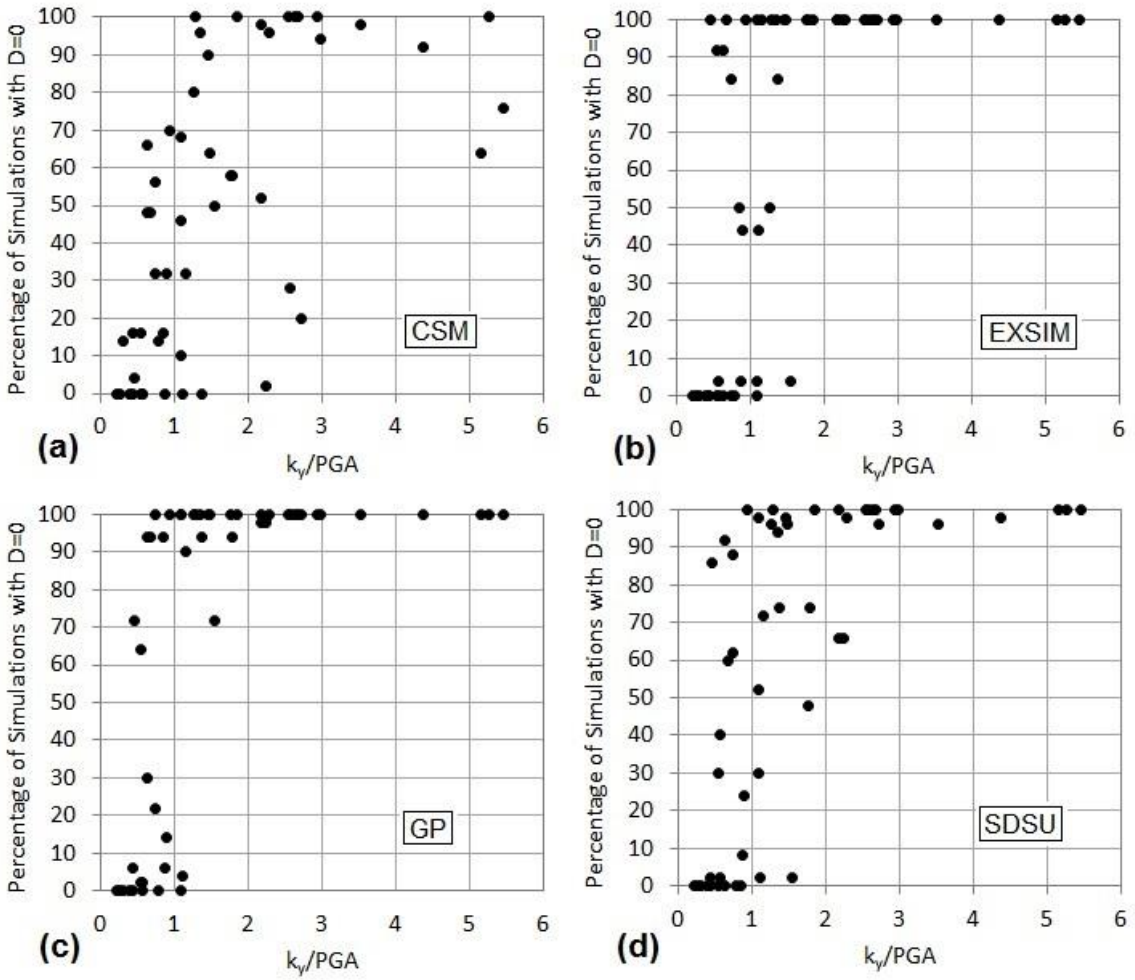

Figure 4.7 Percentage of simulations with zero displacement versus k_y normalized by the PGA of the record for (a) CSM; (b) EXSIM; (c) GP; (d) SDSU.

Next, we consider simulations of recorded ground motions for which nonzero displacements were computed. The difference between the displacement computed for a simulated ground motion and the displacement computed for the recorded motion is quantified with the displacement residual:

$$D_{residual} = ln(D_{record}) - ln(D_{simulation}) \tag{4.3}$$

A mixed effects regression of the displacement residuals was performed to quantify the mean bias and variance of each simulation model.

Mixed effects regression estimates the biases and variances for different subsets of the data (Lindstrom and Bates 1990). Mixed effects regression has previously been used by Rodriquez-Marek et al. (2011) and Kaklamanos et al. (2013) in the context of earthquake engineering. In this study, we group the data by acceleration-time history record and use linear mixed effects regression to compare the simulation models in the context of rigid sliding block displacement. Assuming that the displacements can be described by a lognormal distribution, the displacement residuals (computed as the natural logarithm of displacements) can be described by a normal distribution with mean μ_Y and standard deviation σ_Y. The mixed effects regression model for displacement residual is defined as:

$$y_{i,j} = \alpha + \eta_i + \epsilon_{i,j} \tag{4.4}$$

where α is the average bias (i.e. difference) in the simulation model for all recorded ground motions and simulations, η_i is the inter-recording residual for a particular recording, and $\epsilon_{i,j}$ is the intra-recording residual of a particular simulation. The subscript i denotes the recording number, which varies from 1 to 18, and the subscript j indicates the simulation number, which varies from 1 to 50. In this formulation η_i is assumed to be a normally distributed random variable with a mean of 0 and standard deviation τ. Likewise, $\epsilon_{i,j}$ is assumed to be a normally distributed random variable with a mean of 0 and standard deviation σ. The inter-recording residual measures the difference between the overall residual of the simulation model, α, and the mean residual calculated for

a particular recording. The intra-recording residual measures the difference between the mean residual of a particular recording and the displacement residual of an individual simulation for that recording. Linear mixed effects regression yields estimates of α, τ, and σ. These parameters are used in Equation 4.5 and Equation 4.6 to determine the overall μ_Y and σ_Y of the displacement residuals. The four simulation models can then be evaluated in terms of the μ_Y and σ_Y of their displacement residuals.

$$\mu_Y = \alpha \tag{4.5}$$

$$\sigma_Y = \sqrt{\tau^2 + \sigma^2} \tag{4.6}$$

Figure 4.8 through Figure 4.11 compare the displacements computed using the recorded and simulated motions for the four simulation models. Displacements and displacement residuals are shown, along with the inter-recording (η_i) and intra-recording ($\epsilon_{i,j}$) residuals. The displacement results for the CSM simulations are shown in Figure 4.8. Inspection of Figure 4.8a and Figure 4.8b reveals considerable variability in the displacements computed for the ground motions simulated by the CSM model. In fact, in Figure 4.8a we see that the displacements computed for CSM simulations can range over as much as 7 orders of magnitude for simulations of the same recorded ground motion. This result is not very surprising, given that there was considerable variability in the GMP residuals of the CSM model (Figure 4.3). There are a large number of negative residuals, which indicates that the displacements from the simulated motions are larger than from the recordings. The average residual (α) is equal to -0.64 (Figure 4.8b), which corresponds to the displacements from the simulated

motions being almost twice the value of the displacements from the recorded motions. This result is in agreement with the ground motion residuals (i.e., Table 4-2), which showed that the CSM model over-predicted the recorded PGA and PGV. Through mixed effects regression we were able to determine the inter-recording standard deviation, (τ = 2.40), and the intra-recording standard deviation, (σ = 2.57), as shown in Figure 4.8c and d. The computed τ and σ are both large, indicating there is both significant inter-recording and intra-recording variability.

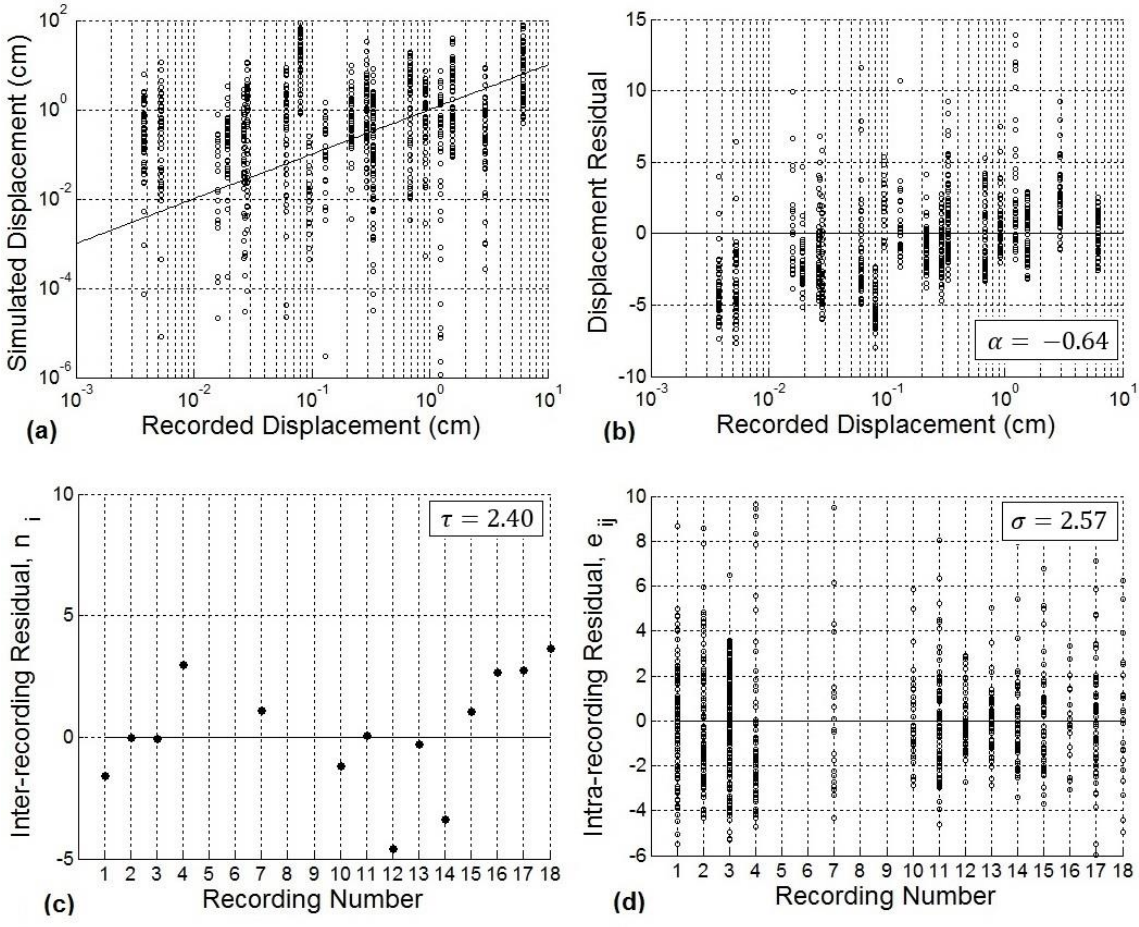

Figure 4.8 Displacements and residual displacements computed for the CSM simulations.

The displacement results for the ground motions simulated by the EXSIM model are shown in Figure 4.9. Similar to the CSM results, there are a significant number of negative residuals, indicating that the displacements from the simulated motions tend to be larger than from the recorded motions. The average displacement residual (α) is equal to -0.14, which corresponds to a 15% over-prediction of displacement, on average. This over-prediction in displacement is in contradiction with the ground motion residuals (Table 4-2) which were all positive (i.e., under-prediction) for EXSIM. This can be explained, at least partially, by the fact that the GMP residuals were computed using all of the simulations, while the displacement residuals were computed using only the simulations with nonzero displacements. Simulations with zero displacement would tend to have smaller values of the GMP, which increases the average GMP residual. However, these simulations do not contribute to the displacement residual. There is a notable difference in the variability of displacements observed for the EXSIM simulations and the variability observed for the CSM simulations. Figure 4.9c shows the inter-recording residuals, which vary more substantially for EXSIM and displays τ = 3.54. The intra-recording variability in displacements (Figure 4.9d) is relatively small for EXSIM with σ = 1.31.

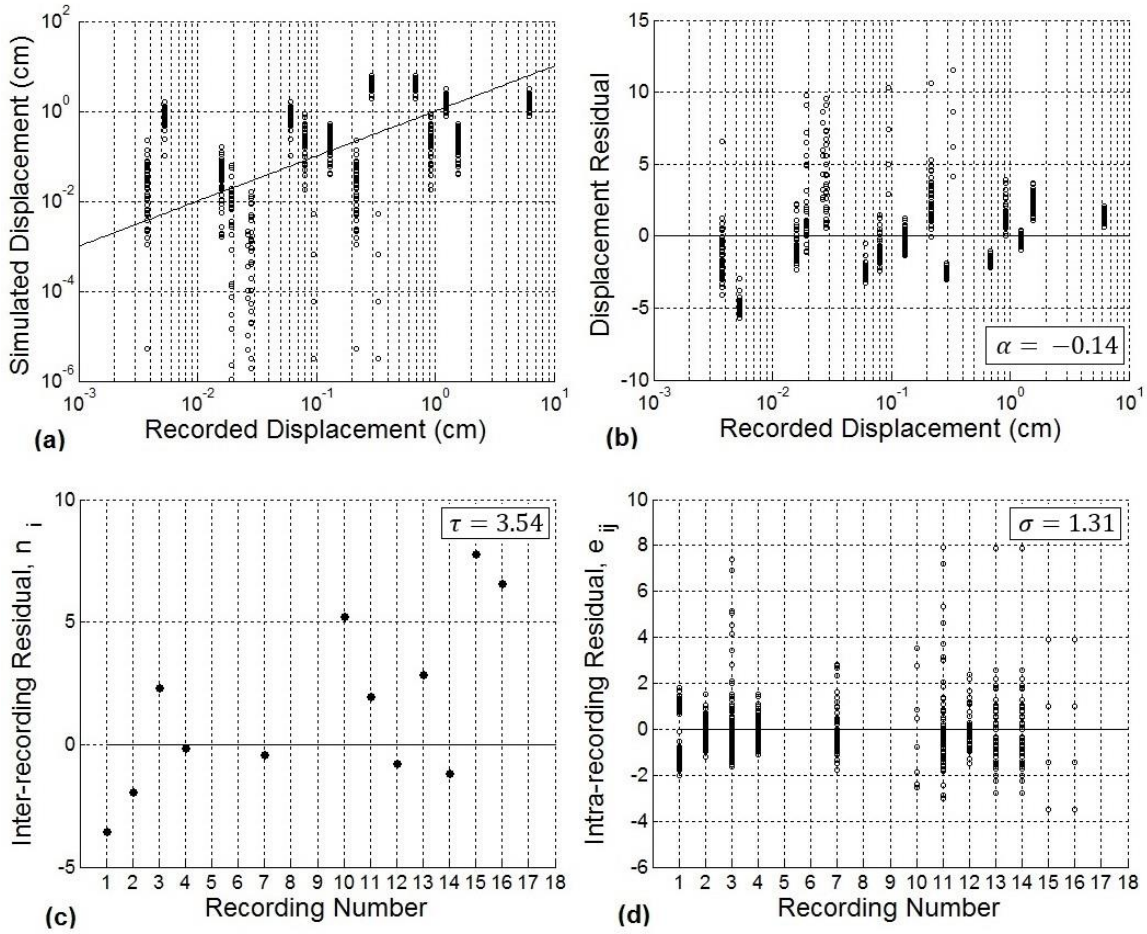

Figure 4.9 Displacements and residual displacements computed for the EXSIM simulations.

The displacement results for the ground motions simulated by the GP model are shown in Figure 4.10. In this case, there are a significant number of positive residuals, indicating that the displacements from the simulated motions are smaller than the displacements from the recorded motions. The average displacement residual (α) is equal to 0.96, which corresponds with average displacements that are only 40% of the displacements from the recorded motion. This under-prediction in displacement is in agreement with the ground motion

residuals (Table 4-2) which were all positive (i.e., under-prediction) for GP. The inter-recording residuals for the GP simulations vary significantly with the resulting τ being very large (τ = 4.14). The displacements computed for the GP simulations are seen to range over as much as 5 orders of magnitude and the resulting intra-recording standard deviation was equal to 2.26.

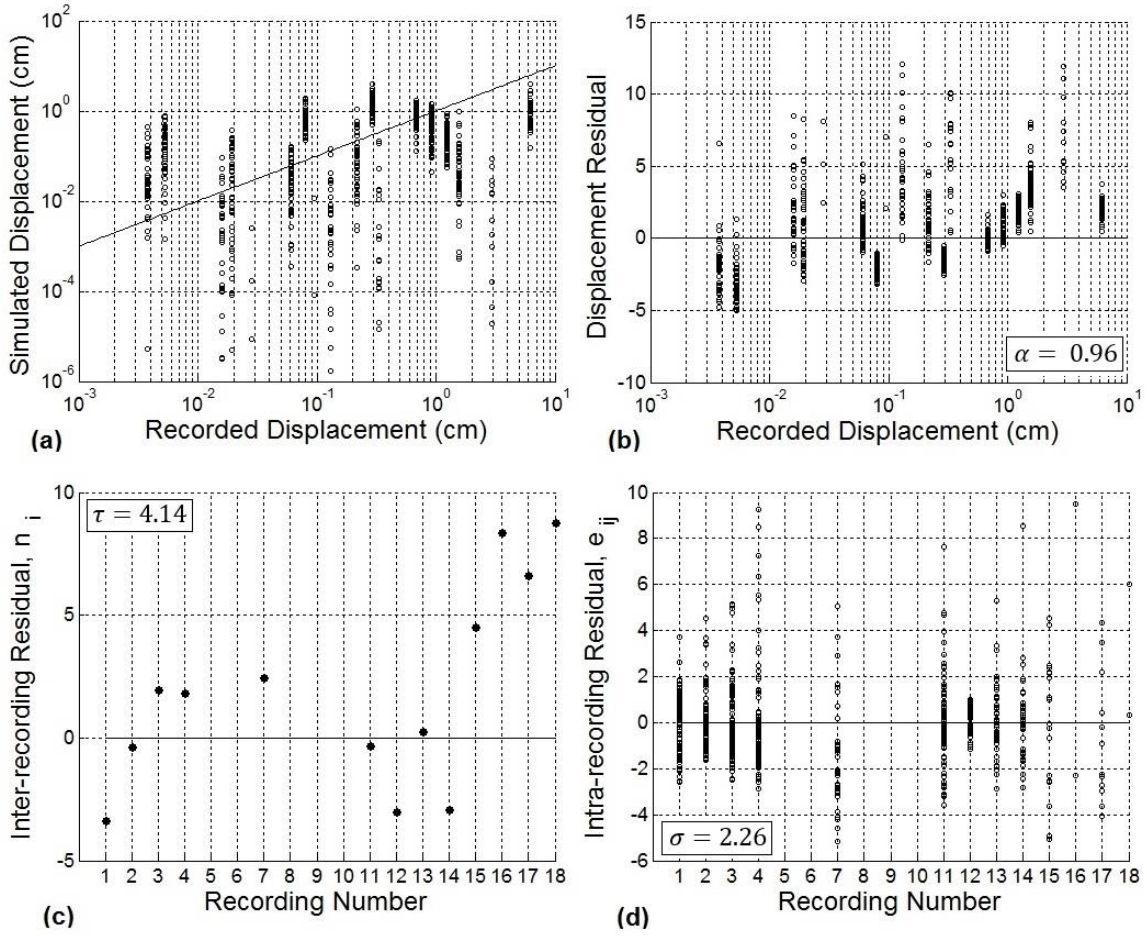

Figure 4.10 Displacements and residual displacements computed for the GP simulations.

The displacement results for the ground motions simulated by the SDSU model are shown in Figure 4.11. In this case, there are similar numbers of

positive and negative residuals and the resulting average displacement residual (α) is equal to -0.06. This value corresponds with only a 5% difference between the displacements from simulated and recorded motions, on average. This good agreement between the simulated and recorded displacements is somewhat surprising given the positive average ground motion residuals for the SDSU model (Table 4-2). However, the SDSU model did have the overall ground motion residuals closest to zero. Inspection of Figure 4.11a reveals that, for some recordings, the displacements from the simulations vary as much as 4 orders of magnitude; in other cases the displacements vary within an order of magnitude. The inter-recording variability (τ) was determined to be 2.51 (Figure 4.11c), while the intra-recording variability in the displacement residual (σ) was determined to be 1.51.

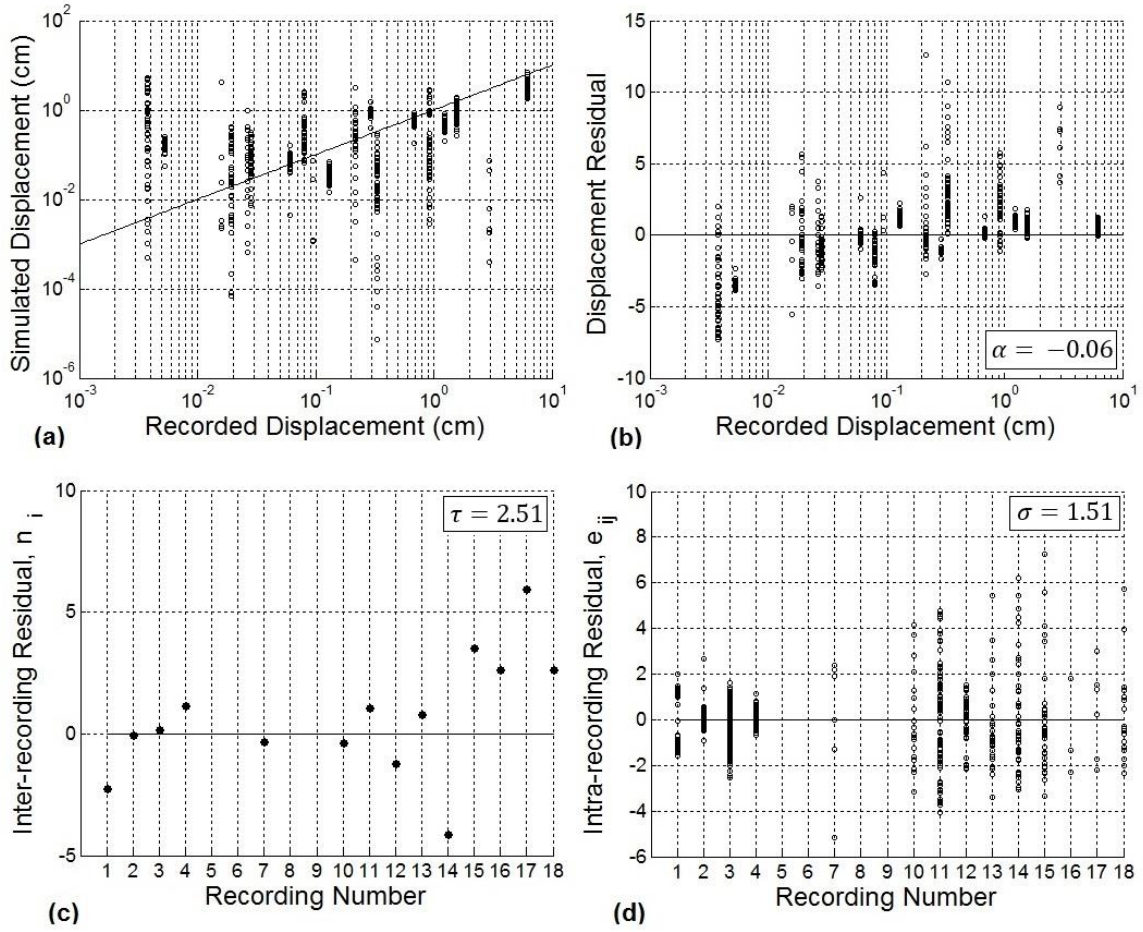

Figure 4.11 Displacements and residual displacements computed for the SDSU simulations.

Table 4-3 summarizes the mixed-effects regression results for the four models in terms of α, τ, σ, and σ_Y. In terms of overall bias (α), the EXSIM and SDSU models provide displacements in the best agreement with displacements from recorded motions; the models over-predict displacement by 5%-15%. CSM significantly over-predicts and GP significantly under-predicts the displacements. Considering variability, the inter-recording variability (τ) is largest for the GP model and smallest for the CSM and SDSU models, while the

intra-recording variability (σ) is smallest for EXSIM and SDSU and larger for CSM and GP. As a result, the GP model displays the largest overall variability in displacement, while the SDSU model displays the smallest overall variability in displacement.

Table 4-3 Mixed effects regression parameters for displacement residuals for the four simulation models.

Simulation	α	τ	σ	σ_Y
CSM	-0.64	2.40	2.57	3.52
EXSIM	-0.14	3.54	1.31	3.78
GP	0.96	4.14	2.26	4.72
SDSU	-0.06	2.51	1.51	2.93

4.4 SUMMARY

In this chapter we evaluate four ground motion simulation models in the context of seismic slope stability analyses. The ground motion parameters (i.e., PGA, PGV, Ia, and T_m) and rigid sliding block displacements of the simulated ground motions are compared to those computed for the recorded ground motions.

The ground motion parameters of the simulated ground motions tend to be smaller than the corresponding ground motion parameters of the recorded ground motions. This was true for most models and most parameters.

The simulations were also evaluated regarding their ability to simulate ground motions with zero displacement when the displacement computed for the recorded ground motion was zero. The EXSIM and GP models were found to be most satisfactory in this respect.

When evaluated in terms of rigid sliding block displacements the SDSU model performed the best. The average displacement residual of the SDSU model was smaller than determined for any other model, as was the overall variability in displacement residual for the SDSU model. The GP model was found to lie on the opposite end of the spectrum. The GP model tends to underestimate displacement more than any other model overestimates displacement. In addition, the GP model was found to have the largest overall variability in displacement residual.

Chapter 5. Conclusions

5.1 Summary and Conclusions

Seismic slope stability is often assessed via permanent displacement analyses, which quantify the cumulative, downslope movement of a sliding mass subjected to earthquake loading. Permanent displacement analyses provide a useful index as to the seismic performance of a slope. Seismic sliding block displacements can be computed for a suite of acceleration-time histories selected to fit a design ground motion.

The objective of this thesis was to investigate the effect of ground motion selection on seismic sliding block displacement. A two-part approach was used to explore this topic. First, ground motions were selected to fit target acceleration response spectra (i.e., uniform hazard spectra, UHS, and conditional mean spectra, CMS) and target conditional intensity measure distributions for peak ground velocity (PGV) and Arias Intensity (Ia) using different selection algorithms. The median rigid sliding block displacements were computed for each suite and compared with one another. Next, the use of simulated ground motions for seismic slope stability analyses was considered. First, the simulated ground motions were compared to the corresponding recorded ground motions in terms of ground motion parameters that are important for seismic slope stability analyses. Then, the simulated ground motions were evaluated in terms of rigid sliding block displacements computed at several yield acceleration values.

In the first part of this study we found that evaluation of the suites in terms of their PGV and Ia distributions provided useful insight into the relative

displacements computed for the suites. Both the PGV and Ia distributions of the UHS suite exceed the theoretical distributions of these parameters, with the difference between the Ia distributions being especially appreciable. The Ia distribution of the UHS suite was found to be inappropriately large; the scaled Ia values of motions in the UHS suite were greater than the largest Ia values in the NGA database. While the information summarized in a ground motion's PGV value is also captured in the motion's response spectrum, the same cannot be said for Ia. Thus, selecting motions to fit an acceleration response spectrum alone may result in inappropriate distribution of Ia. Consequently, the displacements computed for the UHS suite were considerably larger than the displacements computed for the other suites.

The displacements computed for the suite selected to fit the theoretical Ia distribution were smaller than the displacements computed for any other ground motion suite. It is probable that these displacements were so small because the PGV distribution of the Ia suite tended to underestimate the theoretical PGV distribution and the median response spectrum of the Ia suite was below the CMS.

The PGV distributions of the CMS suite and the PGV suite both fit the theoretical PGV distribution quite well. However, the Ia distributions of these suites exceeded the theoretical Ia distribution. Therefore, it is probable that the displacements computed for the CMS suite and the PGV suite were fairly conservative results. If ground motions are to be selected for seismic slope stability analyses considering only two ground motion parameters, we recommend selecting motions to fit a PGV distribution that is conditional on

PGA. Alternatively, selecting motions to fit the CMS provides a suite that generally fits the theoretical PGV distribution and therefore can also be used. Finally, consideration should also be given to selecting motions that adequately fit the PGA, PGV, and Ia distributions expected at the site.

Seismological simulation models were evaluated in the context of seismic slope stability analyses. Four ground motion models were considered: the deterministic Composite Source Model (CSM), the stochastic model EXSIM, the deterministic-stochastic hybrid model by Graves and Pitarka (GP), and the deterministic-stochastic hybrid model developed at San Deigo State University (SDSU). These simulation models were used to generate 50 simulated time series at specific strong motion stations during previous earthquakes.

In general, the ground motion parameters (i.e., PGA, PGV, Ia, and mean period, Tm) of the simulated ground motions tended to underestimate the ground motion parameters of the recorded ground motions. The median displacements from the SDSU simulations were the most similar to those computed using the recorded motions, with the median displacement about 6% larger than the displacement computed for the corresponding recorded ground motion. Also, the displacements from the SDSU simulations provided the smallest variability about the displacements predicted by the recorded motions. For the other simulation models, the displacements were over-predicted, on average, by 15% (EXSIM) to 90% (CSM), or under-predicted by 60% (GP). These models also demonstrated more variability in the predicted displacements. These differences are considerable, which makes the SDSU simulations the most agreeable with the recordings.

5.2 RECOMMENDATIONS FOR FURTHER RESEARCH

When selecting ground motions considering PGA and Ia alone we have seen that there is no guarantee that the spectral shape of the median response spectrum of the site will be appropriate. The displacements computed for the Ia suite were found to be slightly unconservative because the PGV distribution of the Ia suite tended to underestimate the conditional PGV distribution. The displacements computed for the PGV suite were slightly conservative because the Ia distribution of the PGV suite tended to overestimate the conditional Ia distribution.

Bradley (2012) developed the GCIM methodology to simultaneously consider multiple ground motion parameters in the ground motion selection process. This approach allows PGA, PGV, and Ia to be explicitly considered simultaneously in the ground motion selection process, such that both the Ia and PGV distributions of the suite would fit the conditional intensity measure distributions given the design PGA. It would be interesting to compare the rigid sliding block displacements computed for a suite developed considering PGA, PGV, and Ia to the displacements computed for the suites considered in this study.

Appendix A

Table A-1 Summary of properties of PGMD selected horizontal records for Los Angeles UHS. Listed ground motion parameters are for the geometric mean of the two horizontal records.

NGA#	ScaleF	PGA (g)	PGV (cm/s)	Arias Intensity (m/s)	D5-95(s)	Event	Year	Station	Mag .	Mechanism	Rjb(km)	Rrup(km)	Vs30(m/s)
3472	7.92	0.92	67.32	9.61	12.3 18.0	Chi-Chi-Taiwan-06	1999	TCU076	6.3	Reverse	23.8	25.9	615
126	1.41	0.92	95.73	9.58	6.4 6.8	Gazli- USSR	1976	Karakyr	6.8	Unkown	3.9	5.5	659.6
139	2.75	0.92	78.34	10.49	0.0 0.0	Tabas- Iran	1978	Dayhook	7.35	Reverse	0	13.9	659.6
1507	1.50	0.92	84.26	21.30	24.6 23.7	Chi-Chi-Taiwan	1999	TCU071	7.62	Reverse-Oblique	0	5.3	624.9
77	0.83	0.92	53.30	5.45	7.1 7.2	San Fernando	1971	Pacoima Dam (upper left abut)	6.61	Reverse	0	1.8	2016.1
769	5.38	0.92	76.07	9.43	11.7 12.5	Loma Prieta	1989	Gilroy Array #6	6.93	Reverse-Oblique	17.9	18.3	663.3
1626	9.73	0.92	100.13	13.39	28.5 24.9	Sitka- Alaska	1972	Sitka Observatory	7.68	Strike-Slip	34.6	34.6	659.6
1350	4.33	0.92	61.40	12.24	18.4 16.1	Chi-Chi-Taiwan	1999	ILA067	7.62	Reverse-Oblique	33.3	38.8	680
164	5.67	0.92	82.13	41.11	36.0 29.7	Imperial Valley-06	1979	Cerro Prieto	6.53	Strike-Slip	15.2	15.2	659.6
1521	3.21	0.92	99.29	22.12	24.1 24.8	Chi-Chi-Taiwan	1999	TCU089	7.62	Reverse-Oblique	0	8.9	680

Table A-2 Summary of properties of PGMD selected horizontal records for Los Angeles CMS. Listed ground motion parameters are for the geometric mean of the two horizontal records.

NGA#	ScaleF	PGA (g)	PGV (cm/s)	Arias Intensity (m/s)	D5-95(s)	Event	Year	Station	Mag .	Mechanism	Rjb(km)	Rrup(km)	Vs30(m/s)
1051	0.65	0.92	45.69	3.58	6.0 5.3	Northridge-01	1994	Pacoima Dam (upper left)	6.69	Reverse	4.9	7	2016.1
2658	1.50	0.92	35.38	2.40	12.1 14.1	Chi-Chi-Taiwan-03	1999	TCU129	6.2	Reverse	10.9	12.8	664.4
72	5.36	0.92	36.66	6.51	12.9 12.7	San Fernando	1971	Lake Hughes #4	6.61	Reverse	19.4	25.1	821.7
810	2.02	0.92	37.40	9.01	9.3 9.7	Loma Prieta	1989	UCSC Lick Observatory	6.93	Reverse-Oblique	12	18.4	714
3507	3.62	0.92	47.28	6.95	10.0 13.8	Chi-Chi-Taiwan-06	1999	TCU129	6.3	Reverse	22.7	24.8	664.4
2935	11.01	0.92	46.04	6.06	11.3 9.3	Chi-Chi-Taiwan-04	1999	TTN051	6.2	Strike-Slip	37.5	37.6	680
495	0.92	0.92	36.69	3.39	8.2 7.8	Nahanni-Canada	1985	Site 1	6.76	Reverse	2.5	9.6	659.6
2622	3.38	0.92	44.30	5.68	62.8 2.8	Chi-Chi-Taiwan-03	1999	TCU071	6.2	Reverse	15	16.5	624.9
1041	4.95	0.92	31.47	6.15	10.1 9.5	Northridge-01	1994	Mt Wilson - CIT Seis Sta	6.69	Reverse	35.5	35.9	821.7
2820	12.07	0.92	37.36	8.47	11.1 11.7	Chi-Chi-Taiwan-04	1999	KAU050	6.2	Strike-Slip	39.7	39.7	680

Table A-3 Summary of properties of PGMD selected horizontal records for San Jose UHS. Listed ground motion parameters are for the geometric mean of the two horizontal records.

NGA#	ScaleF	PGA (g)	PGV (cm/s)	Arias Intensity (m/s)	D5-95(s)	Event	Year	Station	Mag .	Mechanism	Rjb(km)	Rrup(km)	Vs30(m/s)
1511	1.97	0.70	124.94	13.90	29.5 28.1	Chi-Chi-Taiwan	1999	TCU076	7.62	Reverse-Oblique	2.8	2.8	615
1521	2.44	0.70	75.68	12.85	24.1 24.8	Chi-Chi-Taiwan	1999	TCU089	7.62	Reverse-Oblique	0	8.9	680
126	1.07	0.70	72.97	5.56	6.4 6.8	Gazli- USSR	1976	Karakyr	6.8	Unkown	3.9	5.5	659.6
2111	8.66	0.70	75.08	7.00	18.8 23.7	Denali- Alaska	2002	R109 (temp)	7.9	Strike-Slip	43	43	963.9
143	0.87	0.70	84.12	8.63	0.0 0.0	Tabas- Iran	1978	Tabas	7.35	Reverse	1.8	2	766.8
1507	1.15	0.70	64.23	12.37	24.6 23.7	Chi-Chi-Taiwan	1999	TCU071	7.62	Reverse-Oblique	0	5.3	624.9
139	2.09	0.70	59.71	6.09	0.0 0.0	Tabas- Iran	1978	Dayhook	7.35	Reverse	0	13.9	659.6
1013	1.43	0.70	80.32	3.17	6.5 6.5	Northridge-01	1994	LA Dam	6.69	Reverse	0	5.9	629
1029	8.53	0.70	74.97	6.44	13.1 13.0	Northridge-01	1994	Leona Valley #3	6.69	Reverse	37	37.3	684.9
164	4.32	0.70	62.60	23.89	36.0 29.7	Imperial Valley-06	1979	Cerro Prieto	6.53	Strike-Slip	15.2	15.2	659.6

Table A-4 Summary of properties of PGMD selected horizontal records for San Jose CMS. Listed ground motion parameters are for the geometric mean of the two horizontal records.

NGA#	ScaleF	PGA (g)	PGV (cm/s)	Arias Intensity (m/s)	D5-95(s)	Event	Year	Station	Mag .	Mechanism	Rjb(km)	Rrup(km)	Vs30(m/s)
1051	0.49	0.70	34.83	2.08	6.0 5.3	Northridge-01	1994	Pacoima Dam (upper left)	6.69	Reverse	4.9	7	2016.1
2658	1.14	0.70	26.97	1.39	12.1 14.1	Chi-Chi-Taiwan-03	1999	TCU129	6.2	Reverse	10.9	12.8	664.4
72	4.08	0.70	27.94	3.78	12.9 12.7	San Fernando	1971	Lake Hughes #4	6.61	Reverse	19.4	25.1	821.7
476	11.95	0.70	33.03	6.34	7.3 7.8	Morgan Hill	1984	UCSC Lick Observatory	6.19	Strike-Slip	45.5	45.5	714
3507	2.76	0.70	36.03	4.04	10.0 13.8	Chi-Chi-Taiwan-06	1999	TCU129	6.3	Reverse	22.7	24.8	664.4
2935	8.39	0.70	35.09	3.52	11.3 9.3	Chi-Chi-Taiwan-04	1999	TTN051	6.2	Strike-Slip	37.5	37.6	680
810	1.54	0.70	28.51	5.24	9.3 9.7	Loma Prieta	1989	UCSC Lick Observatory	6.93	Reverse-Oblique	12	18.4	714
495	0.70	0.70	27.97	1.97	8.2 7.8	Nahanni-Canada	1985	Site 1	6.76	Reverse	2.5	9.6	659.6
2622	2.58	0.70	33.76	3.30	62.8 2.8	Chi-Chi-Taiwan-03	1999	TCU071	6.2	Reverse	15	16.5	624.9
765	1.61	0.70	53.56	3.51	5.1 4.8	Loma Prieta	1989	Gilroy Array #1	6.93	Reverse-Oblique	8.8	9.6	1428

Table A-5 Source and site information for the ground motions composing the SigmaSpectra library. Each result listed below is associated with two components of ground motion. Thus, the library consists of 52 acceleration-time history records.

Result #	NGA #	Pulse	Tp (s)	D5-95 (s)	Event	Year	Station	Magnitude	Mechanism	Rjb (km)	Rrup(km)	Vs30 (m/s)	Lowest usable freq (Hz)
1	63	0 0	-- --	12.1 14.2	San Fernando	1971	Fairmont Dam	6.61	Reverse	25.6	30.2	684.9	0.62
2	71	0 0	-- --	10.7 11.9	San Fernando	1971	Lake Hughes #12	6.61	Reverse	14	19.3	602.1	0.62
3	72	0 0	-- --	12.9 12.7	San Fernando	1971	Lake Hughes #4	6.61	Reverse	19.4	25.1	821.7	0.62
4	87	0 0	-- --	11.1 11.5	San Fernando	1971	Santa Anita Dam	6.61	Reverse	30.7	30.7	684.9	0.25
5	126	0 0	-- --	6.4 6.8	Gazli, USSR	1976	Karakyr	6.8	Unkown	3.9	5.5	659.6	0.06
6	139	0 0	-- --	0.0 0.0	Tabas, Iran	1978	Dayhook	7.35	Reverse	0	13.9	659.6	0.12
7	143	0 0	-- --	0.0 0.0	Tabas, Iran	1978	Tabas	7.35	Reverse	1.8	2	766.8	0.06
8	164	0 0	-- --	36.0 29.7	Imperial Valley-06	1979	Cerro Prieto	6.53	Strike-Slip	15.2	15.2	659.6	0.12
9	265	0 0	-- --	8.6 7.6	Victoria, Mexico	1980	Cerro Prieto	6.33	Strike-Slip	13.8	14.4	659.6	0.25
10	284	0 0	-- --	18.1 19.3	Irpinia, Italy-01	1980	Auletta	6.9	Normal	9.5	9.6	1000	0.12
11	285	0 0	-- --	15.4 20.6	Irpinia, Italy-01	1980	Bagnoli Irpinio	6.9	Normal	8.1	8.2	1000	0.12
12	286	0 0	-- --	23.7 25.8	Irpinia, Italy-01	1980	Bisaccia	6.9	Normal	17.5	21.3	1000	0.38
13	289	0 0	-- --	24.8 23.2	Irpinia, Italy-01	1980	Calitri	6.9	Normal	13.3	17.6	600	0.25
14	292	1 1	3.1 3.5	16.6 12.1	Irpinia, Italy-01	1980	Sturno	6.9	Normal	6.8	10.8	1000	0.16
15	295	0 0	-- --	18.6 17.2	Irpinia, Italy-02	1980	Auletta	6.2	Normal	28.7	29.9	1000	0.38
16	296	0 0	-- --	17.5 17.4	Irpinia, Italy-02	1980	Bagnoli Irpinio	6.2	Normal	17.8	19.6	1000	0.38
17	297	0 0	-- --	21.3 21.1	Irpinia, Italy-02	1980	Bisaccia	6.2	Normal	14.7	14.7	1000	0.16
18	300	0 0	-- --	18.3 19.7	Irpinia, Italy-02	1980	Calitri	6.2	Normal	8.8	8.8	600	0.25
19	303	0 0	-- --	14.4 13.5	Irpinia, Italy-02	1980	Sturno	6.2	Normal	20.4	20.4	1000	0.29
20	369	0 0	-- --	9.1 11.6	Coalinga-01	1983	Slack Canyon	6.36	Reverse	26	27.5	684.9	0.25
21	454	0 0	-- --	8.6 8.3	Morgan Hill	1984	Gilroy - Gavilan Coll.	6.19	Strike-Slip	14.8	14.8	729.6	0.12
22	459	1 0	1.2 --	6.9 7.3	Morgan Hill	1984	Gilroy Array #6	6.19	Strike-Slip	9.8	9.9	663.3	0.12
23	471	0 0	-- --	19.0 17.5	Morgan Hill	1984	San Justo Dam (L Abut)	6.19	Strike-Slip	31.9	31.9	622.9	0.25
24	472	0 0	-- --	22.4 19.5	Morgan Hill	1984	San Justo Dam (R Abut)	6.19	Strike-Slip	31.9	31.9	622.9	0.25
25	476	0 0	-- --	7.3 7.8	Morgan Hill	1984	UCSC Lick Observatory	6.19	Strike-Slip	45.5	45.5	714	0.62
26	495	0 0	-- --	8.2 7.8	Nahanni, Canada	1985	Site 1	6.76	Reverse	2.5	9.6	659.6	0.06

Table A-6 Summary of properties of SigmaSpectra selected horizontal records for Los Angeles UHS.

NGA Record	ScaleF	PGA (g)	PGV (cm/s)	Arias Intensity (m/s)	D5-95(s)	Event	Year	Station	Mag .	Mechanism	Rjb(km)	Rrup(km)	Vs30(m/s)
126_GAZ000	1.51	0.92	98.82	10.65	6.4	Gazli, USSR	1976	Karakyr	6.8	Unkown	3.9	5.5	659.6
143_TAB2	1.08	0.92	130.84	13.44	16.1	Tabas, Iran	1978	Tabas	7.35	Reverse	1.8	2	766.8
164_H-CPE237	5.86	0.92	109.10	46.08	36.2	Imperial Valley-06	1979	Cerro Prieto	6.53	Strike-Slip	15.2	15.2	659.6
265_CPE315	1.57	0.92	31.07	2.47	7.6	Victoria, Mexico	1980	Cerro Prieto	6.33	Strike-Slip	13.8	14.4	659.6
286_A-BIS000	9.17	0.92	215.35	15.82	24.2	Irpinia, Italy-01	1980	Bisaccia	6.9	Normal	17.5	21.3	1000
292_A-STU270	2.57	0.92	133.21	9.34	15.2	Irpinia, Italy-01	1980	Sturno	6.9	Normal	6.8	10.8	1000
454_GIL337	9.73	0.92	27.88	5.09	8.2	Morgan Hill	1984	Gilroy - Gavilan Coll.	6.19	Strike-Slip	14.8	14.8	729.6
472_SJR360	15.42	0.92	89.71	24.44	21.3	Morgan Hill	1984	San Justo Dam (R Abut)	6.19	Strike-Slip	31.9	31.9	622.9
476_LOB050	23.49	0.92	47.18	13.39	7.8	Morgan Hill	1984	UCSC Lick Observatory	6.19	Strike-Slip	45.5	45.5	714
495_S1280	0.84	0.92	38.66	2.71	8.1	Nahanni, Canada	1985	Site 1	6.76	Reverse	2.5	9.6	659.6

Table A-7 Summary of properties of SigmaSpectra selected horizontal records for Los Angeles CMS.

NGA Record	ScaleF	PGA (g)	PGV (cm/s)	Arias Intensity (m/s)	D5-95(s)	Event	Year	Station	Mag .	Mechanism	Rjb(km)	Rrup(km)	Vs30(m/s)
265_CPE315	1.57	0.92	31.07	2.46	7.56	Victoria, Mexico	1980	Cerro Prieto	6.33	Strike-Slip	13.8	14.4	659.6
303_B-STU270	11.91	0.92	52.95	10.52	13.9	Irpinia, Italy-02	1980	Sturno	6.2	Normal	20.4	20.4	1000
454_GIL337	9.73	0.92	27.88	5.09	8.2	Morgan Hill	1984	Gilroy - Gavilan Coll.	6.19	Strike-Slip	14.8	14.8	729.6
459_G06000	4.14	0.92	47.18	6.51	7.3	Morgan Hill	1984	Gilroy Array #6	6.19	Strike-Slip	9.8	9.9	663.3
476_LOB320	12.13	0.92	43.63	11.76	7.6	Morgan Hill	1984	UCSC Lick Observatory	6.19	Strike-Slip	45.5	45.5	714
495_S1010	0.94	0.92	43.14	3.93	7.9	Nahanni, Canada	1985	Site 1	6.76	Reverse	2.5	9.6	659.6
63_FTR056	12.92	0.92	60.27	7.40	12.8	San Fernando	1971	Fairmont Dam	6.61	Reverse	25.6	30.2	684.9
71_L12021	2.51	0.92	42.42	5.85	10.7	San Fernando	1971	Lake Hughes #12	6.61	Reverse	14	19.3	602.1
72_L04111	4.78	0.92	26.77	5.68	12.7	San Fernando	1971	Lake Hughes #4	6.61	Reverse	19.4	25.1	821.7
87_SAD273	4.34	0.92	26.29	5.69	11.0	San Fernando	1971	Santa Anita Dam	6.61	Reverse	30.7	30.7	684.9

Table A-8 Summary of properties of SigmaSpectra selected horizontal records for San Jose UHS.

NGA Record	ScaleF	PGA (g)	PGV (cm/s)	Arias Intensity (m/s)	D5-95(s)	Event	Year	Station	Mag .	Mechanism	Rjb(km)	Rrup(km)	Vs30(m/s)
126_GAZ000	1.15	0.70	75.33	6.19	6.405	Gazli, USSR	1976	Karakyr	6.8	Unkown	3.9	5.5	659.6
143_TAB1	0.84	0.70	81.96	8.12	16.5	Tabas, Iran	1978	Tabas	7.35	Reverse	1.8	2	766.8
164_H-CPE147	4.15	0.70	48.00	21.01	29.7	Imperial Valley-06	1979	Cerro Prieto	6.53	Strike-Slip	15.2	15.2	659.6
265_CPE315	1.19	0.70	23.68	1.43	7.6	Victoria, Mexico	1980	Cerro Prieto	6.33	Strike-Slip	13.8	14.4	659.6
285_A-BAG000	5.03	0.70	110.96	8.54	19.5	Irpinia, Italy-01	1980	Bagnoli Irpinio	6.9	Normal	8.1	8.2	1000
286_A-BIS000	6.99	0.70	164.14	9.19	24.2	Irpinia, Italy-01	1980	Bisaccia	6.9	Normal	17.5	21.3	1000
292_A-STU270	1.96	0.70	101.53	5.42	15.2	Irpinia, Italy-01	1980	Sturno	6.9	Normal	6.8	10.8	1000
297_B-BIS000	9.22	0.70	96.16	8.57	20.5	Irpinia, Italy-02	1980	Bisaccia	6.2	Normal	14.7	14.7	1000
300_B-CTR270	4.26	0.70	109.18	9.64	20.0	Irpinia, Italy-02	1980	Calitri	6.2	Normal	8.8	8.8	600
87_SAD003	4.65	0.70	21.87	6.11	11.3	San Fernando	1971	Santa Anita Dam	6.61	Reverse	30.7	30.7	684.9

Table A-9 Summary of properties of SigmaSpectra selected horizontal records for San Jose CMS.

NGA Record	ScaleF	PGA (g)	PGV (cm/s)	Arias Intensity (m/s)	D5-95(s)	Event	Year	Station	Mag .	Mechanism	Rjb(km)	Rrup(km)	Vs30(m/s)
265_CPE315	1.19	0.70	23.68	1.43	4.18	Victoria, Mexico	1980	Cerro Prieto	6.33	Strike-Slip	13.8	14.4	659.6
296_B-BAG000	14.45	0.70	65.27	6.03	5.0	Irpinia, Italy-02	1980	Bagnoli Irpinio	6.2	Normal	17.8	19.6	1000
303_B-STU270	9.08	0.70	40.36	6.11	4.9	Irpinia, Italy-02	1980	Sturno	6.2	Normal	20.4	20.4	1000
454_GIL337	7.42	0.70	21.25	2.96	4.7	Morgan Hill	1984	Gilroy - Gavilan Coll.	6.19	Strike-Slip	14.8	14.8	729.6
459_G06000	3.15	0.70	35.96	3.78	3.1	Morgan Hill	1984	Gilroy Array #6	6.19	Strike-Slip	9.8	9.9	663.3
476_LOB320	9.24	0.70	33.26	6.83	4.3	Morgan Hill	1984	UCSC Lick Observatory	6.19	Strike-Slip	45.5	45.5	714
63_FTR056	9.85	0.70	45.94	4.30	3.2	San Fernando	1971	Fairmont Dam	6.61	Reverse	25.6	30.2	684.9
71_L12021	1.92	0.70	32.34	3.40	2.8	San Fernando	1971	Lake Hughes #12	6.61	Reverse	14	19.3	602.1
72_L04111	3.65	0.70	20.40	3.30	3.6	San Fernando	1971	Lake Hughes #4	6.61	Reverse	19.4	25.1	821.7
87_SAD273	3.31	0.70	20.04	3.31	5.3	San Fernando	1971	Santa Anita Dam	6.61	Reverse	30.7	30.7	684.9

Table A-10 Summary of properties of selected horizontal records for Los Angeles conditional PGV distribution. Listed ground motion parameters are for the geometric mean of the two horizontal records.

NGA Record	ScaleF	PGA (g)	PGV (cm/s)	Arias Intensity (m/s)	D5-95(s)	Event	Year	Station	Mag .	Mechanism	Rjb(km)	Rrup(km)	Vs30(m/s)
822	75.96	0.92	52.40	3.54	5.3 5.8	Roermond, Netherlands	1992	GLA 99999 GSH	5.3	Normal	57.67	59.49	659.6
1657	11.92	0.92	29.60	2.50	9.4 11.1	Northridge-02	1994	CDMG 24157 LA - Baldwin Hills	6.05	Reverse	31.96	32.52	297.1
227	12.93	0.92	38.90	3.12	4.0 3.8	Anza (Horse Canyon)-01	1980	Anza Fire Station	5.19	Strike-Slip	13.7	17.6	338.5
448	2.68	0.92	76.50	5.47	6.5 5.7	Morgan Hill	1984	Anderson Dam (Downstream)	6.19	Strike-Slip	3.2	3.3	488.8
1694	5.20	0.92	36.10	4.07	3.6 2.4	Northridge-06	1994	Beverly Hills - 12520 Mulhol	5.28	Reverse	10.6	15.3	545.7
739	3.85	0.92	75.40	11.86	10.0 11.2	Loma Prieta	1989	Anderson Dam (Downstream)	6.93	Reverse-Oblique	19.9	20.3	488.8
1890	64.73	0.92	48.50	6.75	9.8 9.4	Big Bear-02	2001	Riverside - I215 & 3rd	4.53	Strike-Slip	49.5	50.1	370.8
3188	9.06	0.92	58.60	9.36	13.2 13.1	Chi-Chi, Taiwan-05	1999	TCU067	6.2	Reverse	36.7	41.5	433.6
1873	67.58	0.92	29.70	5.59	13.9 14.3	Big Bear-02	2001	Hemet Fire Station	4.53	Strike-Slip	61.6	62.1	338.5
1941	21.42	0.92	24.60	3.80	8.6 8.4	Anza -02	2001	Hurkey Creek Park	4.92	Normal-Oblique	24	27.7	338.5

Table A-11 Summary of properties of selected horizontal records for Los Angeles conditional Ia distribution. Listed ground motion parameters are for the geometric mean of the two horizontal records.

NGA Record	ScaleF	PGA (g)	PGV (cm/s)	Arias Intensity (m/s)	D5-95(s)	Event	Year	Station	Mag .	Mechanism	Rjb(km)	Rrup(km)	Vs30(m/s)
713	13.48	0.92	42.75	5.23	15.9 11.9	Whittier Narrows-02	1987	LA - Hollywood Stor FF	5.27	Reverse-Oblique	50.9	24.8	316.5
683	3.51	0.92	33.01	4.26	4.9 6.9	Whittier Narrows-01	1987	Pasadena - Old House Rd	5.99	Reverse-Oblique	8.0	19.2	455.4
113	4.67	0.92	7.24	1.43	2.7 2.4	Oroville-03	1975	DWR Garage	4.7	Normal	0.0	6.1	622.9
50	5.11	0.92	54.11	3.56	3.4 2.7	Lytle Creek	1970	Wrightwood - 6074 Park Dr	5.33	Reverse-Oblique	10.9	12.4	486
382	3.98	0.92	34.27	1.86	1.1 2.9	Coalinga-02	1983	Palmer Ave	5.09	Reverse	2.2	11.4	376.1
924	25.13	0.92	26.13	0.66	19.0 19.0	Big Bear-01	1992	Puerta La Cruz	6.46	Strike-Slip	94.5	95.6	370.8
380	2.88	0.92	31.95	2.08	1.7 1.0	Coalinga-02	1983	Oil Fields - Skunk Hollow	5.09	Reverse	1.7	10.7	376.1
825	0.68	0.92	61.78	1.76	6.9 6.5	Cape Mendocino	1992	Cape Mendocino	7.01	Reverse	0.0	7.0	513.7
114	11.75	0.92	26.19	2.51	4.4 4.4	Oroville-03	1975	Duffy Residence (OR5)	4.7	Normal	7.3	10.5	438.3
205	5.71	0.92	49.69	2.27	5.3 6.0	Imperial Valley-07	1979	El Centro Array #7	5.01	Strike-Slip	7.3	10.3	210.5

Table A-12 Summary of properties of selected horizontal records for San Jose conditional PGV distribution. Listed ground motion parameters are for the geometric mean of the two horizontal records.

NGA Record	ScaleF	PGA (g)	PGV (cm/s)	Arias Intensity (m/s)	D5-95(s)	Event	Year	Station	Mag .	Mechanism	Rjb(km)	Rrup(km)	Vs30(m/s)
2771	82.56	0.70	34.70	8.25	21.1 17.7	Chi-Chi, Taiwan-04	1999	HWA020	6.2	Strike-Slip	66	66.3	375.3
924	19.17	0.70	19.90	0.39	19.0 19.0	Big Bear-01	1992	Puerta La Cruz	6.46	Strike-Slip	94.5	95.6	370.8
1714	13.49	0.70	28.50	1.60	2.3 2.4	Northridge-06	1994	LA - W 70th St	5.28	Reverse	30.5	32.4	294.2
1076	5.20	0.70	40.30	8.58	14.7 14.5	Northridge-01	1994	Santa Fe Springs- E. Joslin	6.69	Reverse	48.1	50.2	308.6
1694	3.97	0.70	27.60	2.37	3.6 2.4	Northridge-06	1994	Beverly Hills - 12520 Mulhol	5.28	Reverse	10.6	15.3	545.7
3028	13.92	0.70	39.40	6.29	15.7 19.3	Chi-Chi, Taiwan-05	1999	HWA043	6.2	Reverse	44.3	45	272.6
1647	4.87	0.70	39.20	2.66	5.2 4.7	Sierra Madre	1991	San Marino - SW Academy	5.61	Reverse	15.8	18.7	379.4
3205	9.22	0.70	47.40	6.30	12.4 14.2	Chi-Chi, Taiwan-05	1999	TCU105	6.2	Reverse	59.8	63.8	575.5
2032	100.25	0.70	21.10	4.97	7.4 7.9	Gilroy	2002	Richmond - Point Molate	4.9	Strike-Slip	129.6	130.1	712.8
1680	33.58	0.70	30.90	6.28	16.5 14.1	Northridge-04	1994	LA - Univ. Hospital	5.93	Reverse-Oblique	49.6	51.2	376.1

Table A-13 Summary of properties of selected horizontal records for San Jose conditional Ia distribution. Listed ground motion parameters are for the geometric mean of the two horizontal records.

NGA Record	ScaleF	PGA (g)	PGV (cm/s)	Arias Intensity (m/s)	D5-95(s)	Event	Year	Station	Mag .	Mechanism	Rjb(km)	Rrup(km)	Vs30(m/s)
1974	12.82	0.70	6.92	1.54	11.1 10.8	Anza-02	2001	Sage- Fire Station	4.92	Normal-Oblique	38.6	41.1	622.9
1949	39.16	0.70	10.18	1.04	6.1 5.7	Anza-02	2001	Lake Elsinore - Graham & Poe	4.92	Normal-Oblique	77	78.6	622.9
225	5.85	0.70	22.18	1.04	2.2 1.8	Anza (Horse Canyon)-01	1980	Anza - Pinyon Flat	5.19	Strike-Slip	12	17.4	724.9
1923	31.16	0.70	29.29	2.23	12.5 13.1	Anza-02	2001	Borrego Springs - Scripps Clinic	4.92	Normal-Oblique	38	40	271.4
372	1.21	0.70	23.10	0.97	3.9 1.0	Coalinga-02	1983	Anticline Ridge Free-Field	5.09	Reverse	2.2	11.6	376.1
2398	12.82	0.70	16.53	3.13	11.6 16.7	Chi-Chi, Taiwan-02	1999	TCU088	5.9	Reverse	27.6	28.4	680
924	19.15	0.70	19.92	0.39	19.0 19.0	Big Bear-01	1992	Puerta La Cruz	6.46	Strike-Slip	94.5	95.6	370.8
2871	13.38	0.70	91.50	8.54	15.1 18.1	Chi-Chi, Taiwan-04	1999	TCU084	6.2	Strike-Slip	26.8	27.1	680
3034	14.16	0.70	38.38	5.86	16.2 16.7	Chi-Chi, Taiwan-05	1999	HWA050	6.2	Reverse	53.9	54.4	239.6
71	2.13	0.70	33.02	3.85	10.7 11.9	San Fernando	1971	Lake Hughes #12	6.61	Reverse	14	19.3	602.1

Table A-14 Ground motion parameters of the recorded acceleration-time histories.

Event Station ID	Component	PGA (g)	PGV (cm/s)	I_a (m/s)	T_m (s)
15008-OKYH0	E-W	0.128	11.69	0.292	0.161
	N-S	0.185	8.09	0.264	0.166
15020-SMNH1	E-W	0.233	20.56	0.482	0.498
	N-S	0.158	7.83	0.201	0.354
15025-HYG00	E-W	0.019	1.18	0.005	0.302
	N-S	0.019	1.88	0.006	0.415
2027-ATB	E-W	0.068	4.32	0.029	0.387
	N-S	0.046	3.58	0.030	0.359
2033-ACI	E-W	0.037	1.76	0.021	0.299
	N-S	0.067	3.20	0.074	0.257
5005-A-KRE	E-W	0.112	8.01	0.087	0.455
	N-S	0.089	3.76	0.049	0.318
8028-XSP	E-W	0.087	10.17	0.105	0.661
	N-S	0.057	5.23	0.047	0.509
8029-RIN	E-W	0.092	10.43	0.066	0.837
	N-S	0.078	6.74	0.055	0.682
8031-CFH	E-W	0.108	19.78	0.133	1.047
	N-S	0.075	10.78	0.090	0.767

Table A-15 Rigid sliding block displacements computed for the recorded acceleration-time histories.

Recording Number	Event Station ID	Component	Displacements (cm) for $k_y = 0.05$ g	Displacements (cm) for $k_y = 0.1$ g	Displacements (cm) for $k_y = 0.2$ g
1	15008-OKYH0	E-W	0.294	0.005	0
2		N-S	0.681	0.060	0
3	15020-SMNH1	E-W	6.231	1.557	0.028
4		N-S	1.236	0.131	0
5	15025-HYG00	E-W	0	0	0
6		N-S	0	0	0
7	2027-ATB	E-W	0.016	0	0
8		N-S	0	0	0
9	2033-ACI	E-W	0	0	0
10		N-S	0.027	0	0
11	5005-A-KRE	E-W	0.915	0.019	0
12		N-S	0.080	0	0
13	8028-XSP	E-W	0.215	0	0
14		N-S	0.004	0	0
15	8029-RIN	E-W	0.329	0	0
16		N-S	0.096	0	0
17	8031-CFH	E-W	2.931	0.027	0
18		N-S	0.334	0	0

References

Abrahamson, N., and W. Silva. 2008. "Summary of the Abrahamson & Silva NGA ground-motion relations." *Earthquake Spectra* 24: 67-97.

Ang, A.H.S., and W.H. Tang. 2007. *Probability Concepts in Engineering: Emphasis on Applications in Civil and Environmental Engineering.* New York: Wiley.

Atkinson, G., and K. Assatourians. 2013. "EXSIM: Stochastic finite-fault simulation of time histories." *Broadband Platform Review Panel Meeting.*

Baker, J.W. 2011. "Conditional mean spectrum: tool for ground-motion selection." *Journal of Structural Engineering* 322-331.

Baker, J.W., and A. Cornell. 2005. "A vector-valued ground motion intensity measure consisting of spectral acceleration and epsilon." *Earthquake Engineering and Structural Dynamics* 35: 1193-1217.

Baker, J.W., and C.A. Cornell. 2006. "Correlation of response spectral values for multi-component ground motions." *Bulletin of the Seismological Society of America* 35 (9): 215-227.

Baker, J.W., and N. Jayaram. 2008. "Correlation of spectral acceleration values from NGA ground motion models." *Earthquake Spectra* 24: 299-317.

Boore, D.M. 2003. "Simulation of ground motion using the stochastic method." *Pure and Applied Geophysics* 160: 635-676.

Boore, D.M. 1983. "Stochastic simulation of high-frequency ground motions based on seismological models of the radiated spectra." *Bulletin of the Seismological Society of America* 73: 1865-1894.

Bradley, B.A. 2010. "A generalized conditional intensity measure approach and holistic ground-motion selection." *Earthquake Engineering and Structural Dynamics* 39: 1321-1342.

Bradley, B.A. 2012. "A ground motion selection algorithm based on the generalized conditional intensity measure approach." *Soil Dynamics and Earthquake Engineering* 40: 48-61.

Bray, J.D., and T. Travasarou. 2009. "Pseudostatic coeffcient for use in simplified seismic slope stability evaluation." *Journal of Geotechnical and Geoenvironmental Engineering* 135: 1336-1340.

Bray, J.D., and T. Travasarou. 2007. "Simplified procedure for estimating earthquake-induced deviatoric slope displacements." *Journal of Geotechnical and Geoenvironmental Engineering* 133: 381-392.

Bray, J.D., E.M. Rathje, A.J. Augello, and S.M. Merry. 1998. "Simplified seismic design procedure for geosynthetic-lined, soil-waste landfills." *Geosynthetics International* 5: 203-235.

Graves, R.W. 1996. "Simulating seismic wave propagation in 3-D elastic media using staggered finite differences." *Bulletin of the Seismological Society of America* 86: 1091-1106.

Graves, R.W., and A. Pitarka. 2010. "Broadband ground-motion simulation using a hybrid approach." *Bulletin of the Seismological Society of America* 100 (5A): 2095-2123.

Graves, R.W., and A. Pitarka. 2004. "Broadband time history simulation using a hybrid approach." *Proceedings of the 13th Conference on Earthquake Engineering.* Vancouver.

Hanks, T.C., and R.K. McGuire. 1981. "The character of high-frequency strong ground motion." *Bulletin of the Seismological Society of America* 71: 2071-2095.

Hartzell, S.H., and T.H. Heaton. 1983. "Inversion of strong ground motion and teleseismic waveform data for the fault rupture of the 1979 Imperial Valley, California, earthquake." *Bulletin of the Seismological Society of America* 83: 780-810.

Jayaram, N., and J.W. Baker. 2008. "Statistical test of the joint distrtibution of spectral acceleration values." *Bulletin of the Seismological Society of America* 98: 2231-2243.

Jibson, R.W. 2011. "Methods for assessing the stability of slopes during earthquakes - a retrospective." *Engineering Geology* 122: 43-50.

Jibson, R.W. 2007. "Regression models for estimating coseismic landslide displacement." *Engineering Geology (Amsterdam)* 91: 209-218.

Jibson, R.W., E.M. Rathje, M.W. Jibson, and Y.W. Lee. 2013. "SLAMMER -- Seismic landslide movement modeled using earthquake records." In *U.S. Geological Survey Techniques and Methods, Book 12, Chapter B1*.

Kaklamanos, J., B.A. Bradley, E.M. Thompson, and L.G. Baise. 2013. "Critical parameters affecting bias and variability in site response analyses using KiK-net downhole array data." *Bulletin of the Seismological Society of America* 103 (3): 1733-1749.

Kottke, A., and E.M. Rathje. 2008. "A semi-automated procedure for selecting and scaling recorded earthquake motions for dynamic analysis." *Earthquake Spectra* (Earthquake Engineering Research Institute) 24: 911-932.

Kottke, A., and E.M. Rathje. 2007. "Semi-automated selection and scaling of earthquake ground motions." *4th International Conference on Earthquake Geotechnical Engineering.* Thessaloniki, Greece.

Kottke, A., and E.M. Rathje. 2010. "SigmaSpectra." *NEEShub.* July 26. http://nees.org/resources/sigmaspectra.

Kramer, S.L. 1996. *Geotechnical earthquake engineering.* Upper Saddle River, NJ: Prentice-Hall, Inc.

Lindstrom, M.J., and D.M. Bates. 1990. "Nonlinear mixed effects models for repeated measures data." *Biometrics* 46: 673-687.

Mai, P.M., K.B. Olsen, and W. Imperatori. 2010. "Hybrid broadband ground-motion simulations: combining long-period deterministic synthetics with high-frequency multiple s-to-s backscattering." *Bulletin of the Seismological Society of America* 100 (5A): 2124-2142.

Makdisi, F., and H. Seed. 1978. "Simplified procedure for estimating dam and embankment earthquake-induced deformation." *Journal of the Geotechnical Engineering Division* 104: 849-867.

Motazedian, D., and G.M. Atkinson. 2005. "Stochastic finite-fault modeling based on a dynamic corner frequency." *Bulletin of the Seismological Society of America* 95: 995-1010.

Newmark, N. 1965. "Effects of earthquakes on dams and embankments." *Geotechnique* 15: 139-159.

Pacific Earthquake Engineering Research Center. 2010. "Technical report for the PEER Ground Motion Database web application." http://peer.berkeley.edu/peer_ground_motion_database/site/documentation.

Pinheiro, J., D. Bates, S. DebRoy, D. Sarkar, and R core team. 2008. "nlme: linear and nonlinear mixed effects models."

Rathje, E.M., and G. Saygili. 2009. "Probabilistic assessment of earthquake-induced sliding displacements of natural slopes." *Bulletin of the New Zealand Society for Earthquake Engineering* 42 (1): 18-27.

Rathje, E.M., and G. Saygili. 2008. "Probabilistic seismic hazard analysis for the sliding displacement of slopes: scalar and vector approaches." *Journal of Geotechnical and Geoenvironmental Engineering* 134 (6): 804-8014.

Rathje, E.M., and J. Bray. 2000. "An examination of simplified earthquake-induced displacement procedures for earth structures." *Canadian Geotechnical Journal* 36 (1): 72-87.

Rathje, E.M., F. Faraj, S. Russell, and J.D. Bray. 2004. "Empirical relationships for frequency content parameters of earthquake ground motions." *Earthquake Spectra* 20 (1): 119-144.

Rathje, E.M., J.D. Bray, and N.A. Abrahamson. 1998. "Simplified frequency content estimates of earthquake ground motions." *Journal of Geotechnical and Geoenvironmental Engineering* 124 (2): 150-159.

Rathje, E.M.., and G. Antonakos. 2011. "A unified model for predicting earthquake-induced sliding displacements of rigid and flexible slopes." *Engineering Geology* 122: 51-60.

Rodriguez-Marek, A., G.A. Montalva, F. Cotton, and F. Bonilla. 2011. "Analysis of single-station standard deviation using the KiK-net data." *Bulletin of the Seismological Society of America* 101: 1242-1258.

Saygili, G., and E.M. Rathje. 2008. "Empirical predictive models for earthquake-induced sliding displacement of slopes." *Journal of Geotechnical and Geoenvironmental Engineering* 134: 790-803.

Seed, H.B., and G.R. Martin. 1966. "The seismic coefficient in earth dam design." *ASCE Journal of the Soil Mechanics and Foundations Division* 92: 25-58.

Stewart, J.P., T.F. Blake, and R.A. Hollingsworth. 2003. "A screen analysis procedure for seismic slope stability." *Earthquake Spectra* 29: 697-712.

Terzaghi, K. 1950. "Mechanism of landslides." *Geological Society of America* Application of Geology to Engineering Practice, Berkey Volume: 83-123.

Travasarou, T., J. Bray, and N. Abrahamson. 2003. "Empirical attenuation relationship for arias intensity." *Earthquake Engineering & Structural Dynamics* 32 (7): 1133-1155.

U.S. Geological Survey. 2013. *Landslides 101.* December 18. http://landslides.usgs.gov/learn/ls101.php.

USGS. 2008. "Hazard curve application." *National Seismic Hazard Mapping Project.*

Watson-Lamprey, J., and N. Abrahamson. 2006. "Selection of ground motion time series and limits on Ssaling." *Soil Dynamics and Earthquake Engineering* 26: 477-482.

Zeng, Y., J.G. Anderson, and G. Yu. 1994. "A composite source model for computing reaslistic synthetic strong ground motions." *Geophysical Research letters* 21 (8): 725-728.